Autonoma University of Madrid
Faculty of Science
Department of Inorganic Chemistry

Doctoral Thesis:

Failures and successes in the quest of hybrid systems for efficient catalysis

Azin Hassanpour

Madrid 2015

Autonoma University of Madrid
Faculty of Science
Department of Inorganic Chemistry

Failures and successes in the quest of hybrid systems for efficient catalysis

This dissertation is submitted for the degree of Doctor of Philosophy in Science of **Chemistry**

By

Azin Hassanpour

Supervised by

Dr. Rubén Mas-Ballesté

Madrid, 2015

"I would like to dedicate this thesis to ***Mohammadreza*** *who is my best friend, classmate and beloved husband for his endless support, encouragement and unbelievable love."*

*“I also would like to dedicate this thesis to my kind father (**Dr. Ahmad Hasanpour)**, my self-sacrificing mother (**Fakhri Ghannad**), my lovely sisters (**Ara** and **Anahita**) and my husband’s parents to guiding me on the path of personal discovery for inspiring me to follow my dreams and for sharing in the understanding that distance is nothing when the family´s bond is strong.”*

Albert Einstein:

"Anyone who has never made a mistake has never tried anything new."

I would like to express my gratitude to my thesis advisor Dr. Rubén Mas-Ballesté. He has dedicated enormous energy and countless hours to helping me through every step of my dissertation. His advices and encouragement have been unending and invaluable, guiding me to define the direction of my research.

I would like to express my special appreciation and thanks to Dr. Félix Zamora for his unending assistance and supports.

I am deeply thankful to Professor Tomas Torres for his unbelievable cooperation and unending support.

I also would like to thank Professor Ester Delgado, Dr. Pilar Amo-ocho, Professor Salome Delgado, Dr. Octavio González del Moral, Miguel-Angel Fernandez, Ismael Moreno López and all the staff in the Department of Inorganic Chemistry has also been invaluable during my time at Autónoma University of Madrid. I consider each of them my friends and colleagues; their support and help has kept me grounded and focused during my work.

Special thanks to my lab mates Mohammad-Reza, Octavio, Marta, Khaled, David, Javier, Eva, Cristina and Isadora for their friendship and for sharing their experiences and research during my stay in the lab.

I would also like to thank Dr. Julio Lloret Fillol and Dr. Miquel Costas Salgueiro from University of Girona, Professor José Luis G. Fierro, Dr. José Miguel Campos-Martín and Silvia Morales de la Rosa from Institute of Catalysis and Petrochemical (CSIC) in Madrid, Dr. Veronica Carcelen from Abengoa Companty in Sevilla, Dr. Daniel Granados from IMDEA Nanoscience in Madrid, Benjamin R. Horrocks from School of Chemistry in Newcastle University (UK) for their time and professionalism that has always shown remarkable contributing to the development and quality of the manner of this thesis.

Lastly, and most importantly, I wish to thank my wonderful family, the completion of this work would not have been possible without their encouragement, love and support. Thanks for provided me with so many great memories, opportunities and experiences.

I would like to thank all of my friends and collaborators who have been a part of my life. You have not only made it possible for me to complete graduate school and my dissertation, but also made it a personally and professionally rewarding part of my life.

Abstract:

This thesis has been carried out in the Department of Inorganic Chemistry at the Autonomous University of Madrid and focused on the study of hybrid systems with potential use in a variety of catalytic processes.

After the general introduction, in the second chapter is presented a comprehensive analysis of the H_2 activation process achieved by active species generated by the reaction of H_2O_2 with non-heme iron compound [Fe (BPMCN) $(OTf)_2$] (BPMCN= N,N'-bis(2-pyridylmethyl)-1,2-diaminocyclohexane). This study was derived from the original idea of designing a tandem catalytic process from $H_2 + O_2$ mixture until the formation of epoxides and H_2O from reaction with olefins. However, what was observed is that depending on the presence of acetic acid in the reaction medium, H_2 molecule is activated with varying efficiency by the non-heme iron species with high oxidation state.

In the third chapter of this thesis, different strategies for supramolecular or covalent functionalization of graphene oxide (GO) designing for GO- porphyrin hybrids are presented.

In the fourth chapter, a procedure of sonication of graphite is reported in various mixtures of water and organic solvent, producing stable suspensions of few layers graphene. Optimized spray deposition processes of these graphene suspensions resulted in transparent coatings with excellent electrical conductivity *vs* transparency ratios.

In the fifth chapter is presented the design of electrodes with high surface area, based on carbon microfibers, which can be chemically modified (by an oxidation process using H_2SO_4 / H_2O_2) to make them active in electrocatalytic processes for H_2 generation.

Resumen:

Esta tesis se ha llevado a cabo en el departamento de Química Inorgánica en la Universidad Autónoma de Madrid y se ha centrado en el estudio de sistemas híbridos con potencial uso en diversos procesos catalíticos.

Después de la introducción general, en el segundo capítulo se ha presentado un análisis exhaustivo del proceso de activación de H_2 logrado por las especies activas generadas por reacción de H_2O_2 con el compuesto de hierro no hemo $[Fe(BPMCN)(OTf)_2]$ (BPMCN= N,N'-bis(2-pyridylmethyl)-1,2-diaminocyclohexane). Este estudio se derivó de la idea original de diseñar un proceso catalítico tipo tándem desde la mezcla $H_2 + O_2$ hasta la formación de epóxidos y H_2O a partir de reacción con olefinas. Sin embargo, lo que se observó fue que en función de la presencia de ácido acético en el medio de reacción, se activa con más o menos eficiencia la molécula de H_2 por la correspondiente especie de hierro no hemo con elevado estado de oxidación.

En el tercer capítulo de esta tesis se presentan diferentes estrategias de funcionalización supramolecular o covalente de óxido de grafeno para obtener híbridos de GO-porfirina.

En el cuarto capítulo se reporta un procedimiento de sonicación de grafito en varias mezclas de agua y disolvente orgánico que produce suspensiones muy estables de grafeno de pocas capas. La optimización de procesos de deposición por pulverización de estas suspensiones de grafeno ha resultado en recubrimientos transparentes con una excelente relación transparencia *vs* conductividad eléctrica.

En el quinto capítulo se presenta el diseño electrodos de elevada área superficial, basados en fibra de carbono, los cuales pueden ser químicamente modificados (mediante un proceso de oxidación usando H_2SO_4/H_2O_2) para hacerlos activos en procesos electrocatalíticos para la generación de H_2.

Chapter **1**

General Introduction and Objectives

I. Hybrid:

The research presented in this thesis is focused on the quest of hybrid systems for applications in efficient catalysis. According to the dictionary (oxford dictionary) Hybrid means "anything derived from heterogeneous sources, or composed of elements of different or incongruous kinds."[1] Therefore, we considered as a hybrid system a multicomponent material or homogenous systems.

I.1. Hybrid material:

Hybrid materials are described as a deliberate combination of two or more materials, complimenting each other to have super-functions or new functions, which component materials did not have. They are considered as boundary-area of research, having materials of organic, inorganic and metallic nature.[2]

Inorganic/organic hybrids have received a great attention from materials science and engineering.[3]

Hybridization between different chemical species has effect not only in controlling the physicochemical properties of each component but also in creating new functionality via an interactive coupling between the components. It means chemical interaction between the components such as inorganic–inorganic, organic–inorganic and bio-inorganic nanohybrids that can have different structures with different properties.[4,5]

I.2. Hybrid multicomponent homogenous system:

Chemists are constantly working to discover new and improved reactions. According to the definition of the adjective hybrid, we can consider as a hybrid system a solution with more than one component with a different function in a cooperative process. The final objective in this case, is to design systems consisting in sequence of different reactions that in each one we have a homogenous or heterogeneous catalytic reaction to reach a single goal.

The initial idea of this thesis is the design of hybrid systems both hybrid materials and hybrid multicomponent homogenous systems that could have relevance in several catalytic transformations. Some advantages of the hybrid materials is recyclable catalytic systems with an increased efficiency because of bimolecular decay pathways are avoided, due to the immobilization of the catalyst on the supports. Furthermore, they can be easily incorporated on devices like electrochemical cells.

In addition, with multicomponent homogenous system or multistep one-pot reactions, we can achieve atom economy, more efficient transformations to reach easy synthetic procedures, doing the reaction fast and using clean and cheap reagents.

In comparison with other nanostructured materials, 2D nanosheets can be very useful candidates for the synthesis of nanohybrid material with unique physicochemical properties. A representative example of exfoliated 2D nanosheets is graphene and its derivates.

Currently Graphene-based hybrid materials have been fabricated by the cross-linking of graphene or graphene oxide (GO) through various kinds of inorganic or organic species, like inorganic nanoparticles, polymers, multifunctional organic molecules, and metal ions/ complexes.[6]

To design hybrid materials, catalyst can be attached to solid supports, like carbon-based materials (graphene, graphene Oxide and carbon nanotubes).[7,8] In these hybrid materials the easy separation of catalyst from products is a very convenient feature.[9,10] In addition, high surface areas and sufficient number of reactive sites are some advantages of using carbon based materials as supports in catalytic systems.[11,12]

II. Carbon- based materials:

Carbon is a wonderful element, not only because is necessary for all life processes, but also because of its abundant allotropic forms.[13] Additionally, in lots of synthetic processes, carbon can be tailored into numerous structures, especially those in the nanometer range.[14,15] These carbon nanostructures include: 0D fullerenes, rolled into 1D nanotubes, tightly packed into 2D graphene or stacked into 3D graphite.

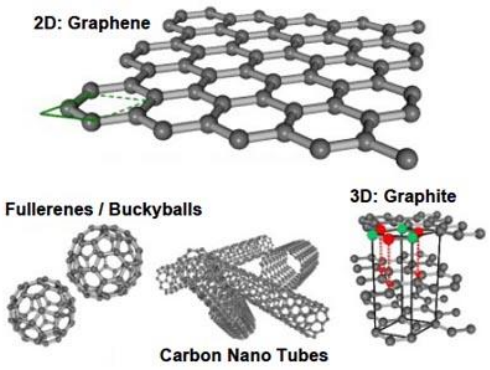

Figure 1.1: Carbon materials as fullerenes, carbon nanotubes (CNTs), graphene and graphite (0D, 1D, 2D and 3D respectively).

II.1. Carbon nanotubes (CNTs):

A single wall carbon nanotube is defined as a cylinder made up of rolled up sheet of graphene. The diameter of carbon nanotubes typically vary from 0.7-3 nm and because of the small diameters, nanotubes are considered as one-dimensional materials. They can have a single shell known as single wall carbon nanotubes, SWNTs or multiple shells known as multiwall carbon nanotubes MWNTs.

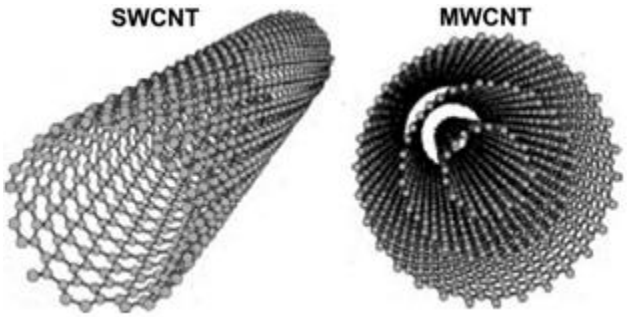

Figure 1.2: Single and multiwall carbon nanotubes.

CNTs play a fundamental role in leading scientific and industrial research effort in nanotechnology due to their especial properties: many-fold stronger than steel, harder than diamond, electrical conductivity higher than copper, thermal conductivity higher than diamond, Kinetic, Electrical and Optical properties.[16]

During the last years, great researches were done in the synthesis of nanotube and their potential application in solar cells, gas storage components of Ar,[17] N_2,[18] and H_2,[19,20] electronic circuits,[21] thin films,[22] STM probes,[23] field emission sources,[24,25] high-power electrochemical capacitors,[26,27] electronic nanoswitches,[28] chemical sensors.[29,30]

The drawbacks of CNTs preparation is insufficient production and uncompetitive cost of CNTs with respect to the common technology. In these years in spite of CNTs developments, researchers are still incapable to produce well-defined CNTs in large quantities with a low-cost technique.

II.2. Carbon fibers (CFs):

Closely related to CNTs are carbon fibers (CFs), which are cylindrical nanostructures, composed by graphene layers arranged as stacked cones, cups or plates.

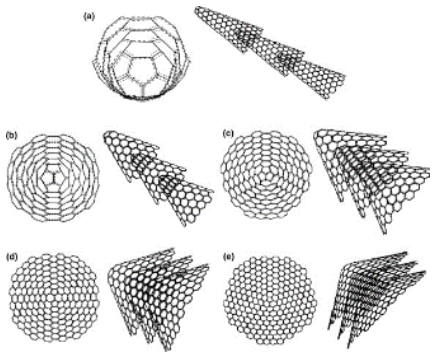

Figure 1.3: Different shapes of building blocks for carbon fibers.

Carbon fibers are very important for the industry due to their properties such as high strength to weight ratio, chemical resistance, and high electrical and thermal conductivity.[31,32] There are generally two methods to produce carbon nanofibers: vapor growth and electrospinning that was explored in 1970s and 1980s.[33,34] In the vapor growth method the primary feedstock is natural gas, while the catalytic iron particles are produced by the decomposition of Fe $(CO)_5$. When the catalyst particles are properly dispersed and activated with sulfur, carbon filaments are abundantly produced in a reactor maintained near 1100 ^oC.

Electrospinning method uses an electrical charge to draw very fine (typically on the micro or nano scale) fibres from a liquid. Also there are several methods of making carbon fibers but basically, it consists of first making fibers out of a carbon rich precursor material. The first steps are carbonizing and stretching precursor fibers, PAN (Polyacrylonitrile), Pitch or Rayon. PAN is the most common precursor for plastic composites.[35,36]

They have been specially used to automotive, aerospace and sport industries. Activated carbon fibers (ACFs) also because of high surface area are using in gas storage, water treatment,[37,38] reinforcement of composites, self-sensing devices,[39,40] electron emission sources, Scanning probe microscopy tips, electrode materials[41] and so on.

In this thesis we have used the carbon fibers that are very cheap and easy to handle.

II.3. Graphene:

Graphene is the two-dimensional (2D) arrangement of carbon atoms in a flat monolayer that tightly packed into a honeycomb lattice and is a basic building block for graphitic materials of all other dimensionalities.

Recently graphene has attracted considerable attention due to its unique structure and extraordinary properties[42,43] such as electronics,[44,45] material sciences,[46] and photo conversion systems,[47] high electron mobility of graphene at room temperature and transparent conducting electrodes.[48]

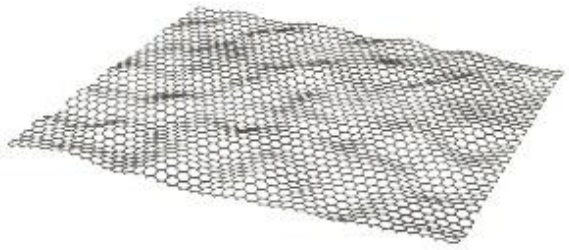

Figure 1.4: Graphene sheet.

Reduced graphene oxide (RGO) is also composed by graphene sheets that can be prepared by reduction of graphene oxide with thermal, chemical or electrochemical treatments. Various C/O ratios and chemical compositions are achieved by using different reducing agents. However, its quality never is comparable to pristine graphene from micromechanical exfoliation.

Chemists and surface scientists have been observed graphitic carbon monolayers on surfaces since the 1960s.[49] Then in 1986, Boehm et al.[50] have been mentioned such single layers of graphite as graphene. Finally in 2004, graphene was separated by using the simple "Scotch tape" method.[51,52]

Large-scale preparation of high purity graphene flakes is necessary for some applications. Today, graphene is prepared typically by one of the following methods:

Bottom-up approaches:

Chemical vapor deposition (CVD) techniques. CVD processes to produce graphene have also been reported, e.g. growth on Ni-surfaces utilizing CH4.[53]

Epitaxial growth on carbides: in this way silicon carbide (SiC) is heated to high temperatures (>1100°C) under low pressures (~10^{-6} torr). Silicon is evaporated and graphene layers are accumulated.[54]

Production of large graphene sheets is the main advantage of these methods. The bottlenecks of these methods are the difficulties to remove and transfer the graphene to other substrates and the limitation in the number of viable substrates because of high temperatures.

Top-down approaches:

Micromechanical cleavage or the Scotch tape technique: In this way graphene layers have pulled from graphite and transferred onto thin SiO_2 on a silicon wafer. The SiO_2 electrically isolated the graphene and weakly interacted with it, providing nearly charge-neutral graphene layers.[55]

Graphite oxidation: the graphene oxide sheets can be easily suspended in a polar solvent, which can be further reduced.[56,57]

Surfactant methods: By using surfactants, graphene can be dissolved and stabilized in suspension.[58,59]

Sonochemical Exfoliation: another approach to produce massive graphene is sonochemical exfoliation. Ultrasonic-treatment and centrifuge are used in this technique. Suspensions of graphene is produced in organic solvents like N-methyl-2-pyrrolidone (NMP).[60,61]

Each of these methods has different advantages and disadvantages. For example the advantage of the oxidation of graphite is that these graphene oxide sheets can be deposited on different substrates.[62] For the mechanical exfoliation low throughput and poor reproducibility is the problem. The drawback of sonochemical exfoliation is long sonication times, small flake sizes and defects on the graphene sheets, also difficulty to remove the solvent residues from graphene layers, which can have effect on the performance of the products.[63] These solvents are usually expensive, toxic and difficult to remove because of their high boiling points, so a large part of the researches today is allocated to the substitution of these solvents with the green, non-toxic and cheap solvents.

Tendency of graphene to aggregate is due to the strong π-π interactions between individual flakes. This aggregation makes difficult construction of graphene based materials.

For this reason, noncovalent[64,65] and covalent[66,67] functionalization of graphene have been developed. By adding functional groups to the graphene, both chemical and physical properties can be significantly changed and this functionalization can be used for biological

sensors,[68,69] drug delivery[70] and tuning electronic properties of graphene.[71] Also, it can increase the ability of graphene to form stable suspensions in different solvents.[72]

Porphyrin derivatives are one of the common functional dyes that have been used for modifying carbon materials to achieve different optoelectronic properties.[73]

Functionalization by covalent bonding, has some limitations in the choice of support materials and complicated synthetic procedures.[74,75] Noncovalent functionalization is achieved through supramolecular interactions such as π-π stacking, electrostatic interaction and hydrogen bonding.[76,77]

II.4. Graphene oxide (GO):

Graphene oxide (GO) is composed by single layers of graphene functionalized by hydroxyl, epoxide and carboxylic groups produced after reacting graphite with strong oxidants.[78]

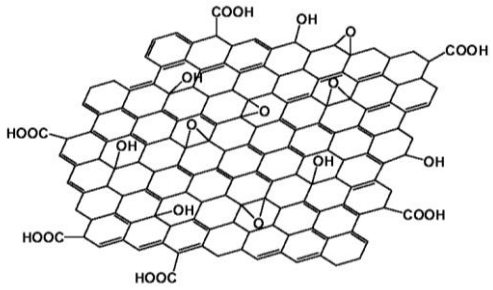

Figure 1.5: Graphene oxide sheet.

The most commonly used procedures for the oxidation of graphite are Hummers and Offeman methods,[79] which involve a mixture of sodium nitrate, potassium permanganate, and concentrated sulfuric acid. The oxygenated groups in GO strongly affect its electronic, mechanical and electrochemical properties.

The covalent oxygenated functional groups in GO can increase structure defects in comparison with pristine graphene, for example they can limit the electrical conductivity of GO.[80] On the other hand, these functional groups can have some advantages for using GO in other applications. For instance, GO is strongly hydrophilic due to the polar oxygen functional groups and it can increase dispersibility of GO in many solvents, especially in water.[81,82] This GO stable dispersion is important in order to prepare thin conductive films as

excellent electrode materials by common methods such as spraying, drop-casting or spin-coating.[83]

GO can be used in electrode surfaces, holding active species and for catalytic electron transfer processes (ET) at electrode surfaces.[84,85]

Functionalities, such as surface functional group,[86,87] holes,[88] oxygen,[89] carbon vacancies and defects, introduce chemically active sites for use in catalytic reactions and also act as anchoring sites for deposition of metal nanoparticles.

In addition, through covalent or supramolecular functionalization these functional groups are sites to immobilize various species.

Until now, the catalytic application of graphene, graphene oxide and reduced graphene oxide has focused on the use of these materials as supports for catalytically active transition metals. In one such example, Mulhaupt and co-workers demonstrated that palladium nanoparticles dispersed on graphite oxide were able to catalyze Suzuki–Miyaura coupling reactions.[90]

Graphenic hybrid materials are proved as highly effective catalysts in oxidation reactions. Graphenic substrate act as support for catalyst by providing sufficient contact between substrate/oxidant and catalyst and help to recovery of the catalyst. In addition, graphene retain catalyst like an active monomer form and preventing it from self-dimerization and avoiding bimolecular deactivation pathways.[91]

III. Reported applications for hybrid systems:

Nowadays, Carbon material- aromatic molecule (porphyrin, phthalocyanine …) hybrid materials have been prepared for a number of applications such as catalysis, solar cells and sensors. Organic nanostructures in terms of porphyrin building blocks have shown great potential in visible-light photocatalytic applications because of their optical, electrical, and catalytic properties. Some examples of these hybrid systems are described below:

Photocatalytic transformations have been studied for hybrids of porphyrin with graphene layers. Accordingly, Yingzhi Chen, et al.[92] have obtained p-THPP/rGO (p-THPP= *meso*-tetra(*p*-hydroxyphenyl)porphyrin) nanohybrid film exhibiting an increased visible-light photocatalytic activity compared to each moiety of the hybrid in degrading organic pollutants under visible light, and this photocatalyst can be easily separated and recycled for consecutive use with excellent stability. This facile fabrication of the p-THPP/rGO

nanohybrid film makes it available for high-performance optoelectronic applications, as well as for device integration.

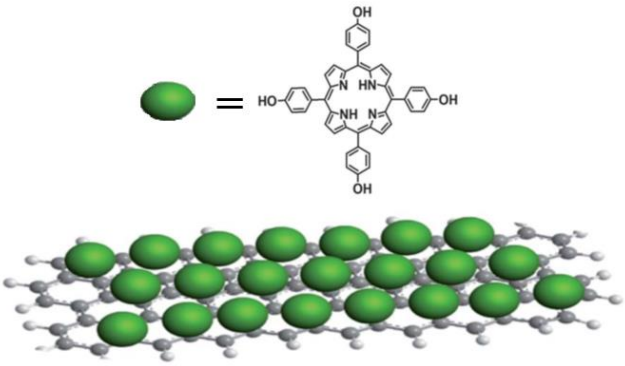

Figure 1.6: Schematic illustration of the structure of the p-THPP NP incorporated rGO film (from reference 90).

In addition, some works have been done to explore the use of complexes formed by transition-metal phthalocyanines covalently attached to the carbon nanotubes as oxygen reduction reaction (ORR) cathode catalysts in fuel cells.

Walter Orellana[93] reported the theoretical study on the covalent functionalization of metallic single-walled carbon nanotubes (CNTs) with transition metal phthalocyanines (MPc, with M = Mn, Fe and Co). The CNT–MPc catalytic activity was investigated for the oxygen reduction reaction (ORR) via the O_2 stretching frequency adsorbed on the phthalocyanine metal center. He found better reduction abilities when the CNT functionalization occurs through sp^2 bonds in comparison with sp^3. The CNT–MPc complexes show metallic characteristics, suggesting favorable conditions to work as ORR cathode catalysts in fuel cells.

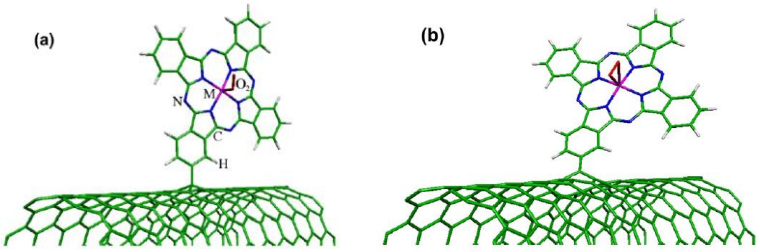

Figure 1.7: Stable geometries of the O2 molecule adsorbed on the phthalocyanine metal center of the CNT–MPc complex. (a) CNT–MPc in the sp^3 bonding structure and M–O2 adduct in the endon geometry. (b) CNT–MPc in the sp^2 bonding structure and M-O2 adduct in the side on geometry (from reference 91).

Very recently, Yuan et al.[94] have used graphene oxide to immobilize Schiff base palladium complex. The supported palladium compound is an efficient catalyst for Suzuki reaction of aryl halides with phenylboronic acid to substituted *trans*-cinnamic acid or *trans*-stilbene at atmospheric condition in aqueous media, and the catalyst could be steadily dispersed in the reaction mixture. The supported catalyst still remains high activity after five rounds.

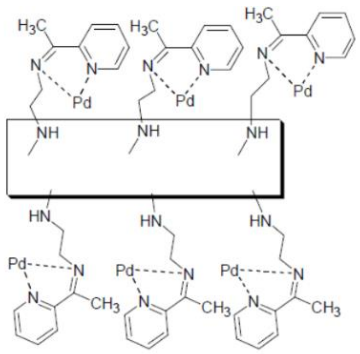

Figure 1.8: GO-Schiffbase-Pd hybrid material (from reference 92).

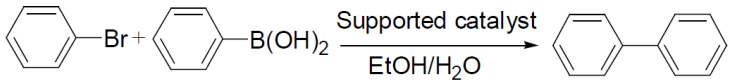

Figure 1.9: Suzuki reaction of aryl bromide with aryl boronic acid.

Magdesieva et al.[95] have used activated carbon fiber nanoporous as supports for Porphyrin and phthalocyanine transition metal complexes to be effective catalysts for CO_2 electroreduction in the form of gas diffusion electrodes, yielding carbon monoxide with current efficiencies up to ca. 70%.

Additionally, Jahan et al. synthesized graphene-iron porphyrin MOF composites with enhanced catalytic activity for the oxygen reduction reaction (ORR) in alkaline media.[77a] Tang et al. prepared the molecular architecture of cobalt porphyrin multilayers on reduced graphene oxide sheets using the layer-by-layer (LBL) assembly technique, which exhibited high ORR performance.[96]

In this thesis, we have tried to make several hybrid systems by using three different kind of carbon-based materials (graphene, graphene oxide and carbon fibers) and complexes to reach to several reactions especially the ones that are related to oxidation or reduction of water and oxidation of organic substrates. We have explored both supramolecular and

covalent interaction between the carbon materials and complexes, and we expected to see if we improve the yields of hydrogen by increasing the surface area in carbon fibers. We have tried to prepare graphene by using green and cheap solvents and prepare the transparent conductive film using this graphene, which could be used in electrocatalytic systems.

IV. Hybrid multicomponent homogenous system:

A main goal in modern research is to discover new and improved reactions and develop cleaner, cheaper, faster synthetic procedures. The strategy of using reactions in tandem is also aimed at increasing efficiency of synthesis. Tandem reactions can be understood as "multistep one-pot reactions".[97] Dr. Ho has defined the tandem reaction as "combinations of two or more reactions whose occurrence is in a specific order, and if they involve sequential addition of reagents the secondary reagents must be integrated into the products."[98]

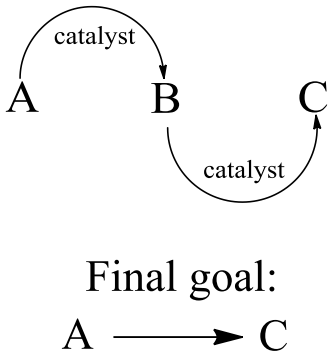

Figure 1.10: Scheme of a sample of tandem reaction with two reactions.

Some advantages of tandem reactions are; 1) making complex structures in as few steps as possible; 2) Eliminate purification steps; 3) Make it easy to work with sensitive or unstable intermediates; 4) Decrease the cost and amounts of reagents, solvents, and reduce the amount of waste.

To reach to a final reaction usually in the nature several systems are coupled. Multienzymatic systems that carry out multistep reactions in nature is a model for the extension of artificial systems that can act like these biological systems.[99,100] Photosynthesis is also an example of tandem reactions or cooperative systems that consists of at least 24 reactions involving 34 metabolites, which is a huge cooperative system.[101]

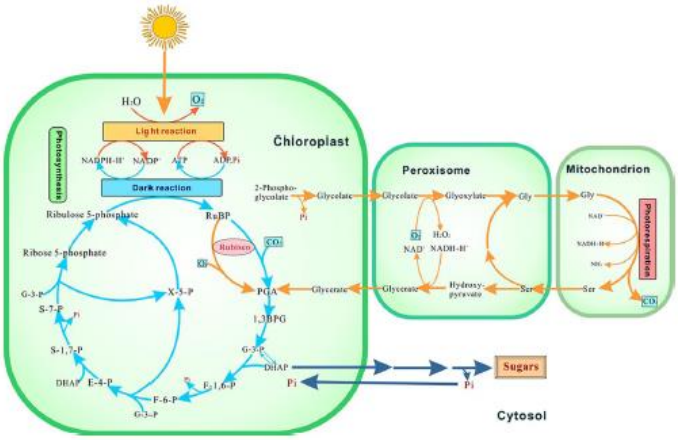

Figure 1.11: Photosynthesis as a huge cooperative system.

Inspired by nature, we wanted to make a hybrid system with two consecutive catalytic reactions. First, Production of H_2O_2 from O_2 and H_2 in the presence of Au/Pd nanoparticles and then oxidation of olefins by using this H_2O_2 in the presence of Iron complexes.

As starting point we used O_2 and H_2 mixtures which could come from efficient water splitting. Whit this idea we wanted to improve the atom economy of the overall process and using O_2 as a cheap and green oxidant for multistep oxidation of organic substrates.

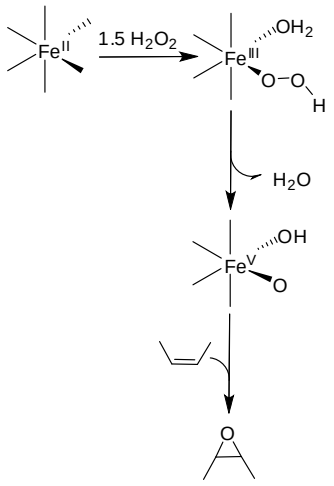

Figure 1.12: Mechanism of the Iron catalyst in presence of the H_2O_2.

As previously reported both H_2O_2 formation and Iron-mediated oxidation of organic substrates using H_2O_2 are efficient processes when they work separately. So, the new idea herein is to make both work together. Specifically, the mechanism described for Iron-catalyzed epoxidation is presented in figure 1.12, which in our experiments we expected to

promote by in situ generation of H_2O_2. However as often accurse in coupled reactions, we observed that the reagent of the first process interferes with the second reaction. Thus, we decided to study in deep the ability of high valent Iron species generated by reaction with H_2O_2 to activate H_2. Such findings although could be understood as failure regarding the initial goals, resulted on an unprecedented understanding of the reactive species of reaction catalyzed by non-heme iron compounds.

Objectives:

1) Study of a multistep cooperative process, consisting on of consecutive formation of H_2O_2 from O_2 and H_2 and H_2O_2 activation in catalytic epoxidation reaction, all in a one-pot system. It would represent a new way to use H_2O_2 in a clean process, avoiding the use of organic species. H_2 role as competitive substrate in epoxidation reactions will be analyzed and possible H-H activation pathway will be considered.

2) Generation of GO-porphyrin hybrid systems relevant to possible design of recyclable catalytic systems with an increased efficiency.

3) Comparison of the effectiveness of the LPE processes in different solvent/water mixtures to obtain graphene suspensions. Isolation of redispersible material to obtain graphene suspensions in water-free solvents. Such work are intended to solve the problem of dispersibility of graphene and its use to prepare transparent conductive coatings, which can be used as solid support in electrocatalytic systems.

4) Design of a carbon fiber based electrode which can be chemically modified to be active in electrocatalytic formation of H_2.

References:

(1) *Oxford Dictionary*.
(2) Y. Hagiwara and H. Suzuki, Ohmsha, Tokyo, Japan, 2000; p 135.
(3) Sanchez, C.; Julian, B.; Belleville, P.; Popall, M. *J. Mater. Chem.* **2005**, *15*, 3559.
(4) (a) Choy, J.-H. *J. Phys. Chem. Solids* **2004**, *65*, 373(b) Ruiz-Hitzky, E.; Aranda, P.; Darder, M.; Rytwo, G. *J. Mater. Chem.* **2010**, *20*, 9306.
(5) Park, D.-H.; Hwang, S.-J.; Oh, J.-M.; Yang, J.-H.; Choy, J.-H. *Prog. Polym. Sci.* **2013**, *38*, 1442.
(6) Zhu, Y.; Murali, S.; Cai, W.; Li, X.; Suk, J. W.; Potts, J. R.; Ruoff, R. S. *Adv. Mater. (Weinheim, Ger.)* **2010**, *22*, 3906.
(7) (a) Zhang, J.-L.; Huang, J.-S.; Che, C.-M. *Chemistry – A European Journal* **2006**, *12*, 3020(b) Liu, C.-J.; Li, S.-G.; Pang, W.-Q.; Che, C.-M. *Chemical Communications* **1997**, 65.
(8) Yu, X.-Q.; Huang, J.-S.; Yu, W.-Y.; Che, C.-M. *J. Am. Chem. Soc.* **2000**, *122*, 5337.
(9) Zhang, J.-L.; Zhou, H.-B.; Huang, J.-S.; Che, C.-M. *Chemistry – A European Journal* **2002**, *8*, 1554.
(10) Sono, M.; Roach, M. P.; Coulter, E. D.; Dawson, J. H. *Chem. Rev. (Washington, D. C.)* **1996**, *96*, 2841.
(11) Zhu, Y.; Murali, S.; Stoller, M. D.; Ganesh, K. J.; Cai, W.; Ferreira, P. J.; Pirkle, A.; Wallace, R. M.; Cychosz, K. A.; Thommes, M.; Su, D.; Stach, E. A.; Ruoff, R. S. *Science (Washington, DC, U. S.)* **2011**, *332*, 1537.
(12) Li, Y.; Zhou, W.; Wang, H.; Xie, L.; Liang, Y.; Wei, F.; Idrobo, J.-C.; Pennycook, S. J.; Dai, H. *Nat. Nanotechnol.* **2012**, *7*, 394.
(13) Coville, N. J.; Mhlanga, S. D.; Nxumalo, E. N.; Shaikjee, A. *S. Afr. J. Sci.* **2011**, *107*, 44.
(14) (a) Zhang, M.; Li, J. *Mater. Today (Oxford, U. K.)* **2009**, *12*, 12(b) Qi, X.; Qin, C.; Zhong, W.; Au, C.; Ye, X.; Du, Y. *Materials* **2010**, *3*, 4142.
(15) Kathyayini, H.; Nagaraju, N.; Fonseca, A.; Nagy, J. B. *J. Mol. Catal. A: Chem.* **2004**, *223*, 129.
(16) Saifuddin, N.; Raziah, A. Z.; Junizah, A. R. *J. Chem.* **2013**, 676815.
(17) Gadd, G. E.; Blackford, M.; Moricca, S.; Webb, N.; Evans, P. J.; Smith, A. M.; Jacobsen, G.; Leung, S.; Day, A.; Hua, Q. *Science (Washington, D. C.)* **1997**, *277*, 933.
(18) Terrones, M.; Kamalakaran, R.; Seeger, T.; Ruhle, M. *Chem. Commun. (Cambridge)* **2000**, 2335.
(19) Dillon, A. C.; Jones, K. M.; Bekkedahl, T. A.; Kiang, C. H.; Bethune, D. S.; Heben, M. J. *Nature (London)* **1997**, *386*, 377.
(20) Liu, C.; Fan, Y. Y.; Liu, M.; Cong, H. T.; Cheng, H. M.; Dresselhaus, M. S. *Science (Washington, D. C.)* **1999**, *286*, 1127.
(21) Yao, Z.; Kane, C. L.; Dekker, C. *Phys. Rev. Lett.* **2000**, *84*, 2941.
(22) Huang, L.; Cui, X.; White, B.; O'Brien, S. P. *J. Phys. Chem. B* **2004**, *108*, 16451.
(23) Dai, H.; Hafner, J. H.; Rinzler, A. G.; Colbert, D. T.; Smalley, R. E. *Nature (London)* **1996**, *384*, 147.
(24) (a) de Heer, W. A.; Bacsa, W. S.; Chatelain, A.; Gerfin, T.; Humphrey-Baker, R.; Forro, L.; Ugarte, D. *Science (Washington, D. C.)* **1995**, *268*, 845(b) Rinzler, A. G.; Hafner, J. H.; Nikolaev, P.; Lou, L.; Kim, S. G.; Tomanek, D.; Nordlander, P.; Colbert, D. T.; Smalley, R. E. *Science (Washington, D. C.)* **1995**, *269*, 1550.
(25) Saito, Y.; Hamaguchi, K.; Hata, K.; Uchida, K.; Tasaka, Y.; Ikazaki, F.; Yumura, M.; Kasuya, A.; Nishina, Y. *Nature (London)* **1997**, *389*, 554.
(26) Britto, P. J.; Santhanam, K. S. V.; Ajayan, P. M. *Bioelectrochem. Bioenerg.* **1996**, *41*, 121.
(27) Niu, C.; Sichel, E. K.; Hoch, R.; Moy, D.; Tennent, H. *Appl. Phys. Lett.* **1997**, *70*, 1480.
(28) Yao, Z.; Postma, H. W. C.; Balents, L.; Dekker, C. *Nature (London)* **1999**, *402*, 273.
(29) Kong, J.; Franklin, N. R.; Zhou, C.; Chapline, M. G.; Peng, S.; Cho, K.; Dailt, H. *Science (Washington, D. C.)* **2000**, *287*, 622.

References:

(30) Collins, P. G.; Bradley, K.; Ishigami, M.; Zettl, A. *Science (Washington, D. C.)* **2000**, *287*, 1801.
(31) Rebouillat S, P. J., Donnet J-B, Ryu S-K 3rd edn. Marcel Dekker, , New York, 1998; p 463.
(32) P, M. CRC Press(Taylor & Francis Group), Boca Raton2005.
(33) Rodriguez, N. M. *J. Mater. Res.* **1993**, *8*, 3233.
(34) Tibbetts, G. G.; Lake, M. L.; Strong, K. L.; Rice, B. P. *Compos. Sci. Technol.* **2007**, *67*, 1709.
(35) Zhang, W.; Liu, J.; Wu, G. *Carbon* **2003**, *41*, 2805.
(36) Sauder, C.; Lamon, J.; Pailler, R. *Carbon* **2004**, *42*, 715.
(37) Yusof, N.; Ismail, A. F. *Journal of Analytical and Applied Pyrolysis* **2012**, *93*, 1.
(38) Wu, J.; Chung, D. D. L. *Carbon* **2002**, *40*, 445.
(39) (a) Zhang, W.; Liu, J.; Wu, G. *Carbon* **2003**, *41*, 2805(b) Vilaplana, J. L.; Baeza, F. J.; Galao, O.; Zornoza, E.; Garces, P. *Materials* **2013**, *6*, 4776(c) Baeza, F. J. G., O.; Zornoza, E.; Garcés, P. *Materials* **2013**, *6*, 841.
(40) (a) Endo, M.; Kim, Y. A.; Hayashi, T.; Nishimura, K.; Matusita, T.; Miyashita, K.; Dresselhaus, M. S. *Carbon* **2001**, *39*, 1287(b) Du, J.-H.; Sun, C.; Bai, S.; Su, G.; Ying, Z.; Cheng, H.-M. *J. Mater. Res.* **2002**, *17*, 1232(c) Wu, F. Y. D., J.H.; Liu, C.G.; Li, L.X.; Cheng, H.M. *New Carbon Mater.* **2004**, *19*, 81.
(41) Rassaei, L.; Sillanpaa, M.; Bonne, M. J.; Marken, F. *Electroanalysis* **2007**, *19*, 1461.
(42) Du, X.; Skachko, I.; Barker, A.; Andrei, E. Y. *Nat. Nanotechnol.* **2008**, *3*, 491.
(43) Novoselov, K. S.; Jiang, Z.; Zhang, Y.; Morozov, S. V.; Stormer, H. L.; Zeitler, U.; Maan, J. C.; Boebinger, G. S.; Kim, P.; Geim, A. K. *Science (Washington, DC, U. S.)* **2007**, *315*, 1379.
(44) Song, E. B.; Lian, B.; Min Kim, S.; Lee, S.; Chung, T.-K.; Wang, M.; Zeng, C.; Xu, G.; Wong, K.; Zhou, Y.; Rasool, H. I.; Seo, D. H.; Chung, H.-J.; Heo, J.; Seo, S.; Wang, K. L. *Appl. Phys. Lett.* **2011**, *99*, 042109/1.
(45) Lin, Y. M.; Dimitrakopoulos, C.; Jenkins, K. A.; Farmer, D. B.; Chiu, H. Y.; Grill, A.; Avouris, P. *Science (Washington, DC, U. S.)* **2010**, *327*, 662.
(46) Lee, C.; Wei, X.; Kysar, J. W.; Hone, J. *Science (Washington, DC, U. S.)* **2008**, *321*, 385.
(47) Yu, H.; Chen, S.; Fan, X.; Quan, X.; Zhao, H.; Li, X.; Zhang, Y. *Angew. Chem., Int. Ed.* **2010**, *49*, 5106.
(48) Kim, K. S.; Zhao, Y.; Jang, H.; Lee, S. Y.; Kim, J. M.; Kim, K. S.; Ahn, J.-H.; Kim, P.; Choi, J.-Y.; Hong, B. H. *Nature (London, U. K.)* **2009**, *457*, 706.
(49) May, J. W. *Surface Sci.* **1969**, *17*, 267.
(50) Boehm, H. P.; Setton, R.; Stumpp, E. *Carbon* **1986**, *24*, 241.
(51) Novoselov, K. S.; Geim, A. K.; Morozov, S. V.; Jiang, D.; Zhang, Y.; Dubonos, S. V.; Grigorieva, I. V.; Firsov, A. A. *Science (Washington, DC, U. S.)* **2004**, *306*, 666.
(52) Novoselov, K. S.; Jiang, D.; Schedin, F.; Booth, T. J.; Khotkevich, V. V.; Morozov, S. V.; Geim, A. K. *Proc. Natl. Acad. Sci. U. S. A.* **2005**, *102*, 10451.
(53) Yu, Q.; Lian, J.; Siriponglert, S.; Li, H.; Chen, Y. P.; Pei, S.-S. *Appl. Phys. Lett.* **2008**, *93*, 113103/1.
(54) Hass, J.; de Heer, W. A.; Conrad, E. H. *J. Phys.: Condens. Matter* **2008**, *20*, 323202/1.
(55) "The Story of Graphene", October 2014.
(56) Stankovich, S.; Dikin, D. A.; Piner, R. D.; Kohlhaas, K. A.; Kleinhammes, A.; Jia, Y.; Wu, Y.; Nguyen, S. T.; Ruoff, R. S. *Carbon* **2007**, *45*, 1558.
(57) Boukhvalov, D. W.; Katsnelson, M. I. *J. Am. Chem. Soc.* **2008**, *130*, 10697.
(58) (a) Lotya, M.; Hernandez, Y.; King, P. J.; Smith, R. J.; Nicolosi, V.; Karlsson, L. S.; Blighe, F. M.; De, S.; Wang, Z.; McGovern, I. T.; Duesberg, G. S.; Coleman, J. N. *J. Am. Chem. Soc.* **2009**, *131*, 3611(b) Vadukumpully, S.; Paul, J.; Valiyaveettil, S. *Carbon* **2009**, *47*, 3288.
(59) Lee, J. H.; Shin, D. W.; Makotchenko, V. G.; Nazarov, A. S.; Fedorov, V. E.; Kim, Y. H.; Choi, J.-Y.; Kim, J. M.; Yoo, J.-B. *Adv. Mater. (Weinheim, Ger.)* **2009**, *21*, 4383.
(60) Hamilton, C. E.; Lomeda, J. R.; Sun, Z.; Tour, J. M.; Barron, A. R. *Nano Lett.* **2009**, *9*, 3460.

(61) Hernandez, Y.; Nicolosi, V.; Lotya, M.; Blighe, F. M.; Sun, Z.; De, S.; McGovern, I. T.; Holland, B.; Byrne, M.; Gun'Ko, Y. K.; Boland, J. J.; Niraj, P.; Duesberg, G.; Krishnamurthy, S.; Goodhue, R.; Hutchison, J.; Scardaci, V.; Ferrari, A. C.; Coleman, J. N. *Nat. Nanotechnol.* **2008**, *3*, 563.
(62) Stankovich, S.; Dikin, D. A.; Dommett, G. H. B.; Kohlhaas, K. M.; Zimney, E. J.; Stach, E. A.; Piner, R. D.; Nguyen, S. T.; Ruoff, R. S. *Nature (London, U. K.)* **2006**, *442*, 282.
(63) Pan, W.; Liu, Y.; Du, L. *J. Mater. Sci. Lett.* **1998**, *17*, 1393.
(64) Stankovich, S.; Piner, R. D.; Chen, X.; Wu, N.; Nguyen, S. T.; Ruoff, R. S. *J. Mater. Chem.* **2006**, *16*, 155.
(65) Xu, Y.; Bai, H.; Lu, G.; Li, C.; Shi, G. *J. Am. Chem. Soc.* **2008**, *130*, 5856.
(66) Niyogi, S.; Bekyarova, E.; Itkis, M. E.; McWilliams, J. L.; Hamon, M. A.; Haddon, R. C. *J. Am. Chem. Soc.* **2006**, *128*, 7720.
(67) Stankovich, S.; Piner, R. D.; Nguyen, S. T.; Ruoff, R. S. *Carbon* **2006**, *44*, 3342.
(68) Mohanty, N.; Berry, V. *Nano Lett.* **2008**, *8*, 4469.
(69) Shan, C.; Yang, H.; Song, J.; Han, D.; Ivaska, A.; Niu, L. *Anal. Chem. (Washington, DC, U. S.)* **2009**, *81*, 2378.
(70) Liu, Z.; Robinson, J. T.; Sun, X.; Dai, H. *J. Am. Chem. Soc.* **2008**, *130*, 10876.
(71) Chen, W.; Chen, S.; Qi, D. C.; Gao, X. Y.; Wee, A. T. S. *J. Am. Chem. Soc.* **2007**, *129*, 10418.
(72) Andersson, C.-H.; Grennberg, H. *Eur. J. Org. Chem.* **2009**, 4421.
(73) Guldi, D. M.; Rahman, G. M. A.; Sgobba, V.; Ehli, C. *Chem. Soc. Rev.* **2006**, *35*, 471.
(74) (a) Che, C.-M.; Lo, V. K.-Y.; Zhou, C.-Y.; Huang, J.-S. *Chem. Soc. Rev.* **2011**, *40*, 1950(b) Nakagaki, S.; Wypych, F. *J. Colloid Interface Sci.* **2007**, *315*, 142.
(75) Fraile, J. M.; Garcia, J. I.; Mayoral, J. A. *Chem. Rev. (Washington, DC, U. S.)* **2009**, *109*, 360.
(76) (a) Xue, T.; Jiang, S.; Qu, Y.; Su, Q.; Cheng, R.; Dubin, S.; Chiu, C.-Y.; Kaner, R.; Huang, Y.; Duan, X. *Angew. Chem., Int. Ed.* **2012**, *51*, 3822(b) Guo, Y.; Deng, L.; Li, J.; Guo, S.; Wang, E.; Dong, S. *ACS Nano* **2011**, *5*, 1282(c) Song, Y.; Chen, Y.; Feng, L.; Ren, J.; Qu, X. *Chem. Commun. (Cambridge, U. K.)* **2011**, *47*, 4436.
(77) (a) Jahan, M.; Bao, Q.; Loh, K. P. *J. Am. Chem. Soc.* **2012**, *134*, 6707(b) Xu, Y.; Zhao, L.; Bai, H.; Hong, W.; Li, C.; Shi, G. *J. Am. Chem. Soc.* **2009**, *131*, 13490(c) Geng, J.; Jung, H.-T. *J. Phys. Chem. C* **2010**, *114*, 8227.
(78) Cai, W.; Piner, R. D.; Stadermann, F. J.; Park, S.; Shaibat, M. A.; Ishii, Y.; Yang, D.; Velamakanni, A.; An, S. J.; Stoller, M.; An, J.; Chen, D.; Ruoff, R. S. *Science (Washington, DC, U. S.)* **2008**, *321*, 1815.
(79) Hummers, W. S., Jr.; Offeman, R. E. *J. Am. Chem. Soc.* **1958**, *80*, 1339.
(80) Mkhoyan, K. A.; Contryman, A. W.; Silcox, J.; Stewart, D. A.; Eda, G.; Mattevi, C.; Miller, S.; Chhowalla, M. *Nano Lett.* **2009**, *9*, 1058.
(81) (a) Park, S.; Ruoff, R. S. *Nat. Nanotechnol.* **2009**, *4*, 217(b) Bissessur, R.; Scully, S. F. *Solid State Ionics* **2007**, *178*, 877.
(82) (a) Paredes, J. I.; Villar-Rodil, S.; Martinez-Alonso, A.; Tascon, J. M. D. *Langmuir* **2008**, *24*, 10560(b) Compton, O. C.; Nguyen, S. T. *Small* **2010**, *6*, 711.
(83) Kim, F.; Cote, L. J.; Huang, J. *Adv. Mater. (Weinheim, Ger.)* **2010**, *22*, 1954.
(84) (a) Liu, H.; Gao, J.; Xue, M.; Zhu, N.; Zhang, M.; Cao, T. *Langmuir* **2009**, *25*, 12006(b) Wang, Z.; Zhou, X.; Zhang, J.; Boey, F.; Zhang, H. *J. Phys. Chem. C* **2009**, *113*, 14071.
(85) Zuo, X.; He, S.; Li, D.; Peng, C.; Huang, Q.; Song, S.; Fan, C. *Langmuir* **2010**, *26*, 1936.
(86) Gao, Y.; Ma, D.; Wang, C.; Guan, J.; Bao, X. *Chem. Commun. (Cambridge, U. K.)* **2011**, *47*, 2432.
(87) Zhu, Z.; Su, D.; Weinberg, G.; Schloegl, R. *Nano Lett.* **2004**, *4*, 2255.
(88) Erickson, K.; Erni, R.; Lee, Z.; Alem, N.; Gannett, W.; Zettl, A. *Adv. Mater. (Weinheim, Ger.)* **2010**, *22*, 4467.

References:

(89) Imran Jafri, R.; Rajalakshmi, N.; Ramaprabhu, S. *J. Mater. Chem.* **2010**, *20*, 7114.

(90) Scheuermann, G. M.; Rumi, L.; Steurer, P.; Bannwarth, W.; Mulhaupt, R. *J. Am. Chem. Soc.* **2009**, *131*, 8262.

(91) Li, Y.; Huang, X.; Li, Y.; Xu, Y.; Wang, Y.; Zhu, E.; Duan, X.; Huang, Y. *Sci. Rep.* **2013**, *3*, 1787.

(92) Chen, Y.; Huang, Z.-H.; Yue, M.; Kang, F. *Nanoscale* **2014**, *6*, 978.

(93) Orellana, W. *Chem. Phys. Lett.* **2012**, *541*, 81.

(94) Yuan, D., Chen, Bibob *Chin. J. Org. Chem.* **2014**, *34*, 1630.

(95) Magdesieva, T. V.; Yamamoto, T.; Tryk, D. A.; Fujishima, A. *J. Electrochem. Soc.* **2002**, *149*, D89.

(96) Tang, H.; Yin, H.; Wang, J.; Yang, N.; Wang, D.; Tang, Z. *Angew. Chem., Int. Ed.* **2013**, *52*, 5585.

(97) Ho, T. In *Tandem Organic Reactions* New York, 1992.

(98) Tietze, L. F. B., U. *Angew. Chem., Int. Ed. Engl.* **1993**, *32*, 131.

(99) (a) Khosla, C. *Chem. Rev. (Washington, D. C.)* **1997**, *97*, 2577(b) Leadlay, P. F. *Curr. Opin. Chem. Biol.* **1997**, *1*, 162.

(100) (a) Staunton, J.; Wilkinson, B. *Chem. Rev. (Washington, D. C.)* **1997**, *97*, 2611(b) Townsend, C. A. *Chem. Biol.* **1997**, *4*, 721.

(101) Luo, R.; Wei, H.; Ye, L.; Wang, K.; Chen, F.; Luo, L.; Liu, L.; Li, Y.; Crabbe, M. J. C.; Jin, L.; Li, Y.; Zhong, Y. *Proc. Natl. Acad. Sci. U. S. A.* **2009**, *106*, 847.

Chapter **2**

H_2 activation by non-heme Iron species in high oxidation state

I. Introduction

Alkenes as well as hydrocarbons of other classes are widely used as raw materials in organic synthesis. Indeed, stereoselective epoxidation and cis-dihydroxylation of alkenes are valuable strategies for the formation of new C-X bonds, particularly attractive due to the creation of two asymmetric carbons next to each other.

Epoxides are important possible initial materials and intermediates for the chemical industry. For example, epoxides can be polymerized for the production of copolymers as polyethers, polyols and polycarbonates. Also they are used in the production of pharmaceuticals, perfumery, plasticizers, epoxy resins, pesticides, etc.[1,2]

Epoxides are commercially produced from olefins through a chlorohydrin process. However, the chlorohydrin process consumes large amounts of chlorine, causing serious environmental issues.

An alternative oxidant to be considered for epoxidation process is oxygen. Oxygen is a cheap, abundant and environmentally friendly oxidant. However, use of O_2 as oxidant needs metal catalysts[3] based on osmium[4] or ruthenium.[5] Alternatively it needs to be used along with sacrificial agents like aldehydes.[6,7] In addition, the reaction conditions required (such as, high temperature and high pressure) limit its practical application.

As an activated form of O_2, hydrogen peroxide has been extensively investigated as a clean (which produces water as a byproduct), cheap and safe oxidant for the epoxidation of olefins.[2,8]

Although H_2O_2 is a very suitable oxidant for this application because of its low price and environmental benignity, its high polarity demands for the use of a suitable solvent to overcome solubility problems of the generally apolar olefins.[9,10] In addition, the industrial production of H_2O_2 implies oxidation of hydroxyanthracene, which can produce accumulation of anthraquinone as subproduct.

Various examples of not only olefin epoxidation but also, alkane hydroxylations with hydrogen peroxide have been achieved by using non-heme iron catalyst with polydentate N-donor ligands (scheme 2.1).[11]

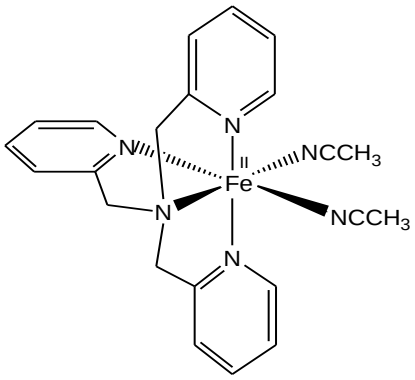

[Fe (TPA)(CH_3CN)$_2$]$^{2+}$

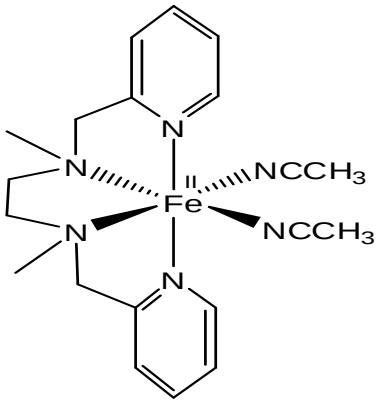

[Fe (BPMEN)(CH_3CN)$_2$]$^{2+}$

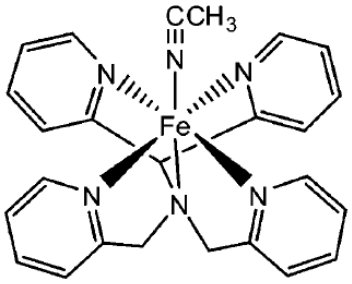

[(N_4Py)Fe^{II}(CH_3CN)]$^{2+}$

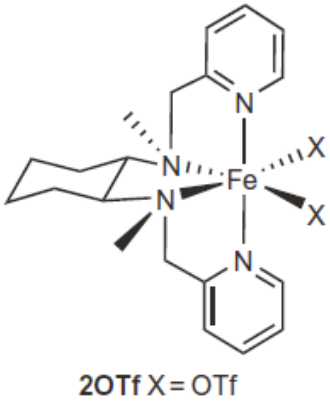

[(α-BPMCN)Fe($NCCH_3$)$_2$](OTf)$_2$

Scheme 2.1. Different non-heme iron catalyst with polydentate N-donor ligands.

Recent experimental observations on the mechanisms of non-heme metal catalyzed oxidations with H_2O_2 have attracted significant interest in the chemical and biochemical communities,[12,13] with an special focus on the more extensively and thoroughly investigated iron catalyzed epoxidations.

Considering the present generally interest of hydrogen production by routes related to artificial photosynthesis, we tried in this chapter to attempt a new twist on the H_2O_2-based catalytic procedures.

The idea of water splitting was taken from photosynthesis in green plants, where sunlight energy is employed to generate O_2 from water molecules and use the subsequent reducing power to reduce CO_2 and form carbohydrates.

Water splitting into H_2 and O_2 is a multielectron process coupled with a multiple-proton transference.

$$2H_2O \xrightarrow{h\nu} 2H_2 + O_2 \qquad \Delta G^0 = 4.92\ eV\ (113\ kcal\ mol^{-1}) \qquad (1)$$

$$4H^+ + 4e^- \longrightarrow 2H_2 \qquad (2)$$

$$2H_2O \longrightarrow O_2 + 4H^+ + 4e^- \qquad (3)$$

Assuming a success on water splitting processes, which every day is closer to become a reality, in this chapter we proposed to use the mixture of H_2 and O_2 as primary precursors for epoxidation processes. The cooperative processes that we would try herein are presented in scheme 2.2.

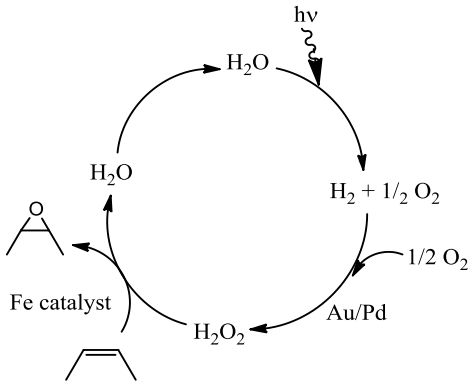

Scheme 2.2. Process of olefins oxidation in a cooperative system.

The first part of this multistep cooperative process is water splitting to produce H_2 and O_2. The hypothesis of this chapter takes as a starting point the successful splitting of water and we take such system a step forward. We studied the possibility of consecutive formation of H_2O_2 from O_2 and H_2 together with the use of H_2O_2 in catalytic epoxidations, all in a one-pot system.

This process would imply the use of only O_2 molecule as final oxidant and light as source of energy. It would represent a new way to use H_2O_2 in a clean process, avoiding the use of organic species.

H_2O_2 formation from direct reaction of O_2 and H_2 catalyzed by Au/Pd nanoparticles was reported several years ago.[14,15] In our laboratory, we have been able to produce significant amounts of H_2O_2 by this method. Thus, we tried to couple such H_2O_2 production with well-known epoxidation and hydroxylation processes catalyzed by non-heme iron

compounds. In all cases no oxidation of organic products were detected, although H_2O_2 was produced. This observation lead us to study possible H_2 activation pathways promoted by the products resulting from Iron complexes and H_2O_2.

Therefore, this investigation presents a new perspective for H_2 activation resulting in normative mechanistic insights.

II-Experimental procedures

At the beginning, according to literature[14,15] we have done the reaction of formation H_2O_2 from direct reaction of O_2 and H_2 catalyzed by Au/Pd nanoparticles. Pressure reactor was charged by acetonitrile: water (9:1) as solvent and 10 mg Au/Pd nanoparticles. A flow of H_2 and O_2 (80 and 20 respectively) was injected through the system. The reaction was stirred under 40 atm pressure at room temperature (25°C) for 1 hour. After the filtration, we have measured a 3.1 mM concentration of the produced H_2O_2 by titration with $KMnO_4$ (details in Materials and Methods).

Afterwards, we wanted to know if we have the oxidation of substrate in presence of catalyst and H_2O_2 directly. Therefore, using the same solvent mixture, we added 1000 eqiv. cyclooctene as substrate and Iron complex (1mM) as catalyst and we have added 10 eqiv. H_2O_2 slowly by syringe pump as shown in figure 2.1. We found around 90% epoxidation of the olefins in the reaction media.

Figure 2.1: Adding H_2O_2 slowly to the substrate by syringe pump.

Thus, we expected to see the same amount of epoxide in the one-pot reaction, where the H_2O_2 (around 3 mM) was generated in situ. However, for the one-pot experiment no epoxidation was observed. Since we knew that, under the reaction conditions, H_2O_2 was generated the most plausible scenario considered was that H_2 behaved as competitive substrate *vs* olefin.

To investigate the role of hydrogen as a competitive substrate, we made a series of catalysis experiments. We used three different organic substrates with marked different tendencies to be oxidized by H_2O_2 in the presence of $[(\alpha\text{-BPMCN})Fe(NCCH_3)_2](OTf)_2$ (BPMCN =N,N'-bis(2-pyridylmethyl)-1,2-diaminocyclohexane) and we compared the effect of hydrogen with and without added acetic acid.

Previously it was observed that as a result of addition of acetic acid to olefin oxidation in the presence of non-heme iron-catalyzed $[(BPMEN)Fe(NCCH_3)_2]^{2+}$ were increased both catalytic activity and selectivity toward epoxidation (scheme 2.3).[16,17] CH_3COOH promotes epoxidation by the following mechanism:[18]

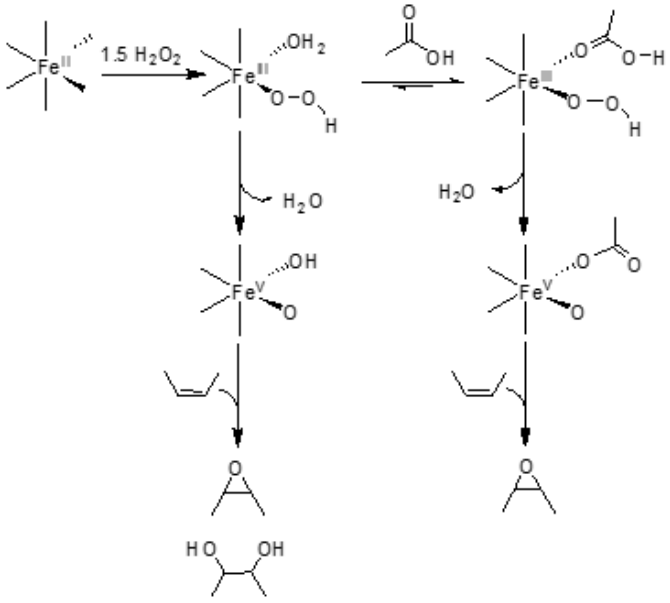

Scheme 2.3: Effect of addition of acetic acid to olefin oxidation.

The iron complexes $[(BPMEN)Fe(OTf)_2]$ [BPMEN) N,N´-bis-(2-pyridylmethyl)-N,N´-dimethyl-1,2-ethylenediamine] catalyze the oxidation of olefins by H_2O_2 to yield

epoxides and cis-diols. The addition of acetic acid inhibits olefin cis-dihydroxylation and enhances epoxidation.

Therefore, according to these observations we have tried to do epoxidation of substrates by Iron catalyst in the absence and presence of acetic acid.

II.1. Running reaction under Ar and H_2 atmosphere

Cyclooctene, thioanisole and cyclohexane were chosen as the substrates for the epoxidation process using H_2O_2 as oxidant. A flask was charged with dry acetonitrile as a solvent, Fe complex (1 mM) and substrate (1 M). Then the system was saturated with Ar or H_2 by successive freeze-drying cycles (3 times) and a solution of 10 equiv H_2O_2 (10 mM) was injected over a period of 30 min (286 μl) by using a syringe pump and stirring for 10 min more. At the end of the reaction, Naphthalene (1mM) as an internal standard was added to the solution and stirred.

For cyclooctene and methyl phenyl sulfoxide our sample after the reaction was ready for doing gas chromatography, just by passing the solution through silica, but for cyclohexane we had to do some treatment for acetylation of produced alcohol. After finishing the reaction, 1 ml of naphthalene (1mM), 1 ml acetic anhydride, 0.1 ml 1-methyl Imidazole were added and stirred for 15 min then around 1g ice was added and stirred. After 15 min, 1 ml H_2SO_4 (1M) and 2 ml CH_2Cl_2 were added. The organic phase was extracted and 2 ml of saturated Na_2CO_3 was added. Organic phase was extracted again and Na_2SO_4 anhydrous was added. Then CH_2Cl_2 solution was filtered with glass wool.

III. Analysis of products obtained at 1 atm. of Ar or H_2

To see the oxidation of the substrates in different condition the solution was subjected to GC analysis. The products were identified by comparison of their GC retention times.

The experiments in hydrogen atmosphere were carried out by saturating the media with hydrogen just by purging the system with H_2 and thereafter bubbling hydrogen to the acetonitrile solution containing the iron catalyst and the organic substrate. Thus, it can be considered that this series of experiments were carried out at 1atm of H_2 pressure. The results are shown in table 2.1.

Table 2.1. Percent of oxidation substrate under Ar and H_2 atmosphere in the presence and absence of acetic acid for different substrates.

Oxidant		H_2O_2		H_2O_2 + CH_3COOH	
Atmosphere		Ar	H_2	Ar	H_2
Reagent	Product				
Cyclohexane	Cyclohexanol	**58**	**22**	**55**	**48**
	Cyclohexanone	**3**	**3**	**2**	**4**
Cyclooctene	Epoxide	**87**	**54**	**91**	**99**
Methyl,Phenyl -Sulfide	Sulfoxide	**32**	**25**	**98**	**103**
	Sulfone	**1**	**1**	**2**	**4**

Oxidation of cyclohexane is reduced by more than a 60% in hydrogen atmosphere. In addition cyclooctene oxidation is reduced by a 40%. However methyl,phenyl sulphide oxidation is just decreased by 20%. These differences are fully consistent with a competitive inhibition scenario in which the hardest substrate to be activated (cyclohexane) is the one that is more inhibited by hydrogen. In contrast, inhibition of the sulfide oxidation, which is the substrate of the series with highest tendency to be oxidized, is barely affected by the presence of hydrogen. Cyclooctene is just in the middle of such tendencies. Is worth to note that sulphide oxidation is the easiest process but the yields are quite low, probably for the tendency of the sulfoxide product to coordinate the iron centres and deactivate by this way the catalysis.

Interestingly, the hydrogen effect is not observed at 1atm of H_2 pressure when acetic acid is added to the reaction media. In fact, as reported before, acetic acid increases the oxidation yields, which is especially significant for sulfide oxidation. This enhancement in oxidation efficiencies is related with the generation of a new high valent iron species that is very active in the oxidation catalysis. However, the oxidant species generated in presence of acetic acid has a lower tendency to activate hydrogen even though is very active in activating different organic substrates.

IV. Reactions at variable H_2 and D_2 pressures

The effect of hydrogen is further confirmed in a series of experiments in which H_2O_2 solutions were injected in a reactor under different hydrogen pressures.

The organic substrate studied was cyclohexane because it was the substrate that is more affected by H_2. Tube of the reactor was charged with dry acetonitrile as a solvent, Fe complex (1 mM) and cyclohexane (1 M). Pressure was set on 10 atm by adding H_2. Thereafter, a solution of 10 equiv H_2O_2 (10 mM) was injected over a period of 30 min under pressure and stirring for 30 min more.

We have done the same experiment, setting the pressure values at 8, 6 and 4 atm and following the acetylation work up. The products were identified by comparison of their GC retention times.

The same setting of experiments was carried out adding acetic acid (1.75 M) and adding D_2 instead of H_2.

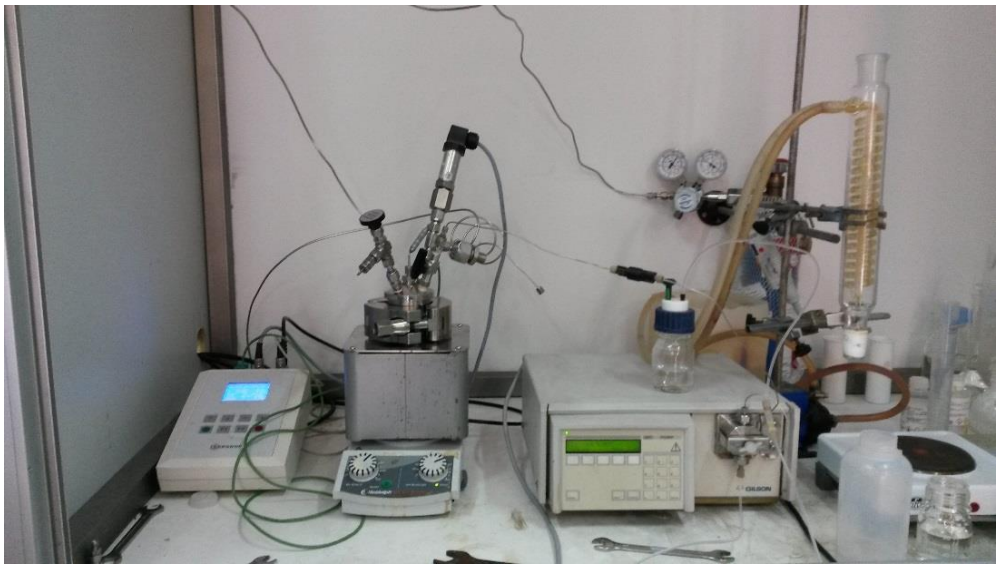

Figure 2.2: Reactions at variable H_2 and D_2 pressures in reactor.

V. Analysis the results of the experiments

The results obtained, as shown in figure 2.3, at higher H_2 pressures complete inhibition of cyclohexanol production can be achieved. In fact, at 10 atm of H_2 pressure, absolutely no cyclohexanol is produced. Such dependence on the H_2-pressure clearly indicates the role of hydrogen as a competitive substrate.

Experiments in presence of acetic acid even at different of H_2 pressures reveal that generation of cyclohexanol is not completely inhibited even at 10 atm. Thus, although a

hydrogen activation pathway is also possible in presence of acetic acid, it is clearly less favourable than without acetic acid.

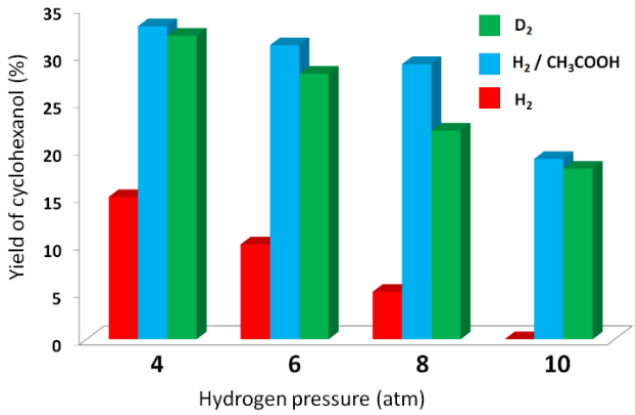

Figure 2.3. Percent of oxidation cyclohexane under H_2 and D_2 pressure in the presence and absence of acetic acid.

In addition, we have performed the experiments by using deuterium instead of hydrogen in different pressures. According to the charts in figure 2.3, there is a decrease in the yield of cyclohexanol production with increasing the pressure of D_2, but there is always more cyclohexanol than for H_2 experiments, which is consistent with a considerable kinetic isotopic effect. Thus, D_2 is a rather sluggish substrate compared to hydrogen, so generation of cyclohexanol is not completely inhibited by D_2 even at 10 tm.

VI. Running reaction without substrate under D_2 atmosphere

In absence of organic substrate, the product of the hydrogen activation by the active high-valent iron species is expected to be simply a water molecule. Thus, in order to facilitate a distinctive detection of water formed, we carried out experiments using deuterium instead of hydrogen because deuterated water generated by deuterium activation can be easily analysed by ^{2}D-NMR. Therefore, injection of 10 eq of hydrogen peroxide was carried out in a reactor pressurized at 10 atmospheres with deuterium gas containing 3mL of a 1mM solution of [Fe(BPMCN)$(OTf)_2$] in CH_3CN.

The integration of the signal was referenced to the natural abundance deuterium signal of acetonitrile solvent. Calibration was made by adding known amounts of deuterated water to an acetonitrile solution containing both the iron compound and the amounts H_2O_2 added in the experiments. On the other hand, control experiment was performed pressurizing with

deuterium a reactor containing a H_2O_2 solution in absence of the iron compound. Spectra from the experiment and from the control are shown in figure 2.4.

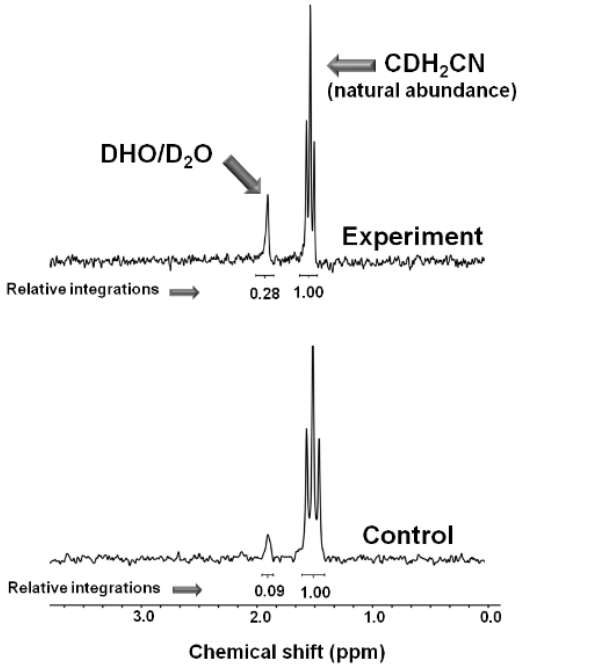

Figure 2.4. Deuterated water from experiment and control shows by ^{2}D-NMR.

From calibration factor (details in materials and methods) experimentally found and discounting the amount of deuterium found in the control (mainly coming from impurity in D_2 gas) can be calculated that *ca* 0.8 eq of D_2 were converted to D_2O by reaction with H_2O_2 in presence of [Fe(BPMCN)(OTf)$_2$].

The overall yield of D_2O could seem scarce, but several factors have to be considered before evaluating such yield. In fact, once the high-valent iron species is generated, D_2 activation competes with self-decay pathways. Such competition is especially relevant considering that certain kinetic isotope effect disfavours D_2 activation vs H_2 reaction and thus the amount of water expected from values shown in table 2.1 are significantly reduced when D_2 is used. This last point was confirmed by performing experiments in presence of cyclohexane as organic substrate at different D_2 pressures. The results observed indicate that D_2 is a rather sluggish substrate compared to hydrogen. However, even under these conditions, formation of D_2O was confirmed in presence of cyclohexane at 10 atm of D_2 (0.8 eq) and at 8 atm of D_2 (0.4 eq).

VII. What about catalysis?

The initial goal of this work was olefins oxidation and alkane hydroxylation by using a cooperative processes started from mixtures starting from H_2 and O_2. As previously reported using Au/Pd nanoparticles as catalyst, we produce H_2O_2. Our idea was coupling it to olefin oxidation by using this H_2O_2 and [Fe (BPMCN)$(OTf)_2$] as catalyst.

However, we could not obtain olefin oxidation by this way due to the presence of hydrogen as a competitive substrate in the system.

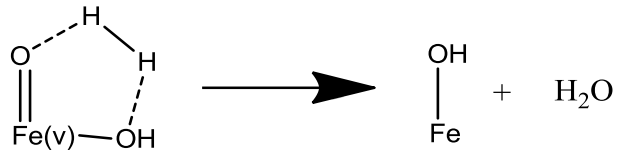

Therefore, we decided to investigate the oxidation of olefin with H_2O_2 and Fe complex, in the presence of H_2 as a competitive substrate.

Thus, on one hand we have not been able to generate olefin oxidation in a cooperative system. However, on the other hand in our quest, we described a new H_2 activation process achieved by the species generated by reaction of H_2O_2 with Fe complex, which is a new pathway for H_2 activation. Such mechanistic insights could have implications on the study of biological hydroxylations and the understanding of hydrogenases.

VIII. Conclusions

The overall data presented in this chapter is consistent with the mechanistic scenario shown in scheme 2.4. As previously reported, a different high valent species is generated by reaction of [Fe(BPMCN)$(OTf)_2$] with H_2O_2 depending on the presence or absence of acetic acid. Both species are active in oxidation catalysis for substrates such alkanes, olefins or organic sulphides. Catalysis results are generally improved by adding acetic acid, what could induce to infer that species generated in presence of acetic acid is more active, has an enhanced oxidative character and is more versatile. However, the results shown herein suggest that this is not always the truth. In fact, while active species generated in presence of acetic acid does not activates hydrogen, active intermediate generated in absence of acetic acid is able to oxidize hydrogen to water. It seems that for the species $[(BPMCN)FeO(OH)]^{2+}$ both the oxo and hydroxo

sites can cooperatively participate in the hydrogen activation process. In contrast, in the intermediate $[(BPMCN)FeO(OOCCH_3)]^{2+}$ the acetate group is less basic and pourly assists the H_2 oxidation.

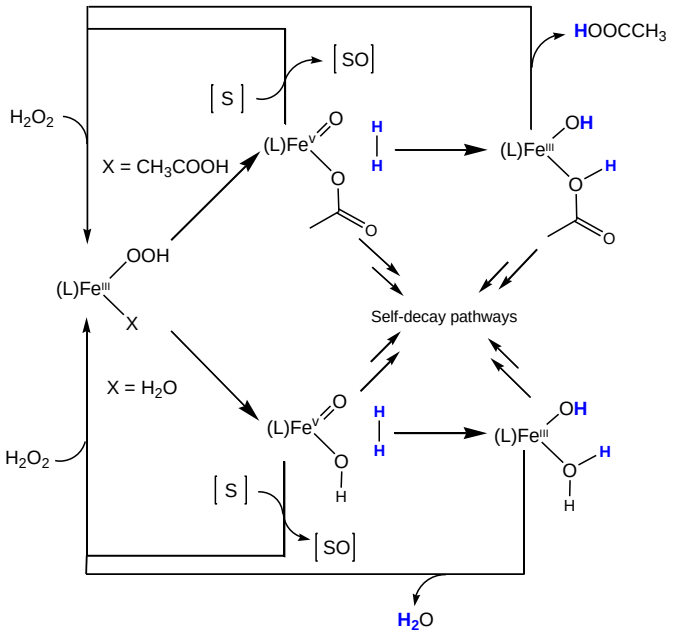

Scheme 2.4. Mechanistic scenario of different high valent species is generated by reaction of $[Fe(BPMCN)(OTf)_2]$ with H_2O_2 depending on the presence or absence of acetic acid.

References:

(1) Oyama, S. T.; Editor *Mechanisms in Homogeneous and Heterogeneous Epoxidation Catalysis*; Elsevier B. V., 2008.
(2) Grigoropoulou, G.; Clark, J. H.; Elings, J. A. *Green Chem.* **2003**, *5*, 1.
(3) Mashkina, A. V. *Catal. Rev. - Sci. Eng.* **1990**, *32*, 105.
(4) Choudary, B. M.; Reddy, C. R. V.; Prakash, B. V.; Kantam, M. L.; Sreedhar, B. *Chem. Commun. (Cambridge, U. K.)* **2003**, 754.
(5) Lee, H. B.; Ren, T. *Inorg. Chim. Acta* **2009**, *362*, 1467.
(6) Rao, T. V.; Sain, B.; Kafola, S.; Nautiyal, B. R. *Energy Fuels* **2007**, *21*, 3420.
(7) Rao, T. V.; Sain, B.; Kumar, K.; Murthy, P. S.; Rao, T. S. R. P.; Joshi, G. C. *Synth. Commun.* **1998**, *28*, 319.
(8) Lane, B. S.; Burgess, K. *Chem. Rev. (Washington, DC, U. S.)* **2003**, *103*, 2457.
(9) (a) Ding, Y.; Gao, Q.; Li, G.; Zhang, H.; Wang, J.; Yan, L.; Suo, J. *J. Mol. Catal. A: Chem.* **2004**, *218*, 161(b) Bu, J.; Yun, S.-H.; Rhee, H.-K. *Korean J. Chem. Eng.* **2000**, *17*, 76.
(10) (a) Figueras, F.; Kochkar, H. *Catal. Lett.* **1999**, *59*, 79(b) Kochkar, H.; Figueras, F. *J. Catal.* **1997**, *171*, 420(c) Woragamon, K.; Jongpatiwut, S.; Sreethawong, T. *Catal. Lett.* **2010**, *136*, 249.
(11) Sheu, C.; Richert, S. A.; Cofre, P.; Ross, B., Jr.; Sobkowiak, A.; Sawyer, D. T.; Kanofsky, J. R. *J. Am. Chem. Soc.* **1990**, *112*, 1936.
(12) Sono, M.; Roach, M. P.; Coulter, E. D.; Dawson, J. H. *Chem. Rev. (Washington, D. C.)* **1996**, *96*, 2841.
(13) (a) Que, L., Jr.; Ho, R. Y. N. *Chem. Rev. (Washington, D. C.)* **1996**, *96*, 2607(b) Wallar, B. J.; Lipscomb, J. D. *Chem. Rev. (Washington, D. C.)* **1996**, *96*, 2625.
(14) (a) Edwards, J. K.; Solsona, B. E.; Landon, P.; Carley, A. F.; Herzing, A.; Kiely, C. J.; Hutchings, G. J. *Journal of Catalysis* **2005**, *236*, 69(b) Solsona, B. E.; Edwards, J. K.; Landon, P.; Carley, A. F.; Herzing, A.; Kiely, C. J.; Hutchings, G. J. *Chem. Mater.* **2006**, *18*, 2689.
(15) (a) Edwards, J. K.; Carley, A. F.; Herzing, A. A.; Kiely, C. J.; Hutchings, G. J. *Faraday Discuss.* **2008**, *138*, 225(b) Edwards, J. K.; Ntainjua N, E.; Carley, A. F.; Herzing, A. A.; Kiely, C. J.; Hutchings, G. J. *Angew. Chem., Int. Ed.* **2009**, *48*, 8512.
(16) White, M. C.; Doyle, A. G.; Jacobsen, E. N. *J. Am. Chem. Soc.* **2001**, *123*, 7194.
(17) Fujita, M.; Que, L., Jr. *Adv. Synth. Catal.* **2004**, *346*, 190.
(18) Mas-Balleste, R.; Que, L., Jr. *J. Am. Chem. Soc.* **2007**, *129*, 15964

Chapter **3**

Hybrid systems composed by Graphene Oxide and Porphyrins

I. Introduction

Porphyrins are nowadays a very active field of research because of their interesting chemical and photochemical properties, and tunability by chemical derivativatization. Interestingly, Inspired by nature, artificially synthesized porphyrinic catalysts have been used to catalyze a number of reactions, from the first use of metalloporphyrin as a catalyst in olefin epoxidation and alkane hydroxylation by Groves et al. in 1979.[1]

Metalloporphyrins can have various metallic centers and because of their unique properties like stability, tunability, catalytic efficiency, and selectivity, they have been used for functionalization (hydroxylation, amination, and alkylation) of hydrocarbons, conversion of alcohols to carbonyl compounds, and recently of sulfides to sulfoxides.[2,3]

In a quest to design heterogeneous systems containing poprphyrinic fragments, mostly, metalloporphyrins have been attached to a solid support, like polymers, or carbon based materials (graphene, graphene Oxide, or carbon nanotubes).[2a,4,5] A main focus of interest for these hybrid materials is the easy separation of catalyst from products and the possibility to avoid bimolecular pathways for catalyst deactivation.[6,7]

Some advantages of using carbon based materials as supports in catalytic systems are their high surface areas and the fact that they can offer a sufficient number of reactive sites that could allow to anchor different chemical structures.[8,9] For example, graphene oxide (GO) is composed by single layers of graphene functionalized by hydroxyl, epoxide and carboxylic groups, produced from extensive oxidation of graphene.[10] Graphene oxide (GO), possesses large specific surface area,[11] being both sides of the nanosheets accessible. The functionalities (such as surface functional groups),[12,13] holes,[14] oxygen,[15] carbon vacancies and defects, introduce chemically active sites for use in catalytic reactions and also act as anchoring sites for deposition of metal nanoparticles or molecular catalyst.

Up to this date, connection of metalloporphyrins to solid supports mostly has been achieved by means of covalent bonding, which limits the choices of support materials and also complicates synthetic procedures.[16,17,18] concerning covalent functionalization, the presence of oxygen containing groups in GO provides an opportunity for its chemical modification using known carbon surface chemistry. Several recent papers demonstrate also the possibility of incorporating porphyrin to Graphene via some simple and versatile noncovalent interactions, such as supermolecular interactions known as π-π stacking, electrostatic interaction and hydrogen bonding.[19,20]

In this chapter, we have studied π-π stacking that takes place between electron–abundant aromatic cores of porphyrins and conjugated surfaces of the GO. In addition, we performed functionalization to incorporate pyridine groups able to coordinate to metal centers. First, we chlorinated the COOH group to the COCl by reaction with $SOCl_2$ and then we performed the esterification reaction with para hydroxypyridine. Thus, we bounded a pyridine as a donor group, which can coordinate to the metal of the porphyrin.

In this chapter, we described different methods to generate hybrid GO-porphyrin systems such findings could offer some hints on how to design recyclable catalytic systems with an increased efficiency due to the fact that bimolecular decay pathways should be avoided.

II. Overview of the results obtained

Applications of graphene are often hindered by its poor processibility, which is mainly caused by the high inter-layer attraction energies. To overcome this problem, graphene oxide is considered a valuable alternative. Following this idea, this part of the thesis focuses on the interaction of a series of metallo-porphyrins to graphene oxide. The GO used contains an O/C ratio of 0.58 and a C-O/C=O ratio of 2.[21] These are typical values for GO obtained by standard oxidation procedures, which contain defect-free graphene areas, together with amorphous regions and defective areas that can contain hydroxyl, epoxy and carboxyl groups.[22,23]

This work allowed to describe the effect of different metals and meso-groups in the supramolecular attachment of porphyrins.

Carboxyl group allowed us to perform a covalent reaction. We can first treat the carboxyl group by $SOCl_2$ to form COCl and then pyridine fragments can be bounded to the GO by esterification process. Finally, we have studied the interaction between the metal center of porphyrin and the pyridine attach to GO.

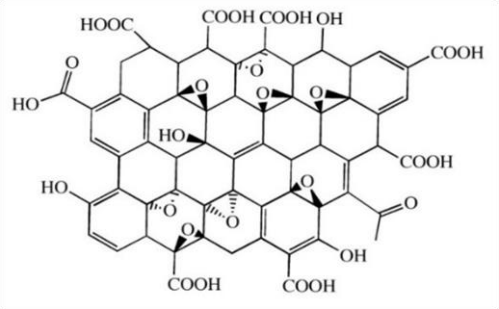

Scheme 3.1. A part of Graphene Oxide that contain hydroxyl, epoxy and carboxyl groups.

III. Experimental procedures

III.1. Synthesis of supramolecular aggregates GO-Porphyrins

Direct reaction of GO with Ph_4- porphyrins

A flask was charged with graphene oxide (25 mg), meso-tetraphenyl porphyrin (25 mg) and dry dichloromethane as a solvent (10 mL). The mixture was stirred during 2 h at room temperature under argon. Then, the solid was isolated by centrifugation (14000 rpm, 5 min.) and washed with dichloromethane until supernatant was observed colorless. Then the solid was dried with vacuum. From mixture it was recovered about 50% of the initial amount of GO. This method was also followed using 5,10,15,20-tetraphenyl-21*H*,23*H*-porphyrin cobalt(II) and 5,10,15,20-tetraphenyl-21*H*,23*H*-porphyrin nickel(II), obtaining final yields of 48% and 46%, respectively.

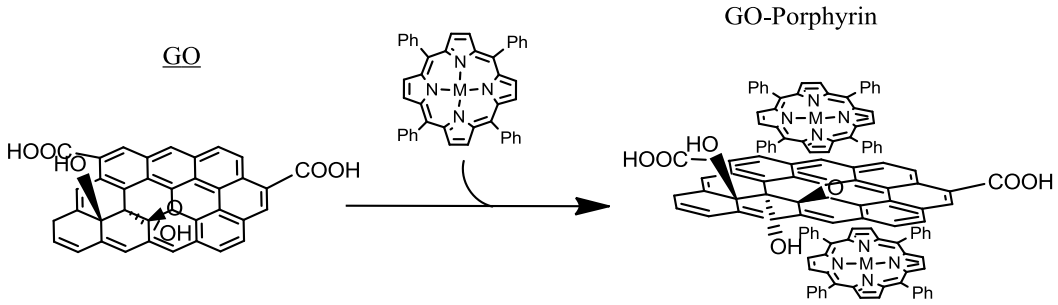

Scheme 3.2. Π-staking interactions between porphyrins and Graphene Oxide.

Direct reaction of GO with C_6F_5- porphyrins

Following analog procedures to what is presented above. A flask was charged with graphene oxide (25 mg), 5,10,15,20-prototetrakis(pentafluorophenyl)porphyrin (F_{20}TPP) (25 mg) and dry dichloromethane as a solvent (10 mL). The mixture was stirred during 2 h at room temperature under argon. Then, the solid was isolated by centrifugation

(14000 rpm, 5 min.) and washed with dichloromethane until supernatant was observed colorless. Then the solid was dried with vacuum. After characterization we found that this solid is only GO and thus fluorinated porphyrin (F_{20}TPP) did not give us GO-(metal)F_{20}TPP adducts. In fact, only residual attachment of Por-F20TPP has been observed (<2 μmol/g of GO), suggesting that electron withdrawing effect of fluoride atoms of phenyl groups in meso positions deactivates porphyrin-GO stacking.

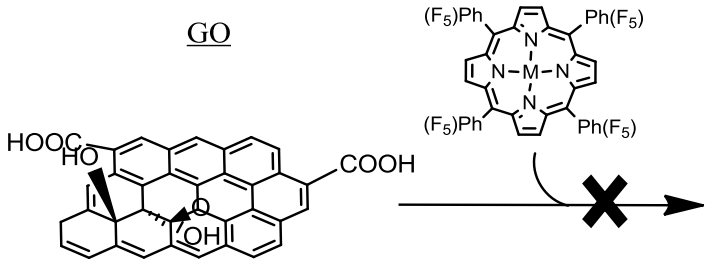

Scheme 3.3. Π-staking interactions between porphyrins- fluorinated and Graphene Oxide.

III.2. Synthesis of GO-Py

In the search of a more versatile and site-specific way to attach porphyrins to graphenoid materials though stronger interactions we attempted the functionalization of graphene oxide according to the procedure summarized in the Scheme 3.4. The final goal is to add a donor group covalently bounded to the graphene oxide flakes, which could allow coordination of the metal centers present in metalloporphyrins. The selected donor groups were pyridines bounded to GO by a simple esterification process between 4-hydroxopyridine and GO previously treated with $SOCl_2$.

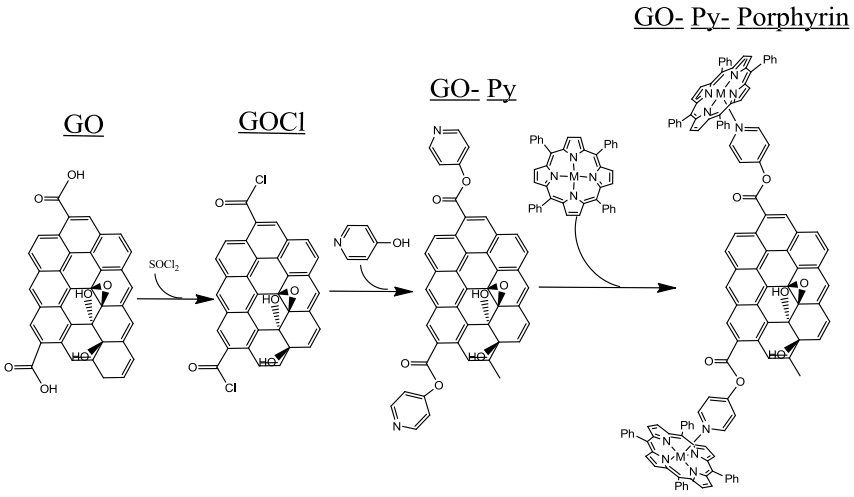

Scheme 3.4. Synthetic strategy to covalent functionalization of graphene oxide that allows attachment of porphyrins through coordination of metal centers to pyridine groups.

Chlorination

In a typical chlorination treatment, graphene oxide (400 mg) was dispersed into dry thionyl chloride (200 mL) with N,N-dimethylformamide (2 mL) and refluxed under argon for 24 h at 70ºC. Excess thionyl chloride was evaporated and the remaining solid washed several times with dry tetrahydrofuran. Then the solid was dried with vacuum. Yield of GO-Cl was 300 mg (75%).

Esterification with 4-hydroxypyridine (GO-Py)

For the esterification process, GO-Cl (270 mg), 4-hydroxypyridine (185 mg), triethylamine (550 □l) and 4-(dimethylamino)pyridine (47 mg) were added in dry tetrahydrofuran (80 mL) and refluxed under argon for 24 h. Thereafter, the excess of THF was evaporated and the remaining solid washed several times with additional amounts of dry tetrahydrofuran. After each washing process, solid was isolated by centrifugation for 5 min. at 5000 rpm. Finally, the solid was washed first with water and later with acetone and then dried under vacuum. The yield of the synthesis of GO-Py from GO-Cl was 77%.

III.3. Reaction of GO-Py with porphyrins

A flask was charged with GO-Py (25 mg), and the corresponding porphyrin (25 mg) and dry dichloromethane as a solvent (10 mL) was stirred during 2 h at room temperature under argon. Then, the solid was filtered off and washed with dichloromethane until we obtained a colorless supernatant. The filtrated solutions were collected and evaporated to dryness. The corresponding product was separated from the excess of porphyrin by extraction in water. Insoluble porphyrin remained as a solid and the product dispersed in water. Solutions were filtered off and the filtrated dispersion evaporated to dryness at 60 ºC and reduced pressure. The yields obtained following this procedure using TPP, CoTPP or NiTPP range from 5% to 20%.

IV. Characterization of the materials obtained

IV.1. UV-Vis Characterization

For the determination of the amount of porphyrin incorporated to GO, we considered the absorbance at 410-420 nm (form porphyrin fragment) and compared with the intensity at 296 nm (characteristic of GO). The absorbance due to the GO was estimated and subtracted

to the measured value in order to evaluate the amount of porphyrin present in the samples. Values provided are expressed as micromoles of porphyrin relative to grams of GO, and were calculated considering the molar absorptivity of GO in water (figure 3.1) and pure porphyrins dissolved in CH_2Cl_2 (figure 3.2) (*vide infra*).

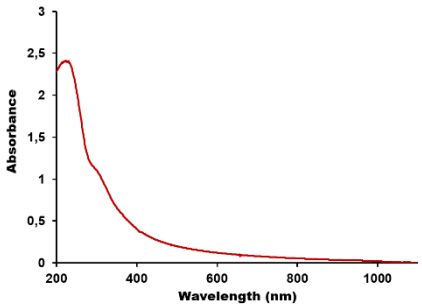

Figure 3.1. UV-vis spectra of GO in water.

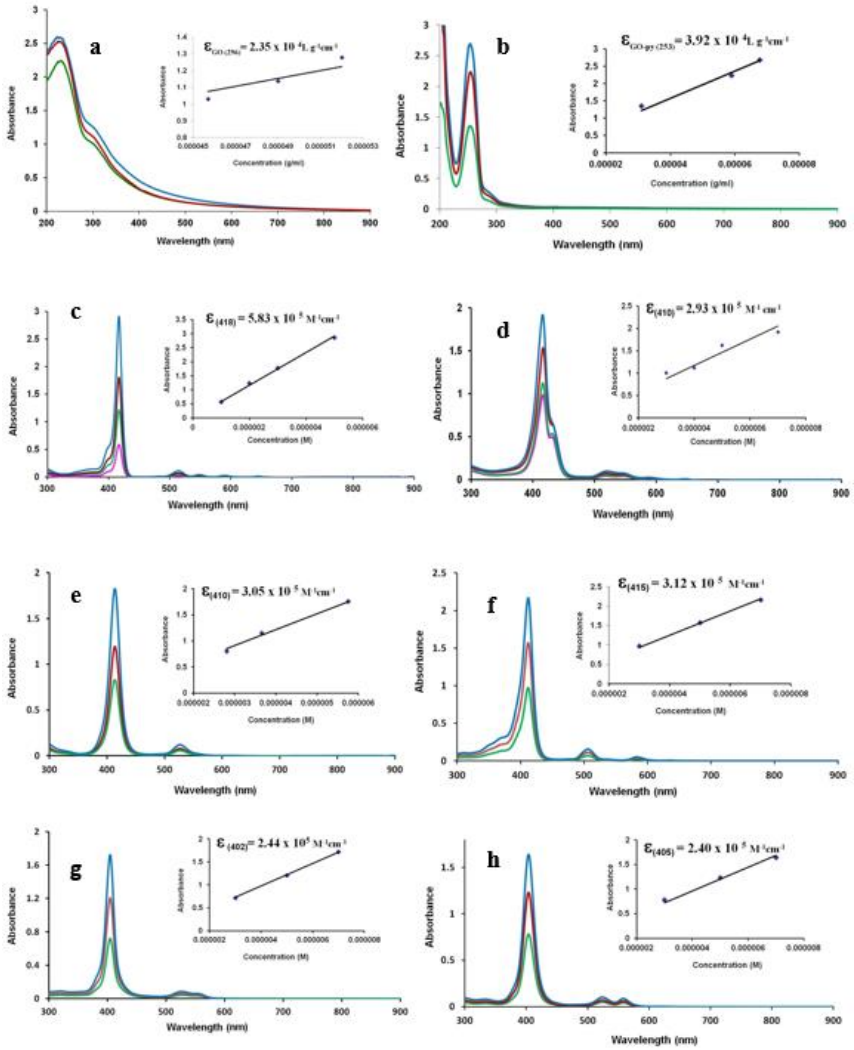

Figure 3.2. Determination of molar absorptivity of GO (a), GO-Py (b),TPP, CoTTP (d), NiTTP (e), F_{20}TTP (f), CoF_{20}TTP (g), CoF_{20}TTP (h).

The product isolated can be analysed by UV-vis, due to the easy dispersibility of GO in water. Dispersibility of both starting GO and the corresponding porphyrin decorated material is crucial. As a consequence experiments with partially reduced GO (with stronger interlayer interactions) have been unsuccessful. The presence of porphyrin attached to GO can be observed and quantified due to the characteristic absorbance at 410-460 nm. As can be observed in figure 3.3, in this region of the spectra, GO slightly absorbs. Thus, in order to evaluate the amount of prophyrin attached to GO, the absorption from GO has to be subtracted. Following this procedure, it has been observed that a hybrid material GO-TPP is produced with a porphyrin content of 9.6 μmol per gram of GO. Taking a step further, we have expanded our study to metal containing porphyrins. Ni(II) and Co(II) containing porphyrins were exposed to GO following the same procedure used for protoporphyrin. These two metal centers offer different coordinative properties, which will allow us to detect differentiated patterns depending on the characteristic features of Ni(II) or Co(II). Figure 3.3 shows UV-vis data found for GO and the corresponding products after reactions with TPP, CoTPP and NiTPP. Incorporation of CoTPP (10.2 μmol/gr of GO) is comparable to that observed for proto TPP, suggesting that π-π interactions are at the end the ultimate responsible for porphyrin incorporation to GO. However, Ni(II) containing porphyrin does not show interaction with graphene oxide. Thus, it is observed an effect of metal center, which probably is due to the reluctance of Ni(II) coordinated to high field ligands (such as porphyrins) to deviate from the square planar geometry. In other words, short contact between the Ni center and the π-electron density of GO disfavors the supramolecular attachment of metalloporphyrins.

UV-vis features of porphyrinic fragments shown in figure 3.3 are very close to that observed for solutions in CH_2Cl_2 of pure porphyrins. This is characteristic of weak interactions that have a scarce effect on the electronic structure of the tetrapyrrolic fragment. However, considering that these UV-vis spectra are measured in water dispersions and that the porphyrins used are absolutely insoluble in water, it is clear that a complex between GO-porphyrin has been formed in each case. In fact, it is interesting to note that GO serves as carrier to "solubilize" in water neutral (metallo)porphyrins that otherwise would not be present in solution.

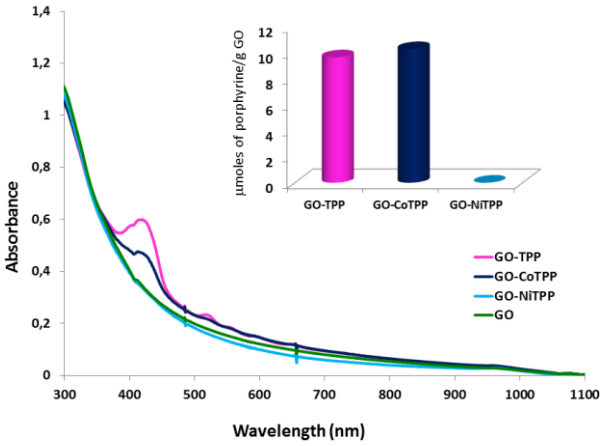

Figure 3.3. UV-vis characterization of adducts of GO and TPP, CoTTP or NiTPP. Spectra correspond to the same GO concentration (47.8 mg/L). Inset shows amounts of porphyrins relative to grams of GO.

It is worth to mention that fluorinated porphyrin (F_{20}TPP) do not give GO-(metal)F_{20}TPP adducts. Considering that proto F_{20}TPP does not attach either to GO, these results reinforce the notion that the main driving force to the formation adducts of GO and porphyrins is π-π stacking that can be established in the graphenic regions of the GO flakes.

A similar procedure was followed for determination of porphyrins ligated to GO-Py. figure 3.4 shows signal characteristic of GO-Py that was found at 253 nm.

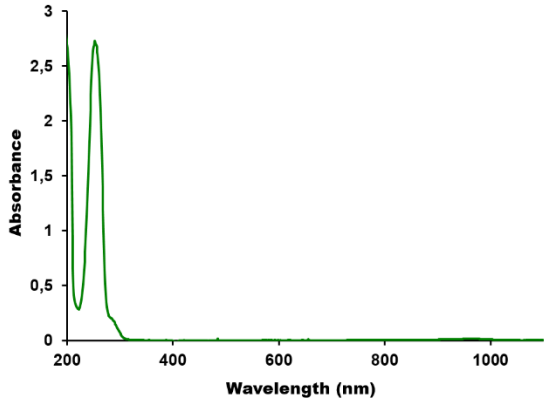

Figure 3.4. UV-vis spectra of GO-Py in water.

Figure 3.5 shows the UV-vis analysis of the products obtained dispersed in water. The porphyrin signal was 30-40 nm red-shifted relative to the spectrum observed for pure porphyrinic compound in CH_2Cl_2. Due to the low content in porphyrin of such samples, signals at 440-460 nm were measured in concentrated suspensions (566 mg/L), and compared to the 253 nm signals in diluted conditions (50 mg/L).

Surprisingly, metal free porphyrin does not attach to GO-Py, probably because functionalization process massively affected to structure of GO hampering the stacking of porphyrins. In contrast, CoTPP and NiTPP interact with GO-Py as shown by the characteristic absorption of porphiryns in the visible region. In this case, the maximum absorbance observed shows a red shift of 30-40 nm with respect to what is observed for solution in CH_2Cl_2 of pure porphyrins. This phenomenon is related to coordination of the pyridine fragment to the metal center as previously reported for Ni[24] and Co[25] containing porphyrins that coordinate to pyridinic fragments.

Level of incorporation of metalloporphyrin to pyridine functionalized GO also depends on the nature of metal center. NiTPP shows a considerable lower tendency to coordinate to pyridine groups in comparison to its cobalt analogous. (0.30 μmol/g of GO-Py *vs* 2.88 μmol/g of GOPy). This observation can be easily related to the low tendency previously observed for NiTPP to coordinate pyridine. In fact, at room temperature, concentrations of pyridine up to 2.0 M in toluene do not induce appreciable changes in the UV-vis spectrum of NiTPP. It is at low temperature (200 K) that evidences for equilibrium between species NiTPP, NiTPP(py) and $NiTPP(py)_2$ have been detected.[26] Thus, our observations indicating a relative low degree of attachment of NiTPP to GO-Py are in good agreement with the known coordination features of such metalloporphyrin. For both NiTPP and CoTPP, the amount of porphyrin detected relative to overall amount of GO-Py is clearly lower than that observed for reaction with pure GO (insets in figures 3.3 and 3.5).This is what should be expected considering that GO-Py offers a limited amount of specific sites to coordinate of metal centers in metallo-porphyrins.

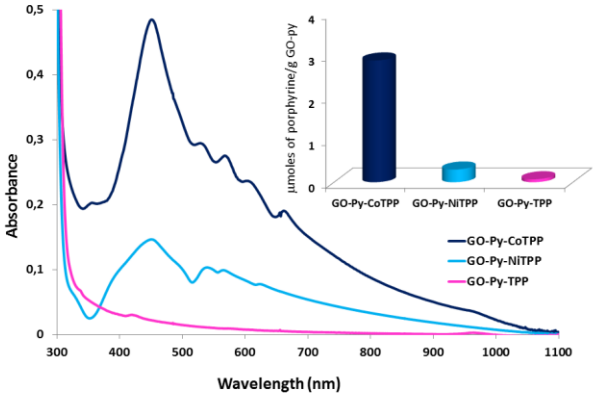

Figure 3.5. UV-vis characterization of adducts of GO-Py and TPP, CoTTP or NiTPP. Spectra correspond to the same GO-Py concentration (566 mg/L). Inset shows amounts of porphyrins relative to grams of GO-Py.

IV.2. IR, Raman and luminescence Characterization

The product obtained (GO-Py) shows a clearly distinct IR. While we can observe a narrow peak at 1735 nm for GO-Py, a wide peak at 1722 nm is observed for GO. In addition, we can see a peak around 1500 nm that corresponds to the pyridine groups of the GO-Py. The most remarkable feature in figure 3.6 is the difference in the singles in the C=O region between Go and GO-Py.

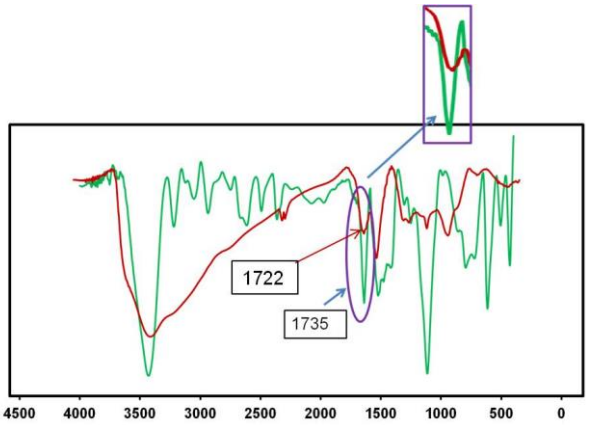

Figure 3.6. FT-Infrared spectra of products GO (red) and GO-Py (green)

Further spectroscopic characterization of the porphyrins attached to GO and GO-Py was obtained from Raman luminescence spectra of cast films on glass slides. In figure 3.7 the luminescence features in the range of 600-720 nm of Co-TPP, GOCoTPP and Go-Py-CoTPP are compared. In all cases, the bands due to the porphyrin are clearly present. The major peak at 650 nm in GO-Py-CoTPP is blue-shifted with respect to GO-CoTPP (662 nm) and with respect to CoTPP (669 nm), which reflects the different mode of interaction of the metalloporpyhrin with GO and GO-Py. It is also noteworthy that the luminescence is more intense for GO-Py-CoTPP, despite its content in porphyrin being lower, than in GO-CoTPP. This observation suggests that the cofacial π-interaction between porphyrin and GO substantially quenches the luminescence of the porphyrin as also observed for cofacial diporphyrins using different spacers.[27]

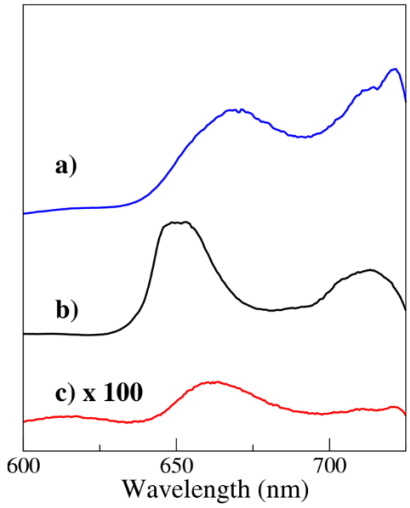

Figure 3.7. Luminescence features in the range 600-720 nm of CoTPP (a), GO-Py- CoTPP (b) and GO-CoTPP (c). The excitation light was the 488 nm line of an argon ion laser and the inelastically scattered / emitted light was dispersed on a grating of 150 lines / mm. The spectrum of GO-CoTPP has been multiplied by a factor of 100 to allow comparison.

IV.3. X-ray photoelectron spectroscopy (XPS) Characterization

The binding energy (BE) of N(1s) core-level recorded at 400.1 eV is characteristic of porphyrinic ligand and also 400.6 eV is characteristic of pyridinic ligand. In addition, Co($2p_{3/2}$) line profile displayed a satellite structure which is the fingerprint of Co^{2+} ions and the main peak appeared at 780.4 eV, smaller than the 781.0 eV found on CoTPP (table 3.1).

The N(1s) core-level spectrum of these samples shows two components at 399.0 eV and 400.9 eV associated to pyridinic and porphyrinic structures, respectively as shown in figure 3.8a. Integration of both N-signals shows four nitrogen atoms from porphyrin are present for each N from pyridine. Thus, all pyridine groups are coordinated to Co-TPP fragments.

The BE of Co^{2+} ions appeared at somewhat higher BE (781.4 eV) than for pure GO-CoTPP (780.4 eV) or CoTPP (781.0 eV). These observations are consistent with coordination of cobalt center to pyridine group as shown in figure 3.8b.

We also estimated Co coverage by the Co/OGO ratio derived from XPS measurements. This value was much higher than the determined by UV-vis experiments. It is likely that the number of Co atoms on the surface is overestimated taking into account that the Co2p signal is very weak and hence the associate error is very high.

Table 3.1. Binding energies (eV) of core-levels of CO/pyGO samples (in parentheses are peak percentages).

sample	C(1s)	O(1s)	N(1s)	Co($2p_{3/2}$)
GO	284.8 (36) 286.3 (56) 288.0 (8)	531.1 (41) 532.4 (59)	-	-
GO-CoTPP	284.8 (51) 386.9 (45) 288.4 (4)	531.5 (32) 532.8 (68)	400.1	780.4
GO-Py	284.8 (55) 286.3 (37) 288.0 (8)	531.1 (47) 532.5 (53)	400.6	-
GO-Py-CoTPP	284.8 (78) 286.5 (22)	531.1 (35) 532.6 (65)	399.0 (81) 400.9 (19)	781.4
CoTPP	284.8 (95) 287.6 (5)	-	399.2	781.0

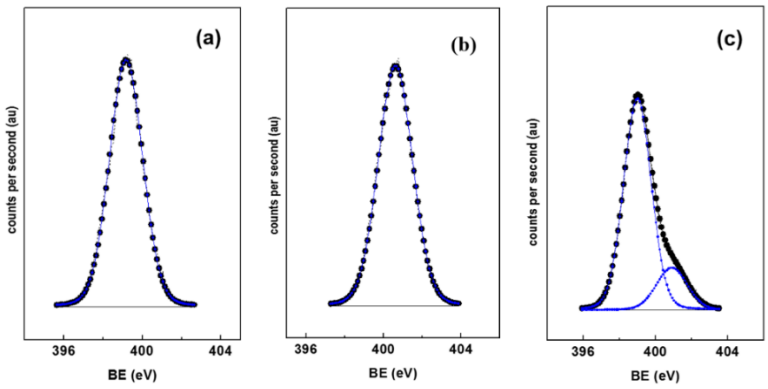

Figure 3.8a. N(1s) core-level spectra of CoTPP (a), GO-Py (b) and GO-Py-CoTPP (c) samples.

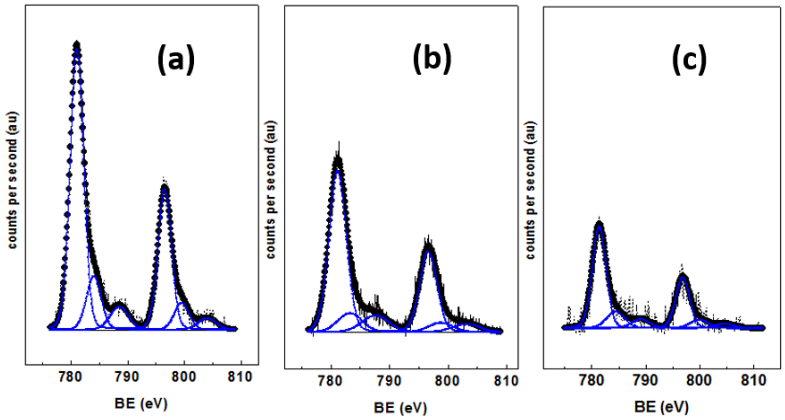

Figure 3.8b. Co (2p) core-level spectra of CoTPP (a), GO-CoTPP (b) and GO-Py-CoTPP (c) samples.

IV.4. Atomic force microscopy (AFM) Characterization

The nanometric dimensions of materials obtained were further confirmed by Atomic Force Microscopy (AFM). In figure 3.9 is shown typical AFM topographic images observed after deposition of water dispersions of GO-CoTPP or GO-Py-CoTPP on SiO_2. Images relative to GO-CoTPP are indicative of isolation monolayers with heights of *ca.* 1 nm. For GO-Py-CoTPP, heights measured are higher (5-15 nm), indicating that functionalization favors certain degree of aggregation. The reasons of these differences are not completely understood. Probably, they are related to the increase number of polar groups incorporated to GO flakes in GO-Py, which could mediate interlayer interactions.

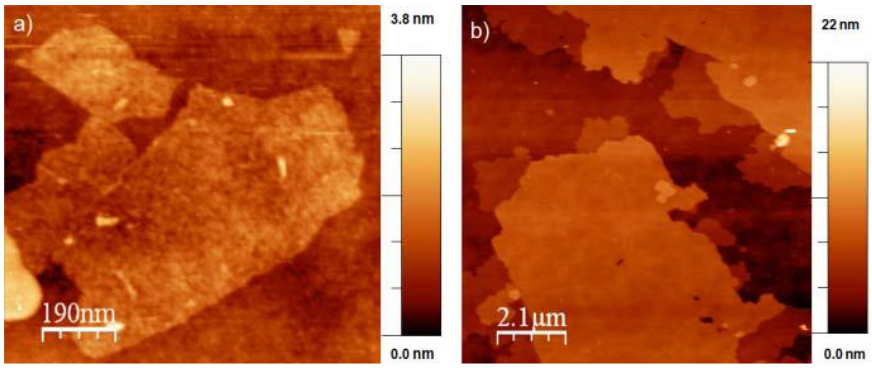

Figure 3.9. AFM topographic images of the nanolayers formed after deposition of suspensions of a) GO-CoTTP and b) GO-Py- CoTTP on SiO_2.

IV.5. Direct reaction of GO with porphyrins in different solvents

In order to get insights on the nature of GO-porphyrin interaction, we determined the effect of solvent on the attachment of porphyrins to GO, by carrying out experiments under comparable conditions using as a solvent toluene, CH_2Cl_2 and a mixture 3:2 CH_2Cl_2/methanol. We did not use pure methanol because porphyrins are insoluble in this solvent. However, the mixture 3:2 CH_2Cl_2/methanol allows complete solubilization of porphyrins in a polar medium. In a typical experiment, we stirred 20 mg of GO and 5 mg of TPP or CoTPP in 10 mL of the corresponding solvent for 2 hours at 20 ºC. Then, the solid was isolated by centrifugation (14000 rpm, 5 min.) and thereafter washed three times with 5 mL CH_2Cl_2. Finally, the GO-porphyrin adduct was extracted with 5 mL of water. In contrast, incorporation of porphyrin is significantly lower in toluene but significantly higher in the mixture 3:2 CH_2Cl_2/methanol. The obtained data is presented in table 3.2 and figure 3.10.

Table 3.2. Amounts of porphyrins (μmols) relative to grams of GO found in experiments carried out in different solvents (toluene, CH_2Cl_2 and a mixture 3:2 CH_2Cl_2/methanol).

	CH_2Cl_2/methanol (3:2)	**CH_2Cl_2**	**Toluene**
GO-TPP	**17.8**	**9.6**	**2.1**
GO- CoTPP	**41.5**	**10.2**	**4.1**

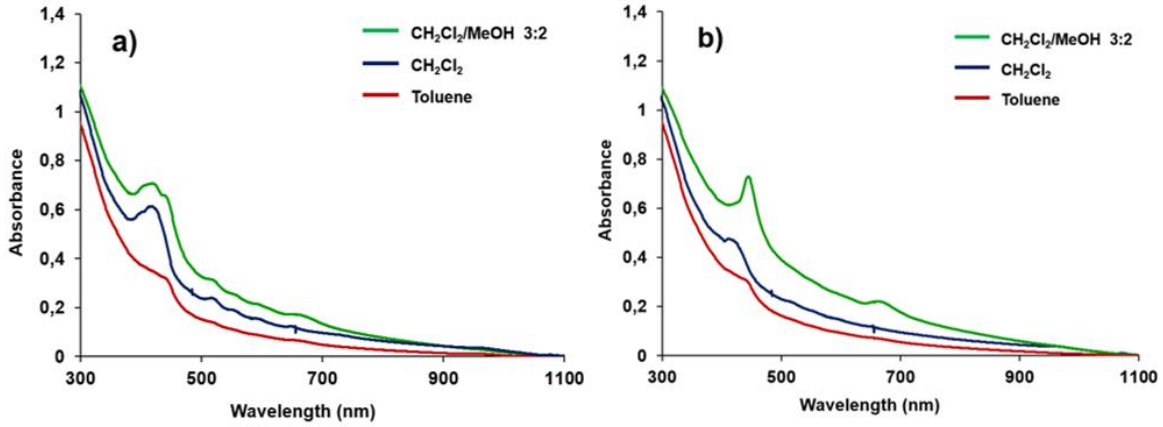

Figure 3.10. UV-vis analysis of the products dispersed in water resulting from experiments carried out in different solvents (toluene, CH_2Cl_2 and a mixture 3:2 CH_2Cl_2/methanol) using TPP (a) or CoTPP (b).

Comparing the results obtained in CH_2Cl_2 with those observed in toluene, a less polar solvent, and in a mixture of CH_2Cl_2/methanol, a more polar medium, it is observed that increasing the polarity, the attachment of TPP and CoTPP to GO is enhanced. In contrast, in the less polar solvent the supramolecular interaction GO-porphyrin is suppressed. These observations indicate that the polar groups of GO do not play the main role in porphyrin attachment. Furthermore, the non-polar regions of GO, that can be more efficiently solvated by toluene, are the ones involved in GO-porphyrin interactions. Consequently, the results of the experiments carried out in solvents of different polarities indicate that π-π stacking is the preferred way to establish the GO-porphyrin interactions.

V. What about catalysis?

The initial goal of this work was the preparation or a hybrid system containing porphyrins to be tested for olefin epoxidation and alkane hydroxylation. Immobilization on GO was a promising strategy to avoid bimolecular decay pathways and to achieve catalyst

recycling. We have been successful on the characterization of new hybrid GO-porphyrins. However, the experimental features of such systems made them hardly applicable in profitable catalytic transformations. It has been observed that supramolecular attachement of prophyrin to GO is quite weak and such system is not stable under catalytic conditions. On the other hand, the yields of the more stable adduct GO-Py-Porphyrin have been also very limited. Furthermore, the total amount of the porphyrins attach to the GO in both types of adducts was quite low, which also hampered its use as catalysts.

Thus, on one hand we have not been able to generate an efficient catalytic system from hybrid GO/porphyrin materials. However, on the other hand, in our quest, we described some new insights on how GO and porphyrins can interact which contributes to the general understanding on how graphene derivatives with predetermined properties, modified by metal centers can be isolated.

VI. Conclusions

Overall, we have presented a new perspective of the ways that can result on incorporation of metalloporphyrins to graphene oxide, offering unprecedented tools in the quest of functional nanostructured materials. On one hand, we have demonstrated that supramolecular assembly of porphyrins directly attached to GO is an efficient method to succeed in having aqueous dispersions of porphyrins that otherwise would be completely water-insoluble. This attachment depends on the nature on the metal center coordinated to the porphyrin and can also be modulated by the substituents in the meso positions on the tertrapyrrolic cycle. The results presented herein suggest that such attachment is mediated through π- π interactions, between graphenic regions of GO and tetrapyrrolic cycle. Covalent functionalization of GO is presented as a new strategy to strongly attach metalloporphyrins to GO flakes through coordination of metal centers to pyridine groups. This alternative is very specific, restricting the presence of metalloporphyrins in the sites where carboxylic acids were originally placed in the parent GO precursor. In summary, the conclusions that can be extracted from our results offer valuable hints to wisely conjugate the unique physical properties of graphene or GO with the optical, electrochemical or catalytic properties of porphyrinic compounds.

References:

(1) Groves, J. T.; Nemo, T. E.; Myers, R. S. *J. Am. Chem. Soc.* **1979**, *101*, 1032.
(2) (a) Zhang, J.-L.; Huang, J.-S.; Che, C.-M. *Chemistry – A European Journal* **2006**, *12*, 3020(b) Lu, H.; Zhang, X. P. *Chemical Society Reviews* **2011**, *40*, 1899.
(3) (a) Chen, L.; Yang, Y.; Jiang, D. *J. Am. Chem. Soc.* **2010**, *132*, 9138(b) Rahimi, R.; Gholamrezapor, E.; Naimi-jamal, M. R. *Inorganic Chemistry Communications* **2011**, *14*, 1561.
(4) Liu, C.-J.; Li, S.-G.; Pang, W.-Q.; Che, C.-M. *Chemical Communications* **1997**, 65.
(5) Yu, X.-Q.; Huang, J.-S.; Yu, W.-Y.; Che, C.-M. *J. Am. Chem. Soc.* **2000**, *122*, 5337.
(6) Zhang, J.-L.; Zhou, H.-B.; Huang, J.-S.; Che, C.-M. *Chemistry – A European Journal* **2002**, *8*, 1554.
(7) Sono, M.; Roach, M. P.; Coulter, E. D.; Dawson, J. H. *Chem. Rev. (Washington, D. C.)* **1996**, *96*, 2841.
(8) Zhu, Y.; Murali, S.; Stoller, M. D.; Ganesh, K. J.; Cai, W.; Ferreira, P. J.; Pirkle, A.; Wallace, R. M.; Cychosz, K. A.; Thommes, M.; Su, D.; Stach, E. A.; Ruoff, R. S. *Science (Washington, DC, U. S.)* **2011**, *332*, 1537.
(9) Li, Y.; Zhou, W.; Wang, H.; Xie, L.; Liang, Y.; Wei, F.; Idrobo, J.-C.; Pennycook, S. J.; Dai, H. *Nat. Nanotechnol.* **2012**, *7*, 394.
(10) Cai, W.; Piner, R. D.; Stadermann, F. J.; Park, S.; Shaibat, M. A.; Ishii, Y.; Yang, D.; Velamakanni, A.; An, S. J.; Stoller, M.; An, J.; Chen, D.; Ruoff, R. S. *Science (Washington, DC, U. S.)* **2008**, *321*, 1815.
(11) Scheuermann, G. M.; Rumi, L.; Steurer, P.; Bannwarth, W.; Mulhaupt, R. *J. Am. Chem. Soc.* **2009**, *131*, 8262.
(12) Gao, Y.; Ma, D.; Wang, C.; Guan, J.; Bao, X. *Chem. Commun. (Cambridge, U. K.)* **2011**, *47*, 2432.
(13) Zhu, Z.; Su, D.; Weinberg, G.; Schloegl, R. *Nano Lett.* **2004**, *4*, 2255.
(14) Erickson, K.; Erni, R.; Lee, Z.; Alem, N.; Gannett, W.; Zettl, A. *Adv. Mater. (Weinheim, Ger.)* **2010**, *22*, 4467.
(15) Imran Jafri, R.; Rajalakshmi, N.; Ramaprabhu, S. *J. Mater. Chem.* **2010**, *20*, 7114.
(16) Che, C.-M.; Lo, V. K.-Y.; Zhou, C.-Y.; Huang, J.-S. *Chem. Soc. Rev.* **2011**, *40*, 1950.
(17) Nakagaki, S.; Wypych, F. *J. Colloid Interface Sci.* **2007**, *315*, 142.
(18) Fraile, J. M.; Garcia, J. I.; Mayoral, J. A. *Chem. Rev. (Washington, DC, U. S.)* **2009**, *109*, 360.
(19) (a) Xue, T.; Jiang, S.; Qu, Y.; Su, Q.; Cheng, R.; Dubin, S.; Chiu, C.-Y.; Kaner, R.; Huang, Y.; Duan, X. *Angew. Chem., Int. Ed.* **2012**, *51*, 3822(b) Guo, Y.; Deng, L.; Li, J.; Guo, S.; Wang, E.; Dong, S. *ACS Nano* **2011**, *5*, 1282(c) Song, Y.; Chen, Y.; Feng, L.; Ren, J.; Qu, X. *Chem. Commun. (Cambridge, U. K.)* **2011**, *47*, 4436.
(20) (a) Jahan, M.; Bao, Q.; Loh, K. P. *J. Am. Chem. Soc.* **2012**, *134*, 6707(b) Xu, Y.; Zhao, L.; Bai, H.; Hong, W.; Li, C.; Shi, G. *J. Am. Chem. Soc.* **2009**, *131*, 13490(c) Geng, J.; Jung, H.-T. *J. Phys. Chem. C* **2010**, *114*, 8227.
(21) **2013**, *12*.
(22) Dreyer, D. R.; Park, S.; Bielawski, C. W.; Ruoff, R. S. *Chem. Soc. Rev.* **2010**, *39*, 228.
(23) Gomez-Navarro, C.; Meyer, J. C.; Sundaram, R. S.; Chuvilin, A.; Kurasch, S.; Burghard, M.; Kern, K.; Kaiser, U. *Nano Lett.* **2010**, *10*, 1144.
(24) Thies, S.; Bornholdt, C.; Koehler, F.; Soennichsen, F. D.; Naether, C.; Tuczek, F.; Herges, R. *Chem. - Eur. J.* **2010**, *16*, 10074.
(25) Nanda, A. K.; Kishore, K. *Macromolecules* **2001**, *34*, 1600.
(26) G. N. La Mar, F. A. W. a. D. D., (Ed.), 1979.
(27) Bolze, F.; Gros, C. P.; Drouin, M.; Espinosa, E.; Harvey, P. D.; Guilard, R. *J. Organomet. Chem.* **2002**, *643-644*, 89.

Chapter **4**

Preparation of Graphene suspensions in volatile solvents

I. Introduction

Graphene, a two-dimensional (2D) sheet of sp^2-hybridized carbon, has attracted considerable attention in the past few years due to its unique structure and properties, such as high electronic[1] and thermal[2] conductivities, great mechanical strength,[3] huge specific surface area[4] and optical properties.[5] The optical properties of graphene can be used in a variety of applications such as transparent electrodes in solar cells or liquid crystal devices.[6,7] Introduction of graphene in thin film technology for transparent conductive films is expected to improve several issues (1) improvement of electrical conductivity (2) enhancement of mechanical flexibility (3) reduction of material cost.[8,9]

Until now, graphene has been prepared mainly by using mechanical exfoliation,[10] dispersion of graphite in selective organic solvents,[11,12] chemical exfoliation,[13] and chemical vapor deposition.[14] Each of these methods has different advantages and disadvantages. For example, mechanical exfoliation and dispersion of graphite in organic solvents suffer from low throughput and poor reproducibility. In addition, the drawback of the chemical exfoliation is creation some defects on the graphene sheets.

The most common approach to produce massive graphene takes place *via* chemical exfoliation. This implies the formation of graphene oxide (GO) by graphite oxidation followed by reduction in order to form reduced graphene oxide (rGO).[15,16] However, the graphitic structure is dramatically affected during the oxidation process and cannot be fully restored and therefore graphene properties are significantly affected.[17,18]

Recently, another liquid-phase method, without oxidation and reduction, was introduced by direct exfoliation of graphite in a certain solvent and formation of graphene in solution just using ultrasonication. Some solvents and surfactant/solvent mixtures have shown positive results for exfoliation and dispersion of graphene,[15,19] however, these solvents are usually expensive, toxic and difficult to remove because of their high boiling points; and their residues in the final samples are certainly detrimental to the expected excellent properties of graphene.[11,20,21]

Probably the most promising LPE procedure is based on the graphite exfoliation using N-methyl-2-pyrrolidone (NMP) as solvent.[11] Despite having high quality graphene layers in graphene- NMP suspensions and high stability of the suspensions,[22] this method has some drawbacks due to the features of NMP, which is a non-green solvent[23] with a high boiling point that may prevent the process ability of the graphene suspensions.

Recently, carbon materials, especially graphene and its derivates, have been used in catalytic oxidation reactions as well as electro-chemical oxidation processes.[24,25,26] Graphene contains a large π-electron structure, appropriate for π-stacking type adsorption, and its open edges also give it an extra electronic state due to a localized state at the edges.[27] Therefore, graphene has been considered as an attractive new material for electrochemical sensors.[28,29]

Graphene, because of the properties like large exposed area and excellent electronic mobility, can be a viable co-catalyst to accept electrons for exciton separation in the photocatalysts.[30,31]

The immobilization of a homogeneous catalyst onto a solid surface is one of the major challenges in catalysis, because it may facilitate the recovery of the catalyst and its separation from the reaction products and may also give rise to the reutilization of the catalyst in multiple subsequent cycles.

By considering these properties of Graphene, in this work, we compared the effectiveness of the LPE process in different solvent/water mixtures and we further developed protocols to obtain graphene suspensions in water-free solvents, to solve the problem of dispersibility of graphene suspensions on different solvents and make more universal the use of graphene in suspensions. This would allow using graphene as additive in photocatalysis system. Graphene could also be used to prepare transparent conductive electrodes, which can be used as solid support for catalyst for reduction electrocatalytic system.

II. Experimental procedures

II.1. Preparation of different solvent-water inks

Graphene-ink dispersion is prepared by sonicating 50 mg graphite in 10 mL *S*:water (*S*= tetrahydrofurane, ethanol, acetone and acetonitrile) during 90 min. at 380 watt with 37 Hz, followed by centrifugation at 550 g for 60 minutes in a glass vial with inner diameter of 20 mm. Several ratios of solvent (*S)* and water mixtures were explored to determine the optimum mixing *S*: water ratio.

Determination of optimal solvent-water mixture

The graphene concentration was calculated by measuring the absorption at 270 nm, being the corresponding absorption coefficient 3180 $L.g^{-1}.m^{-1}$ as experimentally determined (figure 4.1).

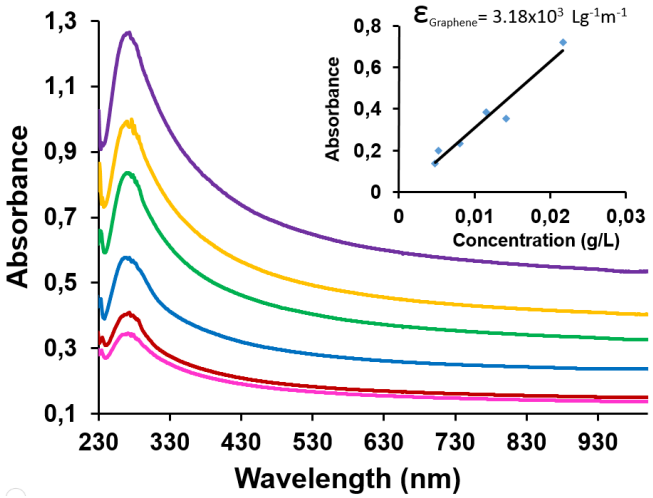

Figure 4.1. UV-vis spectra measured in a 1cm quartz cuvette for graphene suspensions in THF-water (4:1) with concentrations ranging from 0.005 g/L to 0.03 g/L. Molar absorptivity of graphene is determined considering absorption at 270 nm (inset).

In order to optimize the mixtures of organic solvent and water allowing the highest graphene concentration in suspension, several ratios solvent *vs* water were tested (table 4.1).

Table 4.1. Concentration (mg/mL) of graphene-ink in different ratios of different solvents-water mixtures. These suspensions were prepared by using 50 mg graphite in 10 mL solvents with 90 min. sonication (380 watt. 37 kHz) and followed by centrifuge with 550 g for 60 min. All concentrations are in gL^{-1}.

Solvent : water	1:4	1:1	4:1
THF-Water	0.010	0.060	0.097
EtOH-Water	0.006	0.025	0.048
Acetone-Water	0.016	0.05	0.072
Acetonitrile-Water	0.016	0.011	0.006

II.1.1. UV-Vis Characterization

The highest graphene concentration was achieved in the mixture of THF-water (4:1). figure 4.2 shows the UV-vis spectra and optical images of graphite suspended in a THF-water (4:1) mixture after sonication. As shown in table 4.1 different graphene concentrations

were reached by using several organic solvent-water mixtures. Pure water and pure organic solvents did not exfoliate graphite, while the use of an appropriate organic solvent mass fraction results on dark black graphene dispersions.

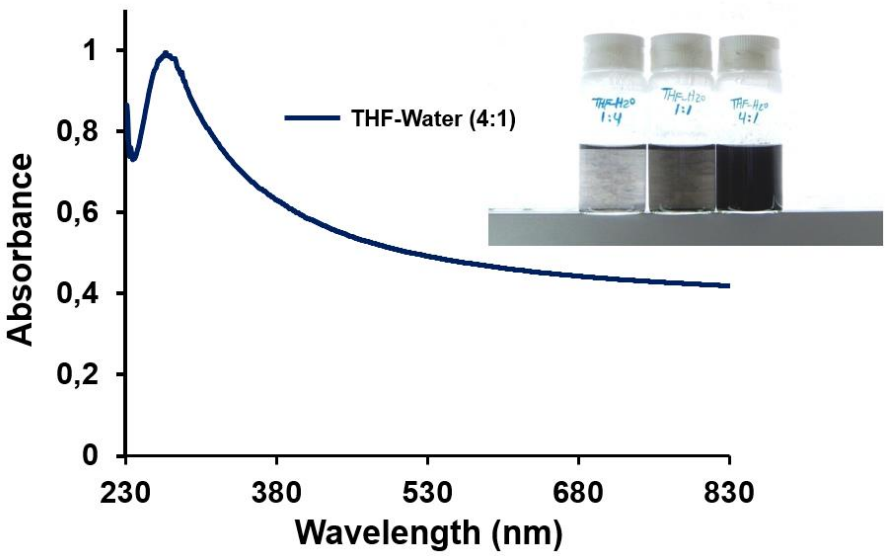

Figure 4.2. Absorbance of graphene suspensions diluted to 10%. The inset shows several vials of undiluted suspensions.

Typically, the UV-vis spectra observed for all organic solvent: water suspensions are comparable to the one shown in figure 4.2, which is mostly featureless, being the peak in the UV region the signature of the van Hove singularity in the graphene density of states.[32] The maximum yield obtained in our exfoliation experiments was found using a 4:1 THF-water mixture, which is several hundred times higher than that in pure water or THF and comparable to that previously reported maximum values in N-methyl-2-pyrrolidone (NMP)[11] and, other mixtures using ionic surfactants in water.[33] Interestingly, the exfoliation procedure reported herein takes only 90 min. of sonication, which is considerably shorter than previous reported methods. In all cases, suspensions were very stable at room temperature being the optical measured sedimentation less 20 % after 3 months at room temperature.

III. Preparation of THF-water inks

As we observed the highest graphene concentration was achieved in the mixture of THF-water (4:1) we have concentrated on this mixture due to the fact that other parameters such as the initial quantity of graphite, time and power of sonication, as well as centrifugal

force (g) and time of centrifuge, play also a key role in concentration, quality and quantity of the flakes in suspensions.[34]

It is worth to mention that with using different amount of initial graphite in the same conditions and mixture, the yield of exfoliation is always constant and it is around 2% of initial graphite. As shown in figure 4.3, for instance, by using 50 mg graphite the concentration of suspension is around 0.1 gL^{-1} while it can be reached to 0.2 gL^{-1} by increasing twice the amount of graphite. Additionally, several cycles of sonication-centrifugation applied to the remaining unexfoliated graphite, phase separated from the graphene-ink by centrifugation, produce additional graphene-inks (2% yield for each cycle according to amount of dried unexfoliated graphite) after recycling to an appropriate treatment based on sonication-centrifugation.

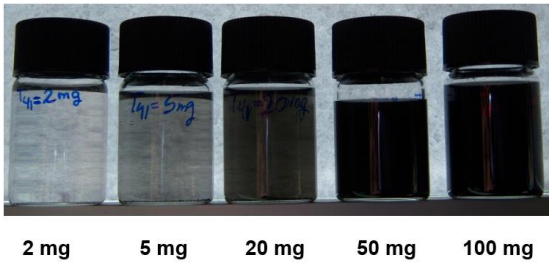

Figure 4.3. Effect of the initial quantity of graphite in the final graphene-ink concentration using the optimized THF-water mixture (80 % wt).

To see the effect of the power of sonication bath and also relative centrifugal force (g) and time of centrifuge a series of experiments were carried out keeping constant the initial amount of graphite (50 mg/ml) were prepared.

Suspension **A**: This suspension is prepared by sonicating 50 mg graphite in10 mL of THF-water (4:1) during 90 min. at 380 watt with 37 Hz, followed by centrifugation at 550 g for 60 minutes.

Suspension **B:** This suspension is prepared by sonicating 50 mg graphite in10 mL of THF-water (4:1) during 90 min. at 310 watt with 40 Hz, followed by centrifugation at 4500 g for 30 minutes.

Suspension **C**: This suspension is prepared by sonicating 50 mg graphite in10 mL of THF-water (4:1) during 90 min. at 310 watt with 40 Hz, followed by centrifugation at 16000 g for 10 minutes.

The graphene concentration of different suspensions, measured by UV-Vis spectroscopy are shown in the table 4.2.

Table 4.2. Different suspension of THF/Water (4:1) with different parameter of sonication and centrifuge.

Suspensions	**A**	**B**	**C**
Sonication (Power-Time)	380 W-90 min	310 W-90 min	310 W-90 min
Centrifuge (Gravitational acceleration-Time)	550- 60 min	4500- 30 min	16000-10 min
Concentration measured by UV-Vis	0.1mg/ml	0.05 mg/ml	0.03 mg/ml

IV. Characterization of the materials obtained

IV.1. DLS and AFM Characterization

The dimensions of the flakes were evaluated by DLS (dynamic light scattering) for all suspensions. As shown in figure 4.4, it is clear that by increasing the speed of centrifuge the dimension of the flakes decreased their average hydro-dynamic radius. As shown in figure 4.4(d), for suspension **C,** additional 90 min. of sonication at 310 W, do not significantly change flakes dimensions

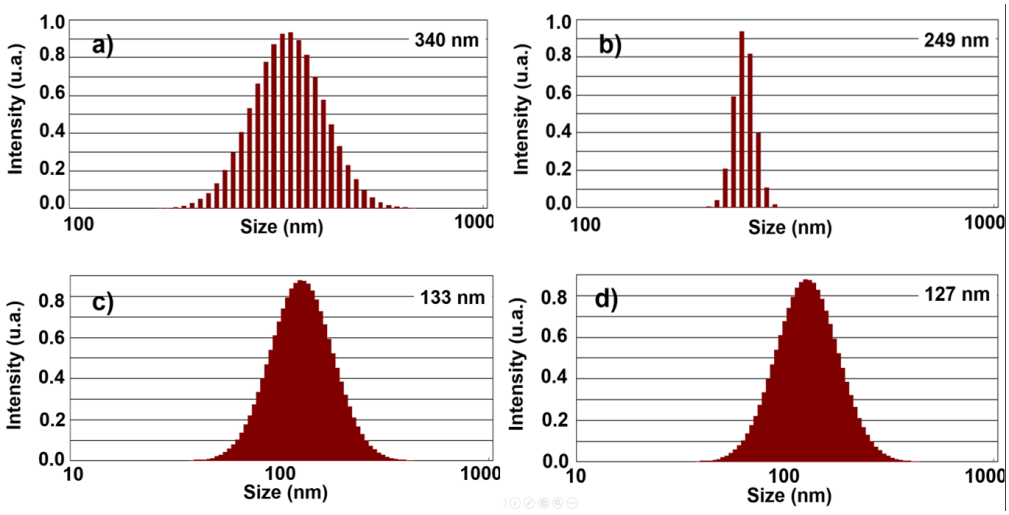

Figure 4.4. DLS of graphene suspension for THF/water (4:1) of suspension a) **A** b) **B** c) **C** and d) 180 min. sonication with 310 W and followed by centrifuge at 16000 for 10 min.

In a further effort to estimate not only the lateral dimensions but also the height of the flakes, AFM measurements for all suspensions were done for more than 20 flakes from at

least three different macroscopic areas of the studied surface (figure 4.5). As it is shown in table 4.3, DLS and AFM results are in good agreement, both indicating that using lower speed of centrifuge, the thickness and the size of flakes significantly increase. It has to be noticed that on surface deposition of graphene suspensions may produce some degree of graphene flakes aggregation affecting to the observed heights.

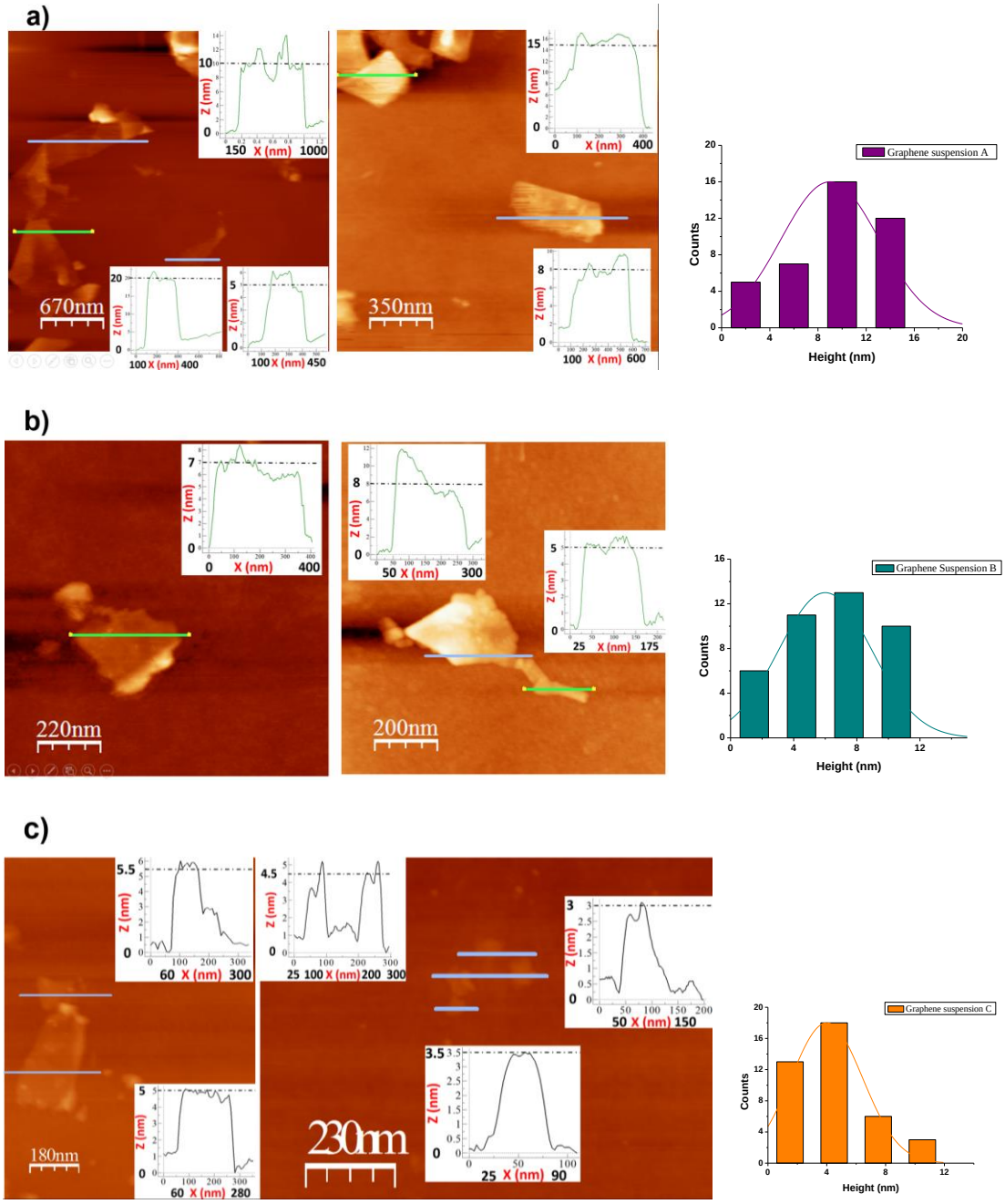

Figure 4.5. Selected representative topographic AFM images of graphene suspensions **A** (a), **B** (b) and **C** (c) deposited on SiO_2 surfaces.

Table 4.3. DLS and AFM results of different suspension of THF/Water (4:1) with different parameter of sonication and centrifuge.

Suspensions	**A**	**B**	**C**
Sonication (Power-Time)	380 W- 90 min	310 W- 90 min	310 W- 90 min
Centrifuge (Gravitational acceleration-Time)	550- 60 min	4500- 30 min	16000- 10 min
AFM (Lateral dimensions-height)	320 nm- 12 nm	220 nm- 8 nm	120 nm- 4 nm
DLS	340 nm	249 nm	133 nm

The height of flakes was determined by AFM and found to be in the range between 3 to 20 nm. Furthermore, thickness discrimination was achieved by adjusting centrifugation parameters (figure 4.5). Thus, the average thickness can be decreased from 12 nm after applying 550 g centrifuge force during 60 min. to 4 nm by applying 16000 g force during 10 min. Thus, higher centrifugal forces allows just the thinner flakes to remain in solution, which is attractive regarding applications such as transparent electrodes (*vide infra*) but also induces a significant decrease of the graphene concentration. In fact, suspensions with flakes averaging 4 nm of thickness have a graphene content of 0.03 mg/ml.

Crystallinity, content of defects and presence functional groups were estimated by electron diffraction, powder X-ray diffraction, Raman and FT-IR spectroscopies (figure 4.6-4.9). The whole set of data supports that highly crystalline flakes with low defect content and non-appreciable amounts of oxidized functional groups were obtained by the already mentioned experimental LPE conditions.

IV.2. TEM Characterization

The dimensions and quality of graphene-ink also were evaluated by TEM and electron diffraction measurements for THF-water (4:1) (suspension **A**) (figure 4.6).

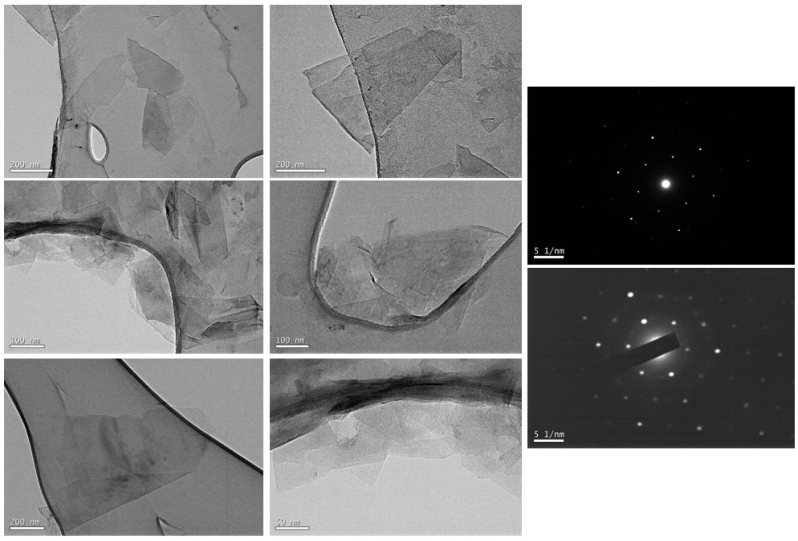

Figure 4.6. TEM images and electron diffraction patterns of dispersion few layers graphene.

To study the graphene film's crystalline grain structure, selected area electron diffraction (SAED) patterns was obtained (figure 4.6), which are an array of hexagonal spots that reflect the graphene sample's internal crystal structure. The simple hexagonal spot pattern is due to the hexagonal carbon lattice from a single crystal of graphene. Changes in the graphene lattice's orientation cause rotations in the hexagonal SAED pattern, and multiple grains of graphene produce multiple hexagonal SAED patterns. The areas in which the spot pattern was identical and nonrotated indicate a single crystal of graphene. Therefore, six diffraction spots in the SAED pattern confirm the single crystalline nature of graphene films, and if it is not hexagonal confirm the multi-layer of the graphene together. As shown in figure 4.6, we have multi-layer of graphene.

IV.3. Raman and IR Characterization

The exfoliation level and the defect content of the graphene obtained were also evaluated by Raman spectroscopy. Figure 4.7 plots typical Raman spectra observed for graphite and suspensions **A-C** deposited on SiO_2. Raman spectra show characteristics D-band (~1360 cm^{-1}), a G-band (~1584 cm^{-1}) and a 2D-band (~2720 cm^{-1}). The intensity ratio of ID/IG gives us an idea of defect contents in the flakes: higher is the ratio, highest is the defect content. Such ratio has been measured for several flakes from different suspensions as shown in figure 4.7 (b-d).The ID/IG values found are in the range of 0.4-0.6 for suspension **C**, 0.4-1.0 for suspension **B** and 0.4- 1.1 for suspension **A**. The spectra show D bands

significantly larger than those of the starting graphite powder, indicating that the preparation process induces some structural defects. Such defects can be of two main types: basal plane defects and edge defects. Basal plane defects can generally result in an obvious broadening of G band, which is found in chemically reduced graphene and it is not the case that it is observed for these suspensions. Edge defects are unavoidable, because cavitation-induced shear force and shock waves cut the initial large crystallite into smaller flakes.

These smaller graphene flakes increases the content of edge defects because they are smaller than the spot of laser.

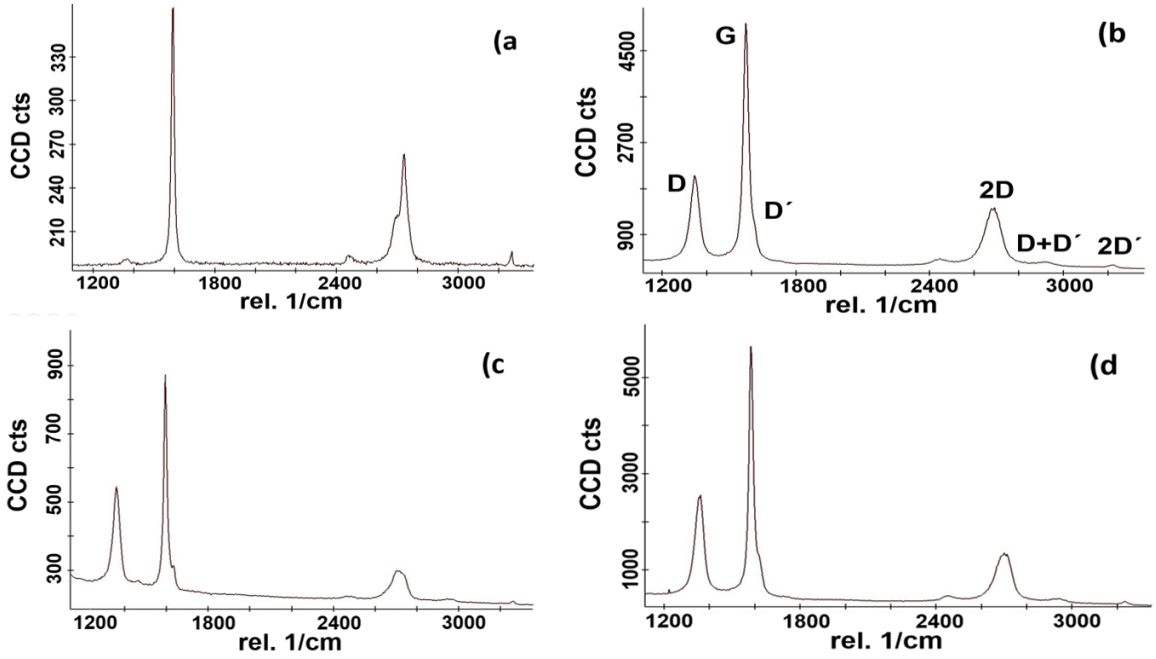

Figure 4.7. Selected Raman spectra measured on SiO_2 surface for graphite (a) and suspensions **A** (b) **B** (c) and **C** (d) on spray-coated SiO_2.

The FTIR spectrum of dried suspension **A** in figure 4.8 shows peaks around 1560 cm^{-1}, which are assigned to the stretching of C=C bonds of graphitic domains. Most importantly, the spectrum shows no peaks associated with C–OH (~1340 cm^{-1}*)* and –COOH (~1700–1800 cm^{-1}*)* groups. This result agrees with non-chemical functionalization of the graphene flakes. As shown in figure 4.8 the same spectrums were observed for suspensions **B** and **C**.

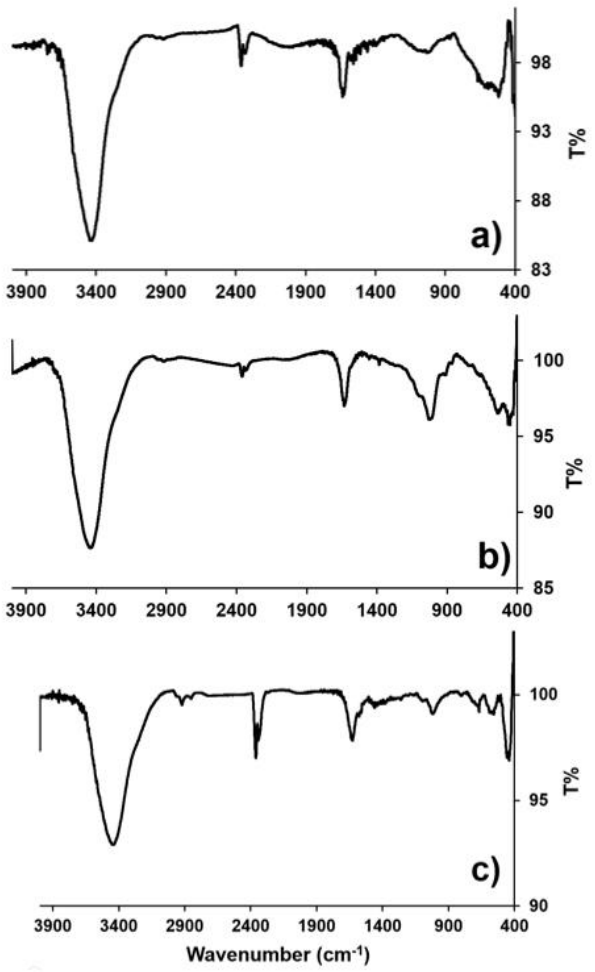

Figure 4.8. FTIR spectra of a dried graphene powder from suspensions **A** (a), **B** (b) and **C** (c) in KBr pellets.

IV.4. X-ray Powder diffraction Characterization

The X-ray powder diffraction from the solution **A** is shown in figure 4.9, together with the data obtained for graphite, shown for comparison. Considering the remarkably thin graphene layers from high degree of exfoliation, the intensity of the (002) peak dramatically decreases. In addition, no (004) peak can be detected for graphene powder, stating that the sub lattices are almost completely excluded for the long-range order greater than four layers.

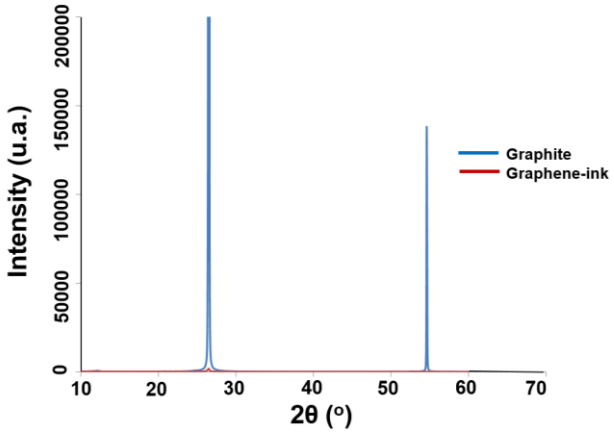

Figure 4.9. X-ray powder diffraction of initial graphite and dried graphene powder.

IV.5. TGA Characterization

TGA results presented in figure 4.10 show a small decrease in the mass of the graphene powder. This reduction takes place in two steps. First, the graphene mass decreases from 100 to 95 % by increasing the temperature from 180 to 500 ºC, this effect can be due to the release of residual solvents. The second peak corresponding to lose of 2 % of graphene mass takes place between 500 and 1000 ºC. This mass reduction is also observed in the TGA of graphite therefore it can be assigned to some small carbon impurities from the graphite starting material. For comparison, TGA of commercial graphene oxide is included in figure 4.10, in which it can be clearly observed a much higher mass decreasing upon heating. Overall, the TGA behavior of exfoliated few layers graphene is much closer to graphite than to graphene oxide, highlighting the chemical integrity of graphene flakes.

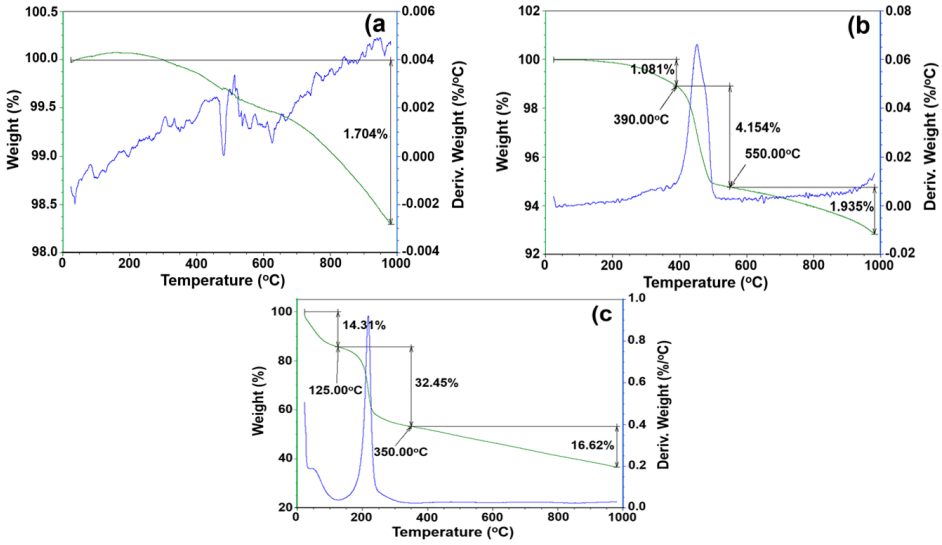

Figure 4.10. TGA of a) graphite, b) dried graphene powder, and c) commercial available graphene oxide.

V. Spray coating procedures

The high quality of the few-layers graphene flakes prompted us to use the suspensions obtained as inks in order to obtain conductive coatings. To get an optimal compromise between conductivity and transparency, we used suspensions containing flakes as thin as possible (graphene-ink of suspension C), resulting from centrifuge at 16000 g (average height flakes: 4 nm; graphene concentration: 0.03 mg/mL).

As shown in figure 4.11, glass substrates on a heater at 175 ºC were sprayed (5 cm distance from spray to the surface) by using a Meinhard TR-30-K1 nebulizer with a flow of argon (0.5 mL/min.). The film thickness can be controlled by the number of spray passing and the ink concentration.

Figure 4.11. Schematic procedure of spraying the glass surfaces on the heater.

V.1. Optical microscope Characterization of the film

After spray-on deposition of graphene inks on the surface the residual solvent was eliminated by a simple annealing process (baking on a hot plate at 350 ºC in air for 15 min.) were used for film preparations. In fact, the initial inhomogeneities distribution of the deposited material is improved by annealing (figure 4.12) with a significant improvement in the conductivity values of the films (*ca*. 2–3 orders of magnitude).

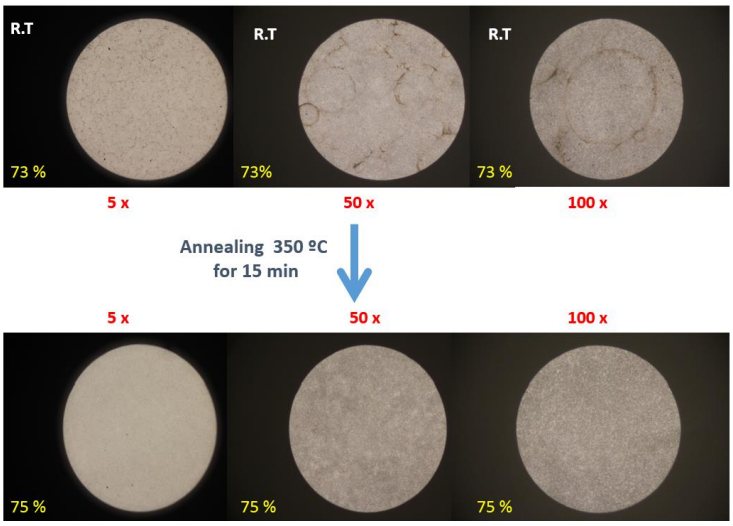

Figure 4.12. Optical images of different zoom of the coated films with suspension C before and after annealing (350 ºC for 15 min.).

V.2. Electrical conductivity Characterization of the film

We examined the respective performance, transmittance *vs* sheet resistance of the sprayed graphene films (figure 4.13). At approximately 80 % transmittance, the sheet resistance reaches to *ca*. 80 kΩsq^{-1}. This value is about 1-2 orders of magnitude lower than that reported for other transparent conductors based on inkjet printed graphene[32] or reduced graphene oxide,[35] and similar to the best graphene-ink reported.[36] It is clear that by spraying a larger amount of graphene ink, we sacrifice the transparency, but the conductivity significantly increased. For instance, on a glass with 73 % transparency, the sheet resistance is *ca*. 20 kΩsq^{-1}. These results show a significant improvement with respect to those recently reported based on graphene sheets produced by liquid phase exfoliation.

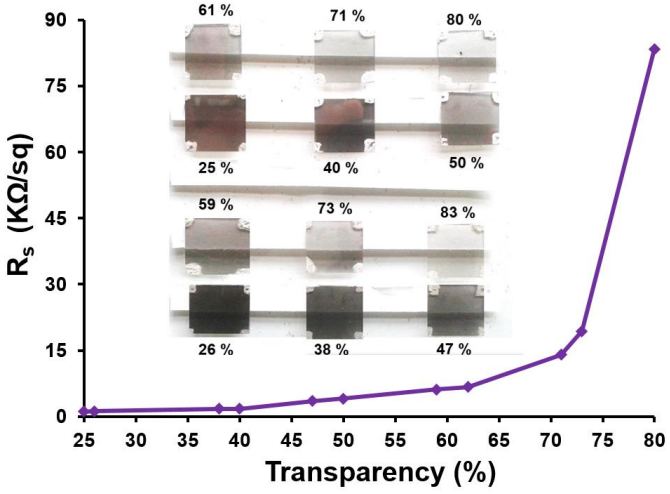

Figure 4.13. Sheet resistance *vs* transmittance for THF-water coated films by spray method.

V.3. AFM Characterization of the film

AFM topographic images were analyzed in order to determine the surface roughness of films generated by spraying graphene-inks sprayed on glass substrates with different levels of transparencies. A general inspection show that the roughness significantly increase upon decreasing the level of transparency. Thus, at *ca*. 80% the mean roughness is ± 20 nm while at a 70 % of transparency increase to ± 35 nm. Additionally, the decrease of the transparency produces an increase of heterogeneous areas. Figure 4.14 shows a topographic AFM image of glass substrate covered with graphene-ink (suspension C) with a level of transparency of 80 %. The image shows a homogeneous coverage with a roughness of ± 20 nm (estimated by analysis of the variations in the height profiles).

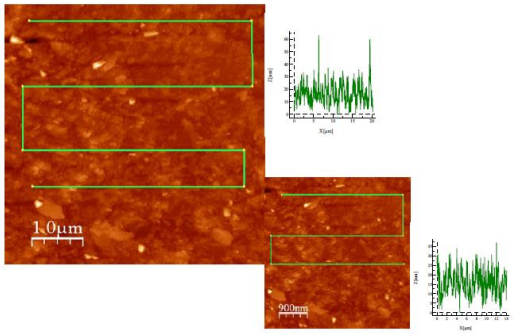

Figure 4.14. Large AFM topographic image and a zoomed area of a glass substrate covered with graphene-ink with a level of transparency of 80 % (inset shows their height profiles).

VI. Preparation of graphene powder

An unreported feature found in this work is the fact that from the graphene suspensions obtained, a powder can be isolated and subsequently re-dispersed in a variety of solvents**,** including even pure solvents where direct exfoliation was not achieved. This is a remarkable achievement because it makes possible to obtain few layers graphene dispersions in a wide range of media, conferring an unreported versatility to LPE techniques. Thus, the results reported herein can enable further implementation of graphene processing methods that make graphene-based technologies more accessible, technically and economically. In fact, the graphene powders isolated from the suspension of graphene in THF/water (4:1) can be obtained by two methods:

1) Powder **1** is obtained upon complete vacuum dryness of a THF-water (4:1) suspension (also named as dried graphene powder).

2) Powder **2** is isolated by adding diethyl ether to the initial THF-water (4:1) suspension provoking a fast precipitation of graphene powder (also named as precipitated graphene powder). Addition of 1 mL diethyl ether to 4 mL freshly sonicated THF-water suspension B results in fast precipitation of a black powder that can be easily collected by using centrifuge with high speed (16000 g for 3 min.), washed several times with only distilled THF, and then completely dried under vacuum. The solid graphene material can be re-dispersed into different solvents such as EtOH or THF.

VI.1. IR Characterization of graphene powders

As shown in figure 4.15 (b, c) no chemical/spectroscopic differences were observed between the two types of graphene powder. In Figure 4.15(d) that corresponds to GO, the spectrum shows peaks associated with C–OH (~1340 cm^{-1}) and –COOH (~1710–1720 cm^{-1}) groups, that we cannot see these peaks in the spectrum of the graphene powder. This result agrees with non-chemical functionalization of the graphene flakes.

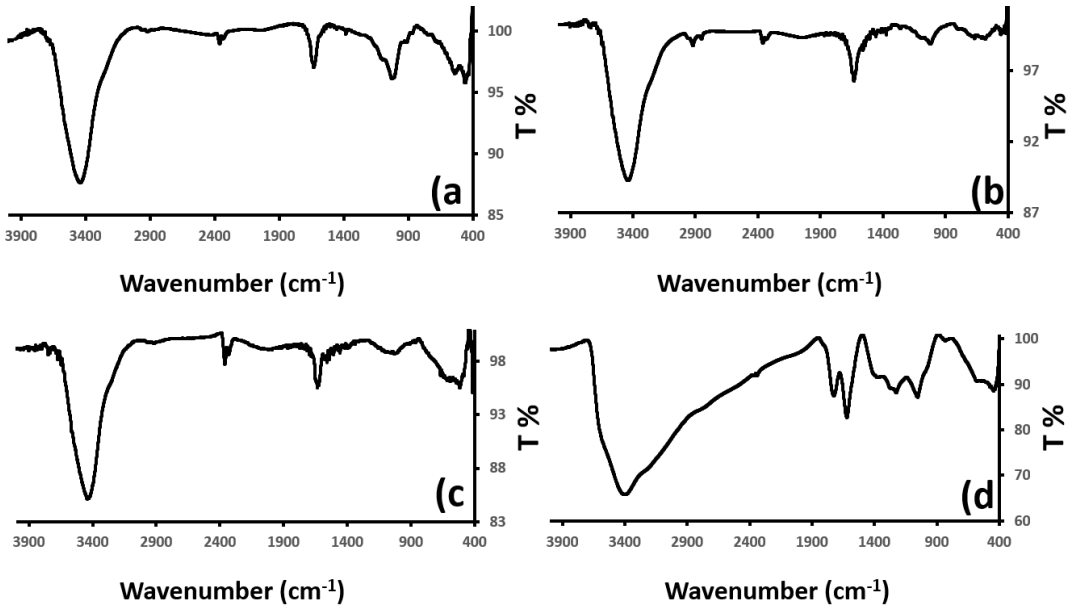

Figure 4.15. FTIR spectra of a) graphite, b) precipitated graphene powder **1**, c) dried graphene powder **2**, and d) commercial graphene oxide.

VI.2. SEM characterization of the powder

Characterization of both graphene powders was carried out by means of scanning electron microscopy (SEM). Typical SEM images of both graphene powders are shown in

Figure 4.16- 4.17. Interestingly, while no chemical/spectroscopic differences (figure 15) were observed between the two types of graphene powders, different morphologies were found depending on the precipitation method. On one hand, globular structures are observed for precipitate graphene powder. In contrast, laminar structures are found in the dried graphene powder. These observations suggest that fast precipitation induced by adding an antisolvent prevents re-aggregation. Consistently, precipitated graphene powder is more efficiently re-dispersed than dried graphene powder (table 4.4).

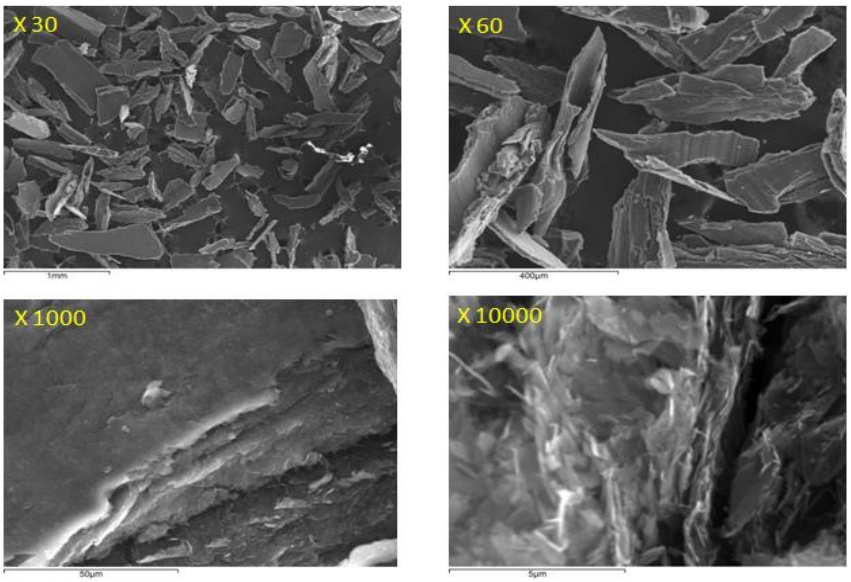

Figure 4.16. SEM images of dried graphene powder (**1**).

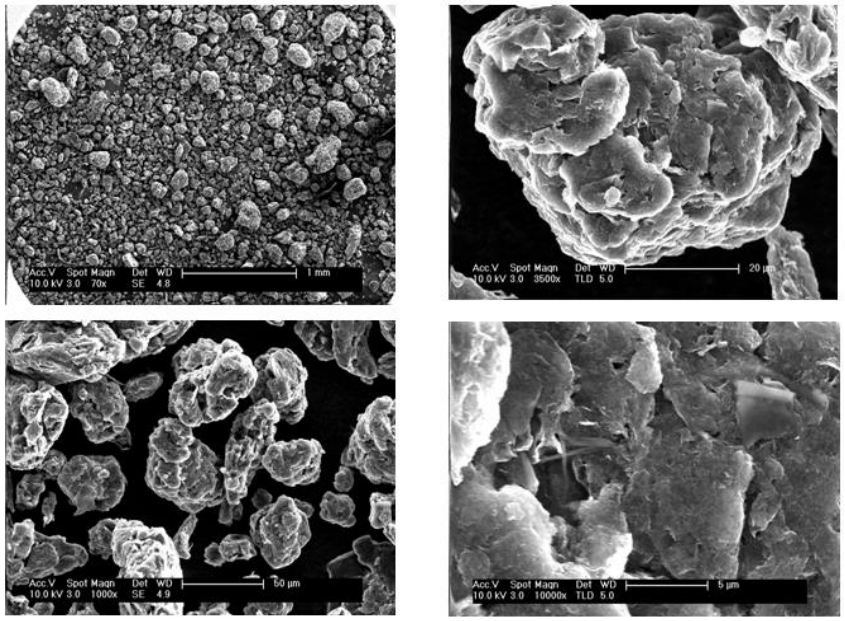

Figure 4.17. SEM images of precipitated graphene powder (**2**).

VII. Preparation of graphene suspensions in anhydrous media

In contrast to graphite, graphene powders **1** and **2** can be dispersed in a variety of solvents including pure organic solvents where direct exfoliation of graphite is not achieved (table 4.4). Dispersion of both powders were obtained using the same experimental conditions of sonication and centrifuge parameters.

In particular, by re-dispersing 1 mg of precipitated graphene powder **2** in 10 mL EtOH or THF by sonicating 90 min. at 310 watt of sonication power, and following by centrifuge at 550 g for 15 min, very stable suspensions of few layers graphene can be obtained (the optical measurements of sedimentation show high stability, > 3 months, with less than 20 % of material precipitated). As measured by UV-vis spectroscopy, the concentrations of graphene obtained were 0.07 and 0.05 mg/mL for EtOH and THF respectively. It means the yields were 70 and 50 % for EtOH and THF, respectively. In contrast, under the same conditions dried graphene powder was re-dispersed with yields of 40 and 20 % for EtOH and THF, respectively.

It is observed that the precipitated graphene powder **1**, is more efficiently re-dispersed than dried graphene powder **2**. This could be due to the structure show by **1** which is less compact in comparison with that observed for **2** (figures 4.16 and 4.17).

Table 4.4. Comparison of degree of dispersion between exfoliation of graphite and graphene powders that were obtained with different methods (90 min. sonication at 380 W and followed by centrifuge at 550 g for 15 min.).

	Solvent (10 ml)	**Concentration (mg/ml) (380 W- 90 min- 550 g- 15 min)**
1 mg precipitated graphene powder	EtOH	0.07 (70%)
1 mg dried graphene powder	EtOH	0.04 (40%)
50 mg- Graphite	EtOH	0.002 (0.04%)
1 mg precipitated graphene powder	THF	0.05 (50%)
1 mg dried graphene powder	THF	0.02 (20%)
50 mg Graphite	THF	0.001 (0.02%)

VII.1. UV-Vis characterization of graphene suspension in anhydrous media

Figure 4.18 shows the UV-vis spectra of dilute suspensions of re-dispersed powders in pure EtOH. UV-vis spectra of both graphene powder **1** and **2** is the same and consisting with non-functionalized graphene flakes in suspensions.

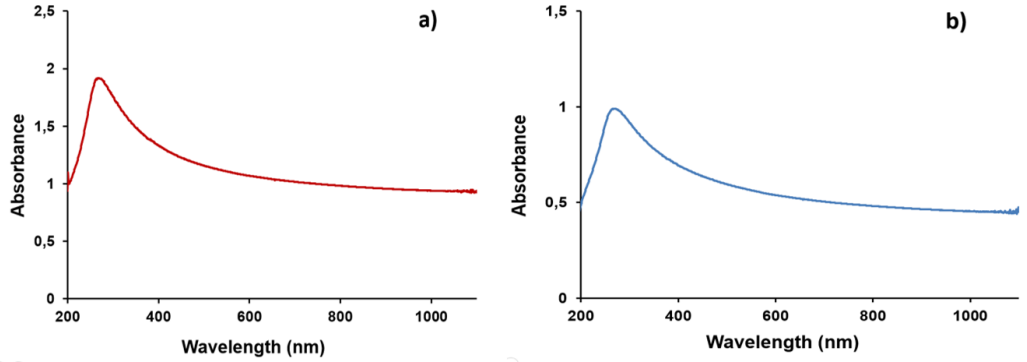

Figure 4.18. UV-vis spectra of a) precipitated graphene powder **1** and b) dried graphene powder **2** in pure EtOH.

VII.2. Raman characterization of graphene suspension in anhydrous media

The intensity ratio of ID/IG of several flakes in Raman spectra (figure 4.19) for redispersed participated graphene powder in pure EtOH or THF are 0.5-1.0 and 0.4-1.1, respectively. Such values are not far from what is observed for original suspensions A-C, indicating that re-dispersion in pure organic solvents do not implies a significant increase of defective structures in graphene flakes.

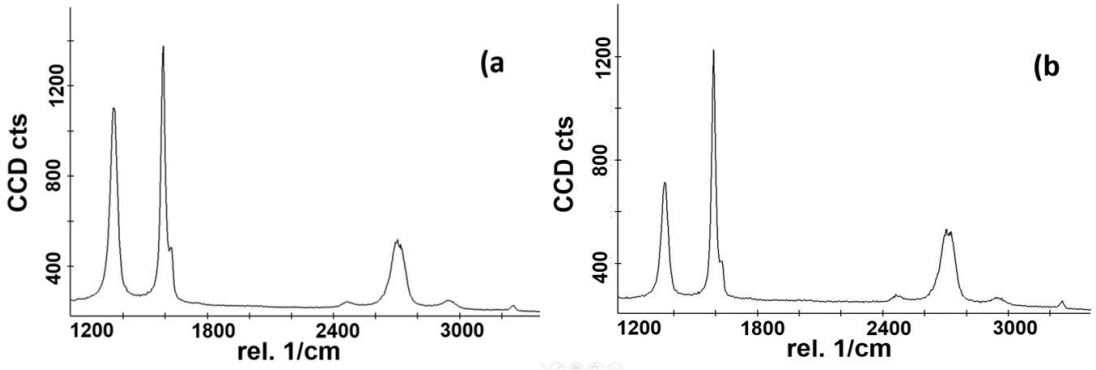

Figure 4.19. Example of Raman spectra measured by depositing re-dispersed participated graphene powder on SiO_2 surface by spray method in pure a) EtOH and b) THF solvents.

VII.3. DLS characterization of graphene suspension in anhydrous media

In order to evaluate the dimension of the flakes, DLS measurements were carried out for graphene suspensions in pure EtOH and THF solvents from precipitated graphene powder. As shown in figure 4.20, the size of the flakes are in both cases close to 200 nm, and also close to what is found in the THF/Water suspension B**,** that is used to produce precipitated graphene powder.

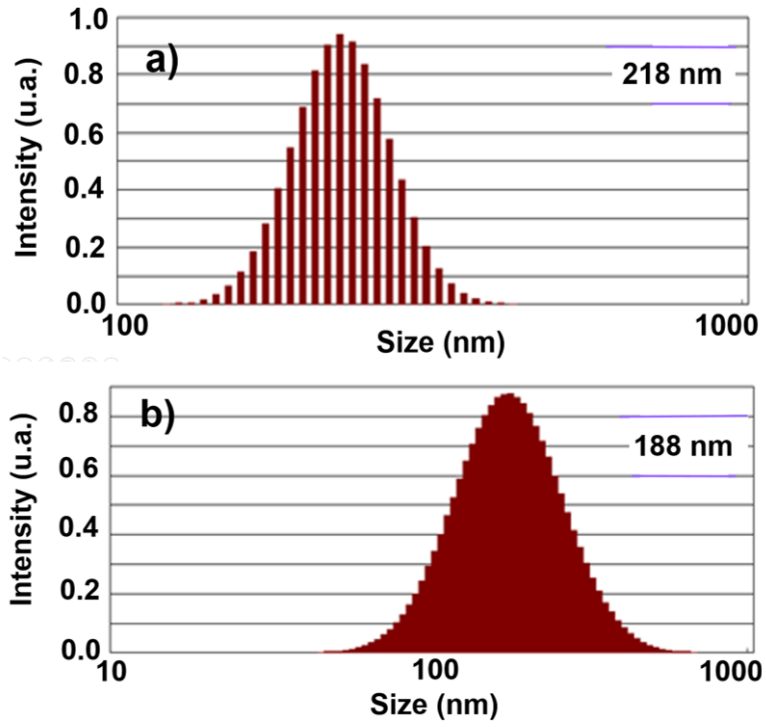

Figure 4.20. DLS of graphene suspension of precipitated graphene powder in pure a) EtOH b) THF solvents.

VIII. Ink preparation and spray coating procedures

Suspensions in pure THF or ethanol can also be used to efficiently coat surfaces. For this purpose, we used suspensions from re-dispersed precipitated graphene powders in THF or ethanol after centrifuge at 16000 g (concentration of graphene: 0.03 and 0.02 mg/mL for EtOH and THF respectively.) The obtained suspensions were sprayed on glass surfaces heated at 175 ^{o}C. After annealing process (350 ^{o}C for 15 min.) conductivity was measured. The values of sheet resistance found as a function of transparency are shown in figure 4.21.

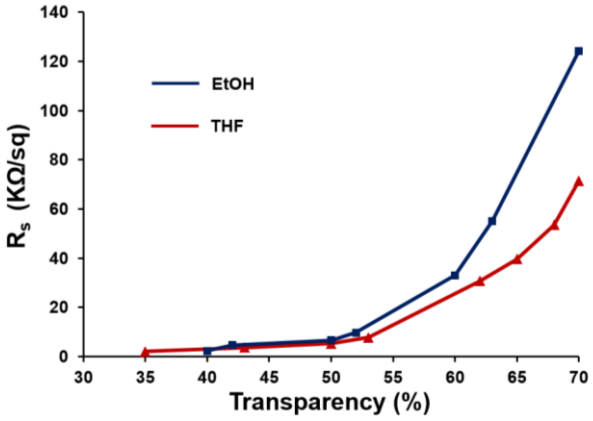

Figure 4.21. Sheet resistance *vs* transmittance for coated films with only THF or EtOH by spray method.

It is noteworthy that the sheet resistance on surfaces with 70 % transparency is less than 70 and 130 $k\Omega sq^{-1}$ for THF and EtOH respectively. The simple procedure here reported enables the possibility to prepare highly stable graphene suspensions in a variety of pure organic solvents, and water-solvent mixtures. These graphene inks are formed from the graphene-powder isolated as a result of LPE of graphite in a mixture of water-organic solvent (organic solvent= THF, ethanol, acetone or acetonitrile). It is worth mentioning that this procedure allows us to form stable graphene suspensions in organic solvents in which graphite exfoliation is not feasible.

These suspensions consists of few-layer high quality graphene flakes with lateral dimensions up to 1 μm which are suitable as inks for spray on a variety of substrates. On glass spray, deposition of these graphene-inks results in electrodes with an electrical conductivity/transparency ratio beyond the state-of the- art in the field of deposited graphene suspensions for production of transparent conductive electrodes.[37] The present technology provides and efficient, scale-up and inexpensive method to fabricate graphene devices.

IX. What about catalysis?

Our initial goal in this chapter, was to use a nanostructured graphene surface where anchor well-known homogeneous HER electrocatalyst to develop a grafted material with good catalytic properties to generate the H_2. The graphene surface was made over a plain material using a graphene-flake ink. To generate a full-covered glass surface was necessary to spray a layer of graphene ink on it. The resistivity of the surface is so high in comparison with ITO or a standard glassy carbon electrode but it is lower than a commercial carbon ink.

However, sprayed graphene is a conductive material but its conductivity is not enough to be a reliable support electrode for HER, also it has a low surface area.

We have been successful on the comparison the effectiveness of the LPE process in different low boiling point and non-toxic solvents/water mixtures and also developed protocols to obtain graphene suspensions in water-free solvents and preparing the transparent and conductive films.

However, on one hand we have not been able to generate an efficient catalytic system from hybrid complex/graphene materials, because supramolecular attachment of complex to graphene surface was quite weak. Furthermore, as a consequence of the overall low electrode surface, the total amount of complex attach to the graphene was quite low, so hampered its use as catalysts. Although relatively high, conduction of graphene coating were not enough to use it as electrocatalyst systems. A different idea was using graphene in suspension as an additive to a system composed by Ruthenium photosensitizer and Cobalt reduction catalyst. We expected to see how graphene mediates between the two components. However, graphene absorption hampered the photoactivation of the system. Thus, again, an efficient catalytic system was not achieved, but in our quest we found new ways to prepare, graphene suspension and we learned how to optimize these inks to generate conductive transparent coatings.

X. Conclusions:

In this chapter, we show results on scalable methods to obtain suspensions in low boiling point solvents such as EtOH, THF and in the mixture of them with water. Those give us uniform size platelets of graphene, suitable for conductive coatings. In fact, for the first time, not only the graphene suspension in reasonable concentration is reported in only THF or EtOH, but also the suspension of THF/water mixture is introduced as a strong mixture to exfoliate the graphite to obtain stable suspension of graphene. A specific expected application of these different suspensions (graphene inks) is their ability to homogeneously coat surfaces by spray deposition in order to fabricate transparent and conductive films that may be useful for the fabrication of organic solar cells or low cost conductive paints.

References:

(1) Geim, A. K.; Novoselov, K. S. *Nat Mater* **2007**, *6*, 183.
(2) Balandin, A. A.; Ghosh, S.; Bao, W.; Calizo, I.; Teweldebrhan, D.; Miao, F.; Lau, C. N. *Nano Lett.* **2008**, *8*, 902.
(3) Lee, C.; Wei, X.; Kysar, J. W.; Hone, J. *Science (Washington, DC, U. S.)* **2008**, *321*, 385.
(4) Stoller, M. D.; Park, S.; Zhu, Y.; An, J.; Ruoff, R. S. *Nano Lett.* **2008**, *8*, 3498.
(5) Geim, A. K. *Science (Washington, DC, U. S.)* **2009**, *324*, 1530.
(6) (a) Eda, G.; Fanchini, G.; Chhowalla, M. *Nat. Nanotechnol.* **2008**, *3*, 270(b) Candini, A.; Klyatskaya, S.; Ruben, M.; Wernsdorfer, W.; Affronte, M. *Nano Lett.* **2011**, *11*, 2634.
(7) Lopes, M.; Candini, A.; Urdampilleta, M.; Reserbat-Plantey, A.; Bellini, V.; Klyatskaya, S.; Marty, L.; Ruben, M.; Affronte, M.; Wernsdorfer, W.; Bendiab, N. *ACS Nano* **2010**, *4*, 7531.
(8) Granqvist, C. G.; Hultaker, A. *Thin Solid Films* **2002**, *411*, 1.
(9) Chen, Z.; Cotterell, B.; Wang, W. *Engineering Fracture Mechanics* **2002**, *69*, 597.
(10) Novoselov, K. S.; Geim, A. K.; Morozov, S. V.; Jiang, D.; Zhang, Y.; Dubonos, S. V.; Grigorieva, I. V.; Firsov, A. A. *Science (Washington, DC, U. S.)* **2004**, *306*, 666.
(11) Hernandez, Y.; Nicolosi, V.; Lotya, M.; Blighe, F. M.; Sun, Z.; De, S.; McGovern, I. T.; Holland, B.; Byrne, M.; Gun'Ko, Y. K.; Boland, J. J.; Niraj, P.; Duesberg, G.; Krishnamurthy, S.; Goodhue, R.; Hutchison, J.; Scardaci, V.; Ferrari, A. C.; Coleman, J. N. *Nat. Nanotechnol.* **2008**, *3*, 563.
(12) Biswas, S.; Drzal, L. T. *Nano Lett.* **2009**, *9*, 167.
(13) Park, S.; Ruoff, R. S. *Nat. Nanotechnol.* **2009**, *4*, 217.
(14) Reina, A.; Jia, X.; Ho, J.; Nezich, D.; Son, H.; Bulovic, V.; Dresselhaus, M. S.; Kong, J. *Nano Lett.* **2009**, *9*, 30.
(15) Bonaccorso, F.; Sun, Z.; Hasan, T.; Ferrari, A. C. *Nat. Photonics* **2010**, *4*, 611.
(16) (a) Hecht, D. S.; Hu, L.-B.; Irvin, G. *Adv. Mater. (Weinheim, Ger.)* **2011**, *23*, 1482(b) Tung, V. C.; Allen, M. J.; Yang, Y.; Kaner, R. B. *Nat. Nanotechnol.* **2009**, *4*, 25.
(17) Stankovich, S.; Dikin, D. A.; Piner, R. D.; Kohlhaas, K. A.; Kleinhammes, A.; Jia, Y.; Wu, Y.; Nguyen, S. T.; Ruoff, R. S. *Carbon* **2007**, *45*, 1558.
(18) (a) Luo, Z.; Lu, Y.; Somers, L. A.; Johnson, A. T. C. *J. Am. Chem. Soc.* **2009**, *131*, 898(b) Tang, L.; Wang, Y.; Li, Y.; Feng, H.; Lu, J.; Li, J. *Adv. Funct. Mater.* **2009**, *19*, 2782.
(19) (a) Dreyer, D. R.; Park, S.; Bielawski, C. W.; Ruoff, R. S. *Chem. Soc. Rev.* **2010**, *39*, 228(b) Gomez-Navarro, C.; Weitz, R. T.; Bittner, A. M.; Scolari, M.; Mews, A.; Burghard, M.; Kern, K. *Nano Lett.* **2007**, *7*, 3499.
(20) (a) Dimiev, A.; Kosynkin, D. V.; Alemany, L. B.; Chaguine, P.; Tour, J. M. *J. Am. Chem. Soc.* **2012**, *134*, 2815(b) Yang, D.; Velamakanni, A.; Bozoklu, G.; Park, S.; Stoller, M.; Piner, R. D.; Stankovich, S.; Jung, I.; Field, D. A.; Ventrice, C. A., Jr.; Ruoff, R. S. *Carbon* **2009**, *47*, 145(c) Guardia, L.; Fernandez-Merino, M. J.; Paredes, J. I.; Solis-Fernandez, P.; Villar-Rodil, S.; Martinez-Alonso, A.; Tascon, J. M. D. *Carbon* **2011**, *49*, 1653.
(21) (a) Hamilton, C. E.; Lomeda, J. R.; Sun, Z.; Tour, J. M.; Barron, A. R. *Nano Lett.* **2009**, *9*, 3460(b) Bourlinos, A. B.; Georgakilas, V.; Zboril, R.; Steriotis, T. A.; Stubos, A. K. *Small* **2009**, *5*, 1841.
(22) Paton, K. R.; Varrla, E.; Backes, C.; Smith, R. J.; Khan, U.; O'Neill, A.; Boland, C.; Lotya, M.; Istrate, O. M.; King, P.; Higgins, T.; Barwich, S.; May, P.; Puczkarski, P.; Ahmed, I.; Moebius, M.; Pettersson, H.; Long, E.; Coelho, J.; O'Brien, S. E.; McGuire, E. K.; Sanchez, B. M.; Duesberg, G. S.; McEvoy, N.; Pennycook, T. J.; Downing, C.; Crossley, A.; Nicolosi, V.; Coleman, J. N. *Nat. Mater.* **2014**, *13*, 624.
(23) Capello, C.; Fischer, U.; Hungerbuehler, K. *Green Chem.* **2007**, *9*, 927.
(24) (a) Jiang, L.; Liu, C.; Jiang, L.; Peng, Z.; Lu, G. *Anal. Sci.* **2004**, *20*, 1055(b) Fujishima, A.; Rao, T. N.; Popa, E.; Sarada, B. V.; Yagi, I.; Tryk, D. A. *J. Electroanal. Chem.* **1999**, *473*, 179.

(25) (a) Heien, M. L. A. V.; Phillips, P. E. M.; Stuber, G. D.; Seipel, A. T.; Wightman, R. M. *Analyst (Cambridge, U. K.)* **2003**, *128*, 1413(b) Ramesh, P.; Suresh, G. S.; Sampath, S. *J. Electroanal. Chem.* **2004**, *561*, 173.

(26) (a) Gao, Y.; Ma, D.; Hu, G.; Zhai, P.; Bao, X.; Zhu, B.; Zhang, B.; Su, D. S. *Angew. Chem., Int. Ed.* **2011**, *50*, 10236(b) Gao, Y.; Ma, D.; Wang, C.; Guan, J.; Bao, X. *Chem. Commun. (Cambridge, U. K.)* **2011**, *47*, 2432(c) Gao, Y.; Hu, G.; Zhang, W.; Ma, D.; Bao, X. *Dalton Trans.* **2011**, *40*, 4542.

(27) (a) Ruoff, R. *Nat. Nanotechnol.* **2008**, *3*, 10(b) Nakada, K.; Fujita, M.; Dresselhaus, G.; Dresselhaus, M. S. *Phys. Rev. B: Condens. Matter* **1996**, *54*, 17954.

(28) (a) Wang, Y.; Li, Y.; Tang, L.; Lu, J.; Li, J. *Electrochem. Commun.* **2009**, *11*, 889(b) Alwarappan, S.; Erdem, A.; Liu, C.; Li, C.-Z. *J. Phys. Chem. C* **2009**, *113*, 8853.

(29) (a) Mallesha, M.; Manjunatha, R.; Nethravathi, C.; Suresh, G. S.; Rajamathi, M.; Melo, J. S.; Venkatesha, T. V. *Bioelectrochemistry* **2011**, *81*, 104(b) Kim, Y.-R.; Bong, S.; Kang, Y.-J.; Yang, Y.; Mahajan, R. K.; Kim, J. S.; Kim, H. *Biosens. Bioelectron.* **2010**, *25*, 2366.

(30) Yeh, T.-F.; Cihlář, J.; Chang, C.-Y.; Cheng, C.; Teng, H. *Materials Today* **2013**, *16*, 78.

(31) An, X.; Yu, J. C. *RSC Advances* **2011**, *1*, 1426.

(32) Torrisi, F.; Hasan, T.; Wu, W.; Sun, Z.; Lombardo, A.; Kulmala, T. S.; Hsieh, G.-W.; Jung, S.; Bonaccorso, F.; Paul, P. J.; Chu, D.; Ferrari, A. C. *ACS Nano* **2012**, *6*, 2992.

(33) Lotya, M.; Hernandez, Y.; King, P. J.; Smith, R. J.; Nicolosi, V.; Karlsson, L. S.; Blighe, F. M.; De, S.; Wang, Z.; McGovern, I. T.; Duesberg, G. S.; Coleman, J. N. *J. Am. Chem. Soc.* **2009**, *131*, 3611.

(34) Khan, U.; O'Neill, A.; Lotya, M.; De, S.; Coleman, J. N. *Small* **2010**, *6*, 864.

(35) Kong, D.; Le, L. T.; Li, Y.; Zunino, J. L.; Lee, W. *Langmuir* **2012**, *28*, 13467.

(36) Li, J.; Ye, F.; Vaziri, S.; Muhammed, M.; Lemme, M. C.; Oestling, M. *Adv. Mater. (Weinheim, Ger.)* **2013**, *25*, 3985.

(37) Parvez, K.; Li, R.; Puniredd, S. R.; Hernandez, Y.; Hinkel, F.; Wang, S.; Feng, X.; Mullen, K. *ACS Nano* **2013**, *7*, 3598.

Chapter **5**

Electrocatalytic H_2 generation using chemical modified electrodes based on carbon fibers

I. Introduction

Non-renewable energy sources like coal, oil and natural gas are excessively used to satisfy the human needs, increasing the rate of depletion of the natural resources. So, human kind has to find the alternatives for non-renewable energies for the future. Utilization of solar energy, wind, tidal, geothermic and bio energy, which in principle are renewable, are possible alternatives.[1]

Recently, interest on hydrogen as a fuel has increased a lot due to the highest gravimetric energy density in comparison with all fuels and also because it is compatible with electrochemical and combustion processes for energy conversion without creating environmental pollution. In addition, hydrogen is a colorless, odorless gas corresponding to almost 75% of the universe's mass. Hydrogen is usually found in combination with other elements like oxygen, carbon and nitrogen. Thus, to obtain pure hydrogen should be separated from these other elements. NASA has used liquid hydrogen as fuel for space shuttle and rockets since the 1970s.[2,3] Hydrogen is used there as fuel to power the electrical systems and as byproduct pure water for drinking is produced.[4]

There are different types of processes for hydrogen production like steam reforming, partial oxidation of sub stoichiometric fuel-air mixture, plasma reforming, water electrolysis, water thermolysis, photocatalytic water splitting.

Hydrogen Evolution Reaction (HER) by electrolysis of water is the simplest way to produce hydrogen of high purity. To make this reaction economically desirable is necessary a good electrocatalyst that improve the process, reducing the over potential and increasing the reaction rate. Hydrogen evolution reaction (HER) has been studied on noble metal catalysts, especially such as polycrystalline and single-crystal surfaces of Pt,[5,6] also on the metals such as Ru,[7,8] Co,[9] Pb,[10] Zn-Ni,[11] Ni-P[12,13] and Ni-Mo.[14] Recently, nanostructured-type materials, such as carbon felt and glassy carbon have attracted major attention as catalyst supports, due to their outstanding physical and chemical properties.[15,16] Also, there are two reports in 2014 on the development and utilization of activated carbon nanotubes (CNTs) and some graphitic carbons, as a highly-active metal-free electrocatalyst for the hydrogen evolution reaction (HER) with good durability in acidic electrolytes.[17,18]

As an alternative to graphene electrodes, which proved to be in our case inefficient, we considered Carbon fiber as conducting carbon material, which is usually employed as

structural material. Carbon fiber has been described as a fiber about 5–10 μm in diameter containing at least 90% carbon obtained by the controlled pyrolysis of appropriate fibers.Carbon fibers, are made of carbon crystals aligned in long flattened ribbons. This crystal row makes the fiber strong. The existence of carbon fiber created in 1879 when Edison took out a patent for the manufacture of carbon filaments suitable for use in electric lamps.[19]

There are several methods of making carbon fibers but basically, it consists of first making fibers out of a carbon rich precursor material. The first steps are carbonizing and stretching precursor fibers, PAN (Polyacrylonitrile), Pitch or Rayon. PAN is the most common precursor for plastic composites.[20,21]

This process eliminates most of other elements, mainly H_2 and N_2, of the starting material. It also allows the carbon to slowly crystallize to graphitic structures. Degree of carbonization and orientation of the ribbons, are the most important factors determining the physical properties of carbon fiber.[22,23]

Duo to the properties of carbon fibers, such as high hardness, high tensile strength, low weight, high chemical resistance, high temperature tolerance and low thermal expansion, they are very useful in aerospace, civil engineering, military, and motorsports, along with other competition sports.[24,25]

In addition, they have other applications as composite materials, microelectrodes and catalysis.

The chemically inert carbon fiber (CF) has excellent mechanical and electrical properties and for electrophysiological, electrochemical and biosensor applications providing a very good base electrode. Activated carbon powders[26,27] and fibers[28,29] because of their high surface area and electric conductivity have been used as electrode materials.

Until now, carbon blacks have been successfully used as supports for catalysts in fuel cells, however, self-aggregation of the carbon particles reduced the electrocatalyst efficiency of the fuel-cell because it prevents the approach of the fuel and oxidant to the active sites.

In comparison with the other carbon- based materials, fibers have flexibility. The advantages of fibrous catalytic packs is immobilization the catalyst, huge surface area, short diffusion distance, their low resistance to flow of liquid and gases through a bundle of fibers. Thus, they can be used as an attractive alternative in fuel cells.[30]

Therefore, the final goal in this chapter is electro catalysis of the H_2 generation by using carbon fibers as modified electrodes.

II. Experimental procedures

II.1. From graphene to carbon fibers

The initial goal of this study was using the graphene suspensions that we have produced in the previous chapter to fabricate a modified electrode. Thus the idea was to use nanostructured graphene surfaces to anchor well-known homogeneous HER electrocatalysts, aiming to find grafted materials with good catalytic properties. The graphene surfaces were grown on plain materials using graphene-flake ink in EtOH or THF. This ink was sprayed over a hot surface several times to generate a full-cover.

Initial attempts using a transparent conducting glass as ITO shown that ITO is reactive at HER working conditions, disabling it as supporting material. Because of that, we decided to explore more inert supporting materials to spray the graphene ink. The selected material was glass, which is a completely inert material that supports perfectly a thin layer of graphene (chapter 4). We sprayed 12-15 ml of graphene suspension (0.05 mg/mL) over a 1 cm^2 glass slide at 175°C to generate a full blackish graphene cover. It was annealed at 350°C during one hour to increase homogeneity, reducing the surface resistivity until 2 kOhm□. This resistivity is quite high compared to ITO or standard glassy carbon electrodes but it is lower than the achieved using commercial carbon inks. Although sprayed graphene is somehow a conductive material, its conductivity is not enough to be a reliable supporting electrode for HER, so the allowed currents are too tiny to be useful. In addition, in this way the surface area is not too much, so the amount of the catalyst on the surface in very low. To solve this problem, we have tried to find another carbon-based material that would be used as supporting electrode with high surface area.

In the literature, recently appeared a paper from Gray et al[31] where they suggested the utilization as conducting supporting substrate a commercial high surface-area carbon material known as Ketjenblack. This material provides a high surface for non-covalent immobilization of electrocatalysts. Ketjenblack is a commercial brand for an electro-conductive carbon black dust from AzkoNobel. This material is carbon with a known nano-metric particle size that has to be supported on a matrix to work. It lead us to think about

carbon fibers as another microstructured carbon material with good electro-conductive properties that is widely used in several fields.

Finally, to have a homogenous electrode with very high surface areas, we prepared carbon fiber brushes. The area was estimated to be ≈80 cm^2 by each centimeter into the working solution by considering the number and dimensions of fibers thread. However, active area was estimated to be approximately the half by normalizing their response to ferrocene as electrochemical standard.

II.2. Preparation the carbon fiber brushes

The carbon fiber electrodes (C-Brushes) are made identically using a copper wire, 50 cm of carbon fiber thread and some Teflon tape to tight everything together. The electrodes are hand-made.

The carbon fiber thread has around 3000 filaments of 5-8 □m of diameter. It was turned (7 times) around a 3 cm plastic strip to make a 6 cm long bundle of fibers. Then, it was joined to a copper wire and finally everything is tight with a Teflon tape (figure 5.1).

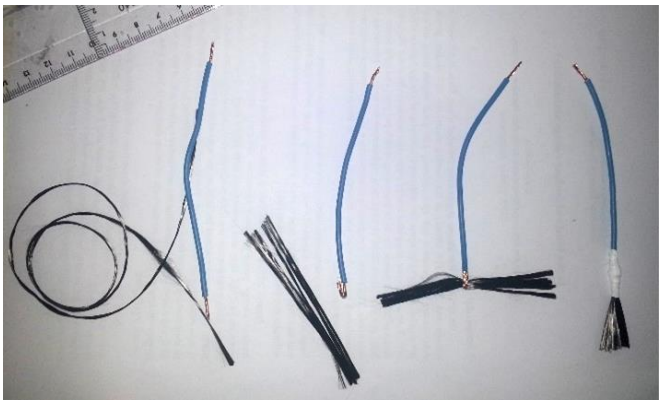

Figure 5.1: Steps to make a carbon fiber brush.

Cleaning the C-Brushes electrodes in two ways:

After preparation the C-Brushes electrodes, all of them were washed and sonicated in only Isopropanol and then dried with Ar.

Then some of them were cleaned by H_2SO_4 with this procedure: the clean electrodes were stirred 1 hour in commercial H_2SO_4, at room temperature (25°C), then the electrodes have washed and sonicated in distilled water several times to remove all the acid traces among fibers. Finally, the electrodes have sonicated 10-15 minutes in Isopropanol and dried

with Ar. All the characterization data suggest no difference between one or another way to clean electrodes, so from now in this chapter we refer as clean electrodes to electrodes just washed with Isopropanol.

Chemical activation of C-Brushes:

Oxidized C-Brushes electrodes:

The clean electrodes by Isopropanol were stirred 30 min. in commercial H_2SO_4 and then 30 min. in the mixture of H_2SO_4/H_2O_2 (1:1) at room temperature (25^{o}C), then the electrodes were washed and sonicated in distilled water and isopropanol several times and dried with Ar.

Addition of Co salts:

Cobalt salts ($CoCl_2$ or $Co(NO_3)_2$) were deposited on the C-Brushes (clean and oxidized) to check the possible catalytic behavior of Cobalt cations. These C-Brushes were stirred in the corresponding solutions in dry MeCN (1mg/mL) for 4 hours and then washed several time with dry MeCN and then dried with Ar.

III. Characterization

The chemical composition of the electrodes has been studied by several analytical techniques such as SEM, TXRF and XPS.

Besides, the carbon electrodes have been characterized by several redox techniques such as linear sweep voltammetry, cyclic voltammetry or chronoamperometry.

III.1. Scanning electron microscopy (SEM) Characterization

Typical SEM images of clean electrodes are shown in figure 5.2. Independently that the washing were carried out using just Isopropanol, or also H_2SO_4, or even H_2SO_4/H_2O_2, SEM images do not show any differences. However, on the surface of the electrodes, washed with H_2SO_4/H_2O_2 treatment with Cobalt salts implies a much bigger amount of material deposited, as it is clear in the figure 5.3.

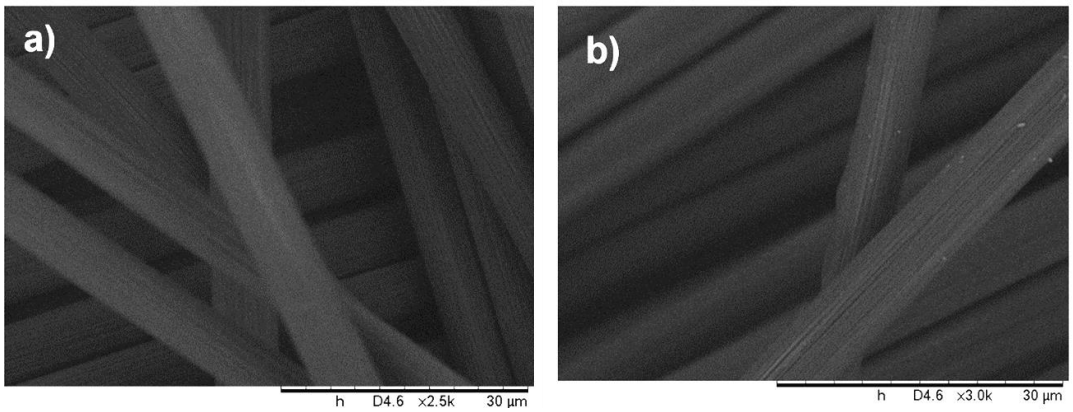

Figure 5.2: SEM images of carbon fibers after cleaning with a) H_2SO_4 and chemical attack with b) mixture of H_2SO_4/H_2O_2.

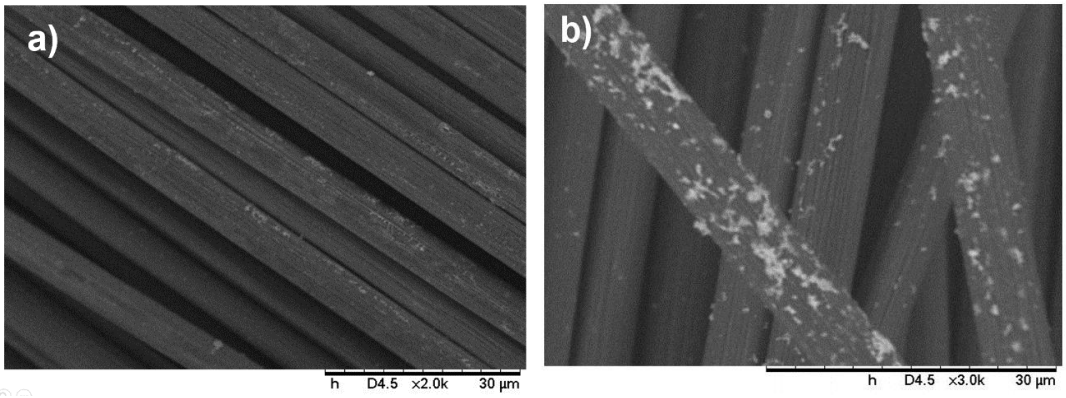

Figure 5.3: SEM images of carbon fibers after cleaning with a) H_2SO_4 and chemical attack with b) mixture of H_2SO_4/H_2O_2 and cobalt salts.

III.2. X-ray photoelectron spectroscopy (XPS) Characterization

To see the chemical composition of surface of carbon fibers, XPS characterization was done. Figure 5.4 shows C (1s) spectra of three different C-brush electrodes. First, the one just cleaned with Isopropanol (a), second the one cleaned with only H_2SO_4 (b) and finally the one activated with the mixture of H_2SO_4/H_2O_2 (c).

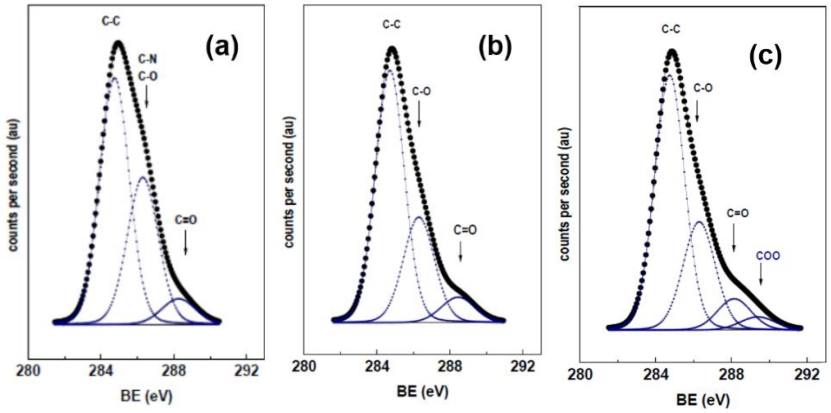

Figure 5.4: Carbon atom ratio of carbon fibers a) washed with the Isopropanol, b) washed with H_2SO_4 and c) activated by mixture of H_2O_2/H_2SO_4.

Analysis of the results are shown in figure 5.5 and also table 5.1. Interestingly there is around 4% of COO in the third one that was activated with the mixture of H_2SO_4/H_2O_2 that has not been observed in the others. Thus, it seems clear that H_2SO_4/H_2O_2 treatment result and chemical functionalization generating new oxidized groups such as carboxylates.

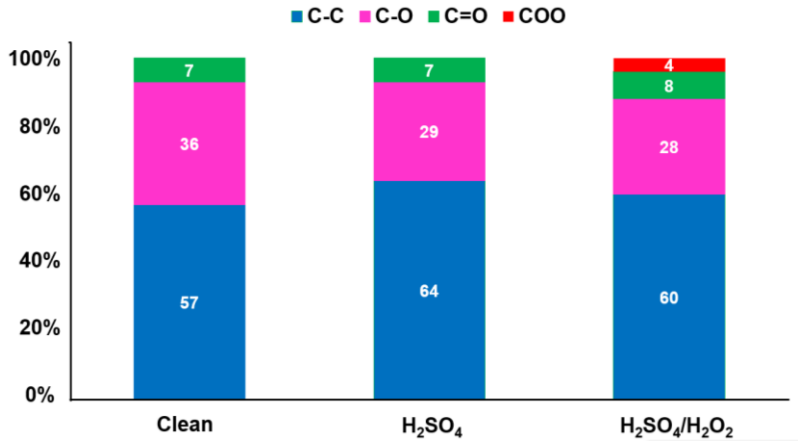

Figure 5.5: CO relationship on Carbon fibers.

Table 5.1: Binding energies (eV) and atomic ratios of samples C functionalized.

	C1s	O1s	N1s	S2p
Clean with Isopropanol	284.8 (57) 286.3 (36) 288.3 (7)	532.9	400.0	-
H_2SO_4	284.8 (64) 286.3 (29) 288.4 (7)	532.3	400.7 (54) 402.2 (46)	168.6
H_2SO_4/H_2O_2	284.8 (60) 286.3 (28) 288.1 (8) 289.4 (4)	532.3	400.6 (69) 402.2 (31)	168.8

Those functional groups could explain the increase of activity of the oxidized carbon fibers and the larger immobilization of cobalt on the carbon surface.

III.3. Total reflections X-ray fluorescence (TXRF) Characterization

TXRF analysis was done for C-Brushes electrodes with several carbon salts to see the amount of cobalt that get plug on the carbon fibers.

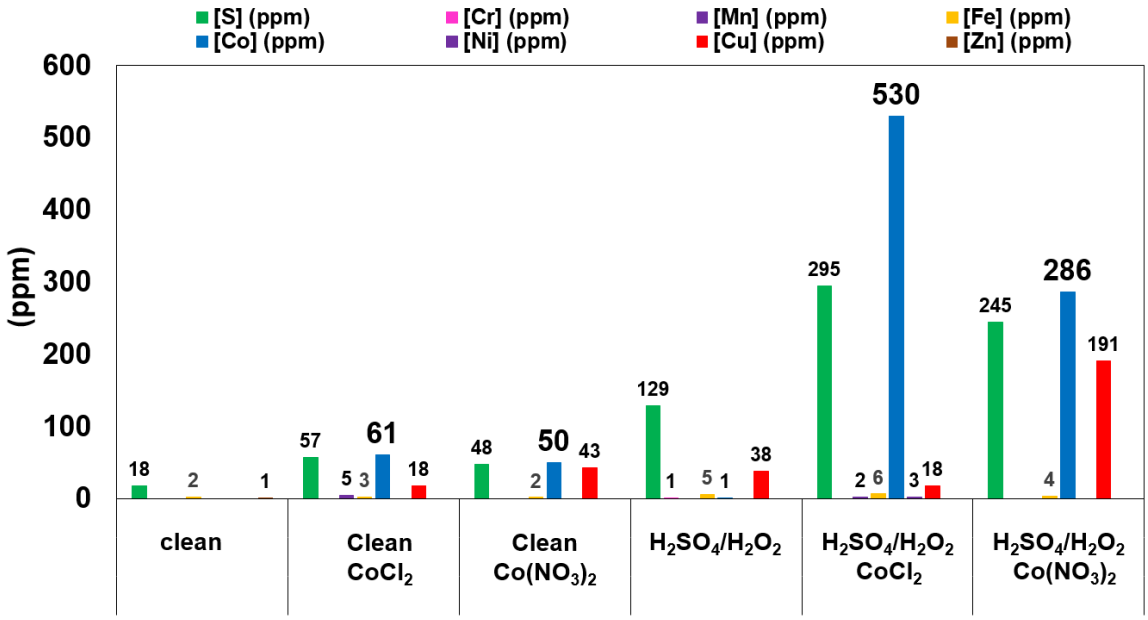

Figure 5.6: TXRF analysis of carbon fiber brushes.

As it is clear in the figure 5.6, between the different treated C-Brushes, the one that activated with H_2SO_4/H_2O_2, incorporates more metal than the others and $CoCl_2$ was more deposited on the oxidized C-Brushes than the $Co(NO_3)_2$, but finally we have used the $Co(NO_3)_2$. The idea was that Chlorides are ligand in the $CoCl_2$ but nitrates are not coordinative and we could have problem with the lability of the Chloride. So, the $Co(NO_3)_2$ can be more efficient for catalysis than the $CoCl_2$, even if we have more $CoCl_2$ on the C-Brushes. In addition, the unique metal impurity is copper, which comes from the copper wire. If we do not consider the copper, we can say that before adding the Co salts the C-Brushes are metal free electrodes.

IV. Electrochemistry

IV.1. Cyclic voltammetry (CV)

To evaluate the electrocatalytic behavior of these electrodes, we have carried out several experiments with the C-Brushes.

We carried out several cyclic voltammetries at increasing H^+ concentrations (trifluoroacetic acid as H^+ source). The working solution was made with fresh dry acetonitrile (10 ml) and Bu_4NPF_6 as electrolyte (100 mM). All the experiments were done under argon atmosphere, bubbling argon into it few minutes and dipping 1 cm of the C-Brushes into the working solution.

The active area of the C-Brushes depends of how much deep is the electrode into the solution. To evaluate the real electrode area we have tried to use a ferrocene standard.

Once the experiment was done, a solution of ferrocene (1 mM) were added and the oxide-reduction wave of ferrocene with the studied C-Brushes and a standard glassy carbon were recorded. Comparison of the both CV's, can determine an area relationship with the known area of the glassy carbon (0.0707 cm^2) and we could extrapolate the electrode area, being the average area of C-Brushes electrodes of 40 cm^2 approximately.

Comparison between the CV of proton reduction of several C-Brushes, can show us, how the reduction wave is more intense for oxidized electrodes than the initial electrode without any chemical treatment (figure 5.7). The electrodes clean and acid-attacked without oxidant shown similar activity on the CV's.

At low proton concentration, the presence of cobalt increase the activity of the electrodes, but when the $[H^+]$ grows up the activity of both, H_2SO_4/H_2O_2 and Co-doped H_2SO_4/H_2O_2, gets equal and we cannot see any difference between them.

An important step for the C-Brushes activation was the correct oxidation of the carbon fibers. To generate COO groups on the carbon surface, the H_2O_2 should not be opened long time ago. If the oxidant activation is not correct, the HER activity is just a little bit higher than a regular C-Brushes clean and there is no any important catalytic effect.

Here have shown some several CV's of C-Brushes; all of them has a specific area.

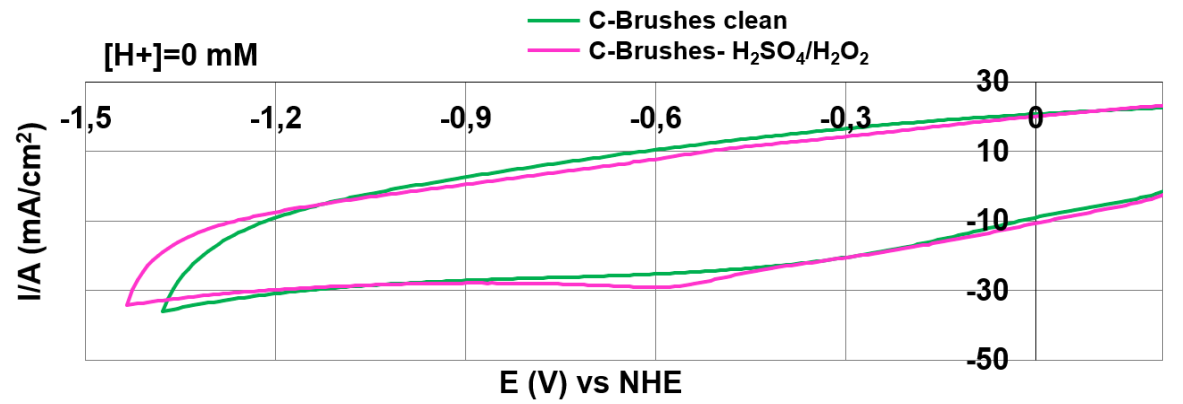
C-Brushes clean
C-Brushes- H_2SO_4/H_2O_2
[H+]=0 mM
I/A (mA/cm²)
-1,5
-1,2
-0,9
-0,6
-0,3
0
30
10
-10
-30
-50
E (V) vs NHE

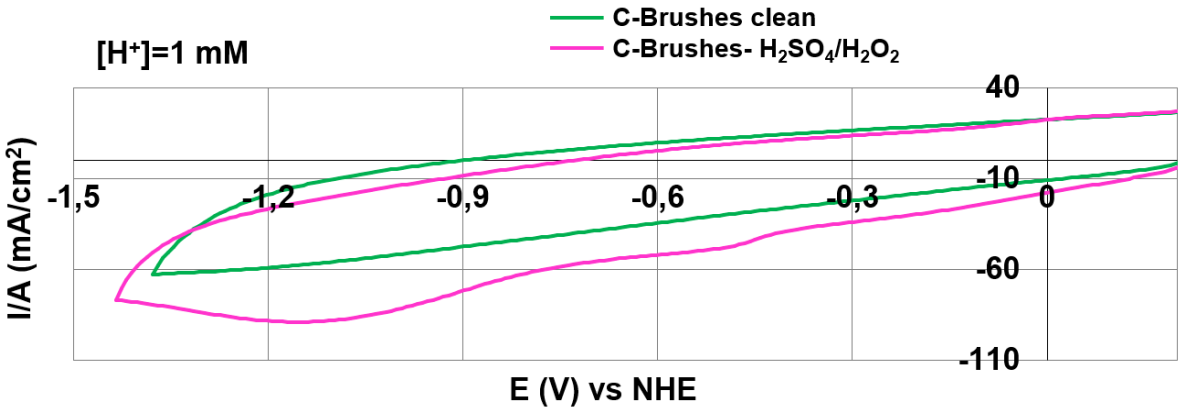
C-Brushes clean
C-Brushes- H_2SO_4/H_2O_2
[H⁺]=1 mM
I/A (mA/cm²)
-1,5
-1,2
-0,9
-0,6
-0,3
0
40
-10
-60
-110
E (V) vs NHE

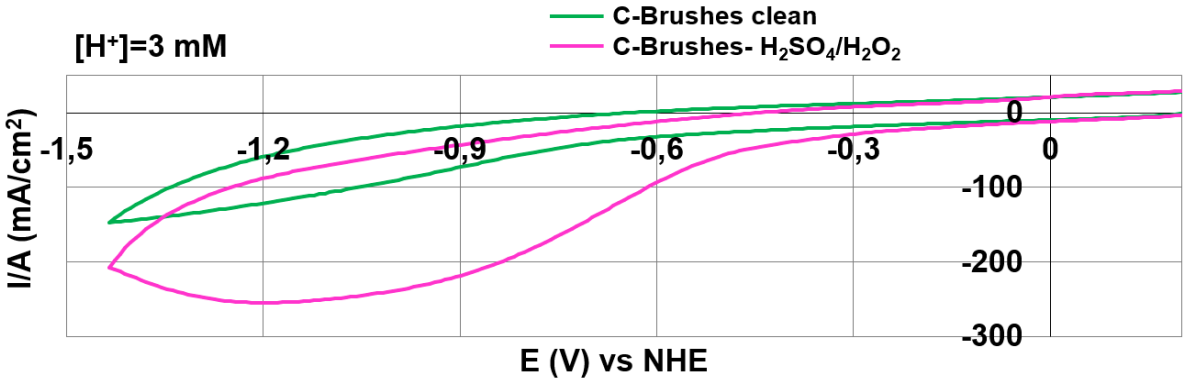
C-Brushes clean
C-Brushes- H_2SO_4/H_2O_2
[H⁺]=3 mM
I/A (mA/cm²)
-1,5
-1,2
-0,9
-0,6
-0,3
0
0
-100
-200
-300
E (V) vs NHE

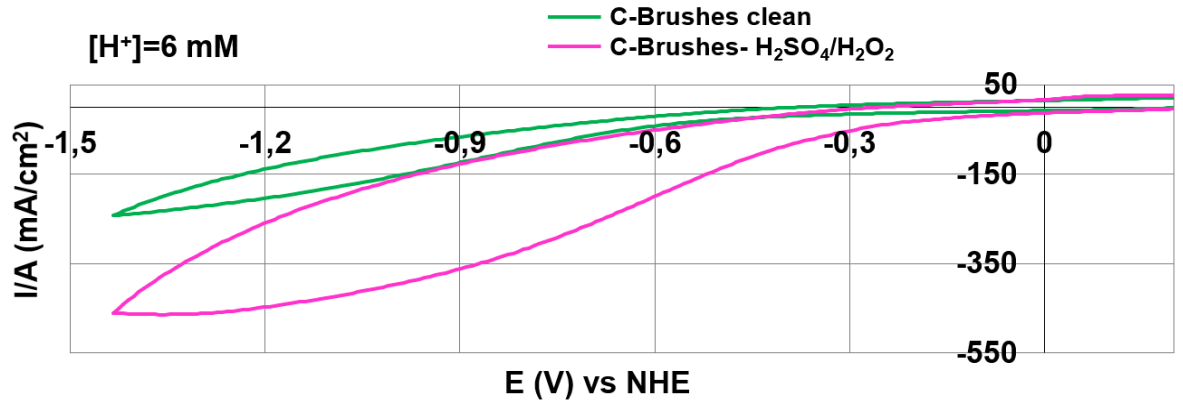
C-Brushes clean
C-Brushes- H_2SO_4/H_2O_2
[H⁺]=6 mM
I/A (mA/cm²)
-1,5
-1,2
-0,9
-0,6
-0,3
0
50
-150
-350
-550
E (V) vs NHE

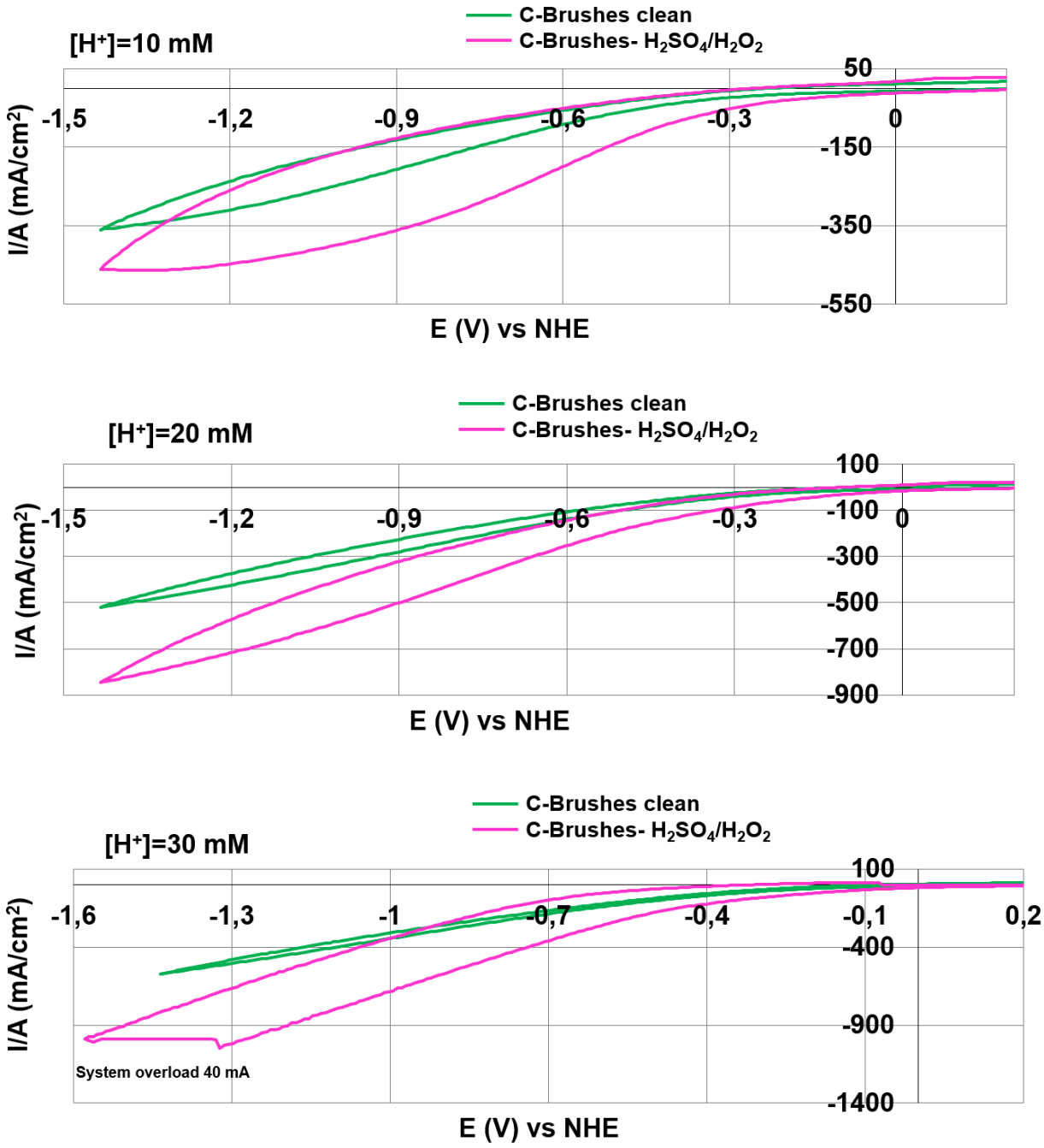

Figure 5.7: Cyclic voltammetry of C-Brushes clean and activated with H_2SO_4/H_2O_2 in different concentration of TFA.

A correct activation of the carbon fibers implies that HER starts 0.15-0.25 V before a regular clean one. 30 mM is the highest concentration because the used system saturates at higher currents.

According the data that is shown in the figure 5.6, in the characterization we saw some amount of Co on the C-Brushes and it was more on the C-Brushes treated with

H_2SO_4/H_2O_2. Here with the cyclic voltammetry also we can see the effect of the Co on the electrodes. As shown in figure 5.8, the addition of cobalt improves a little bit of the cathodic currents and increase the intensity of the currents especially at low proton concentrations. So, there is an effect of the Co, but this effect is not too much, because the amount of the Co on the electrodes is low. However, this increment vanishes at high proton concentration because the cobalt effect is overwhelmed.

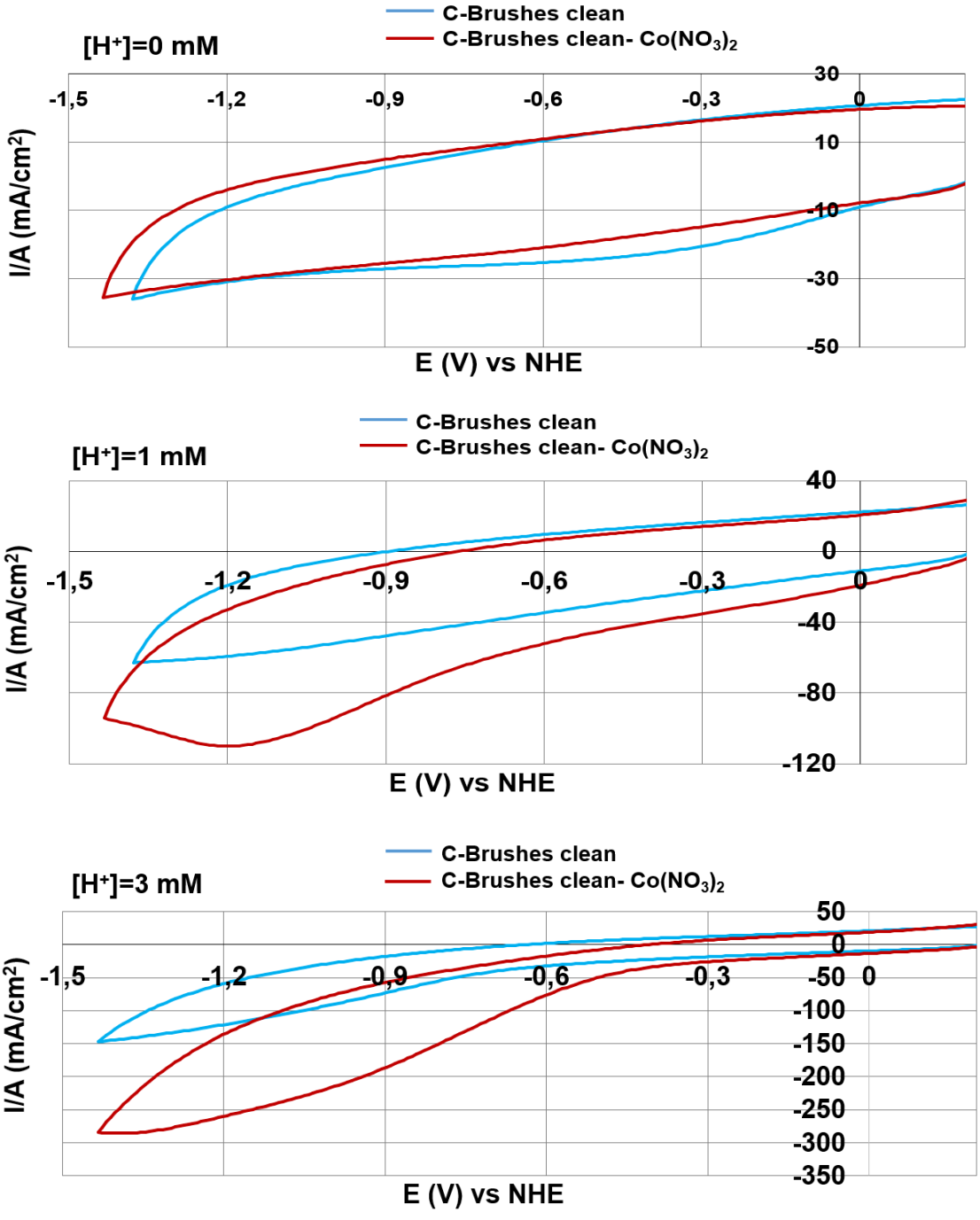

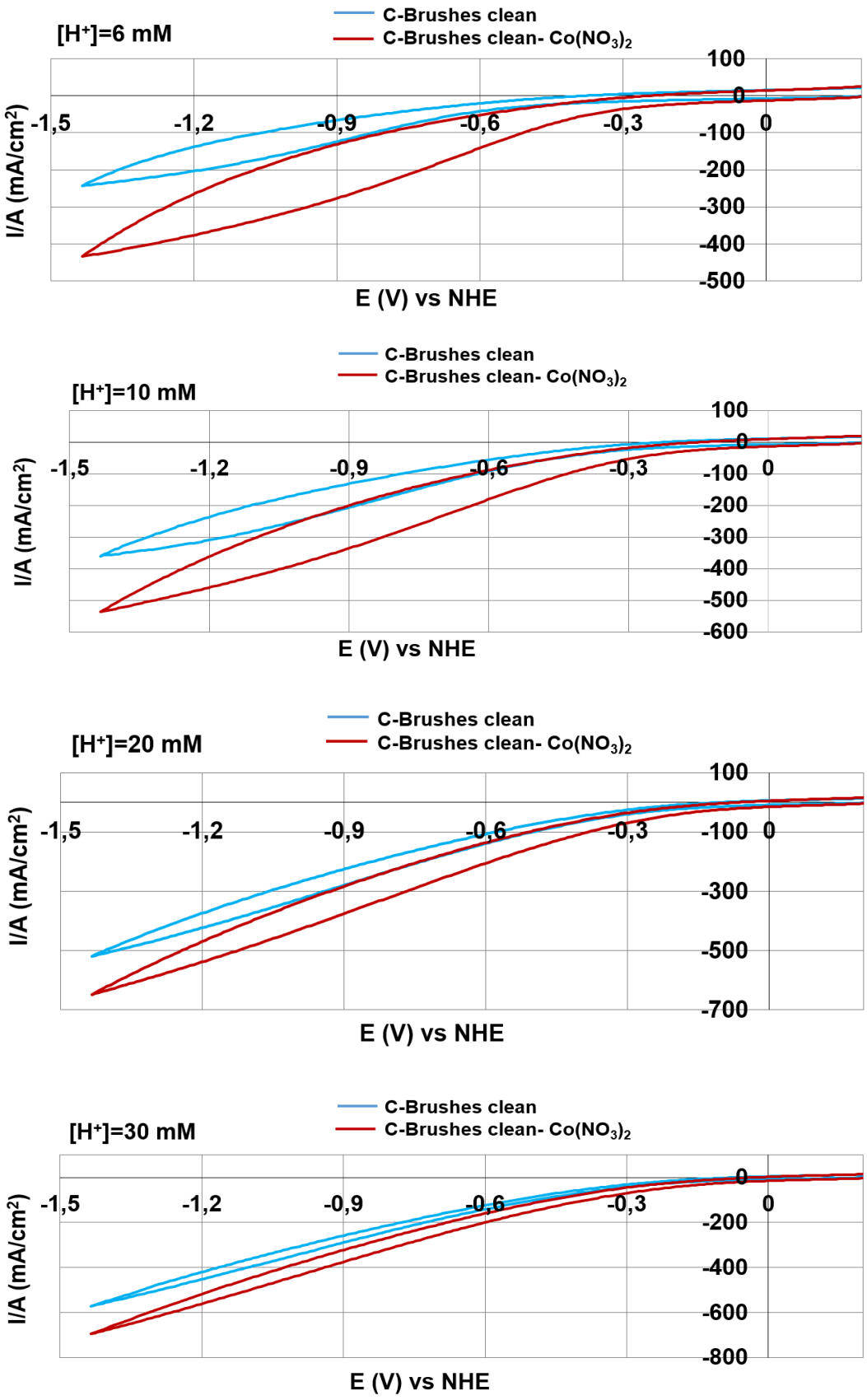

Figure 5.8: Cyclic voltammetry of clean C-Brushes with and without cobalt.

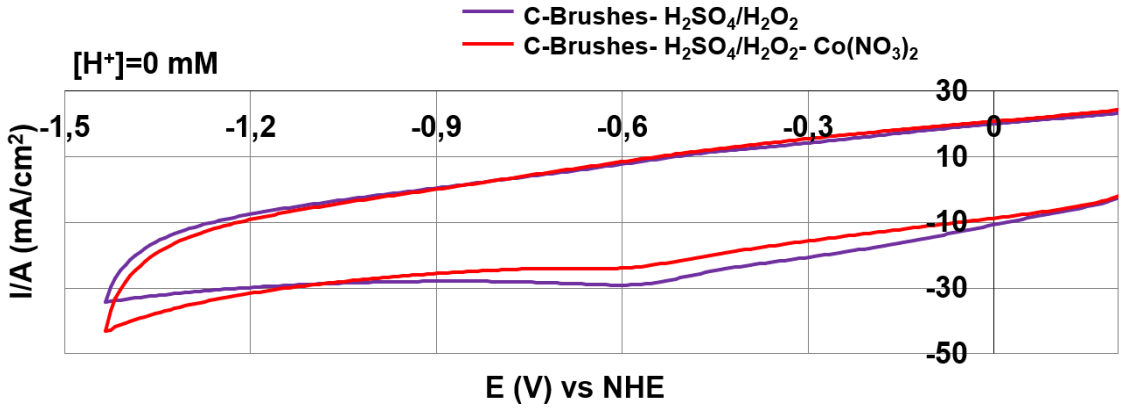
C-Brushes- H_2SO_4/H_2O_2
C-Brushes- H_2SO_4/H_2O_2- $Co(NO_3)_2$
[H+]=0 mM
I/A (mA/cm²)
-1,5
-1,2
-0,9
-0,6
-0,3
0
30
10
-10
-30
-50
E (V) vs NHE

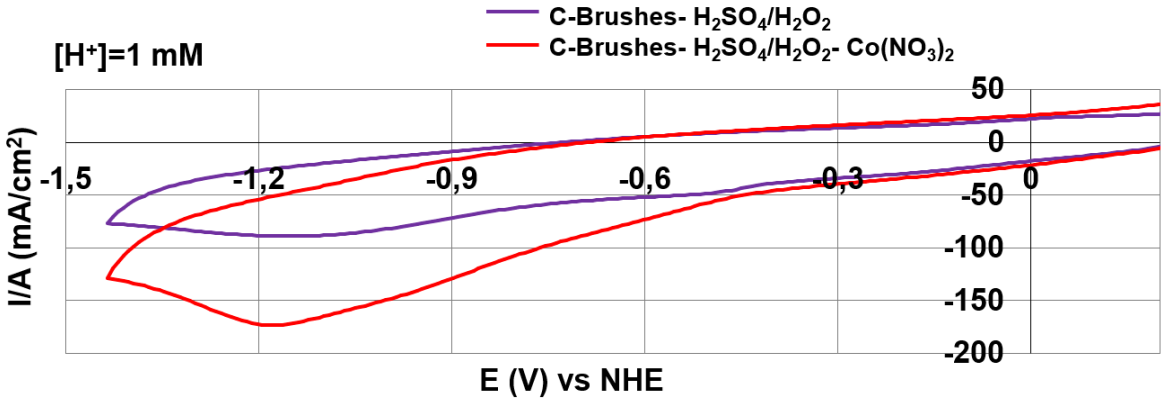
C-Brushes- H_2SO_4/H_2O_2
C-Brushes- H_2SO_4/H_2O_2- $Co(NO_3)_2$
[H+]=1 mM
I/A (mA/cm²)
-1,5
-1,2
-0,9
-0,6
-0,3
0
50
0
-50
-100
-150
-200
E (V) vs NHE

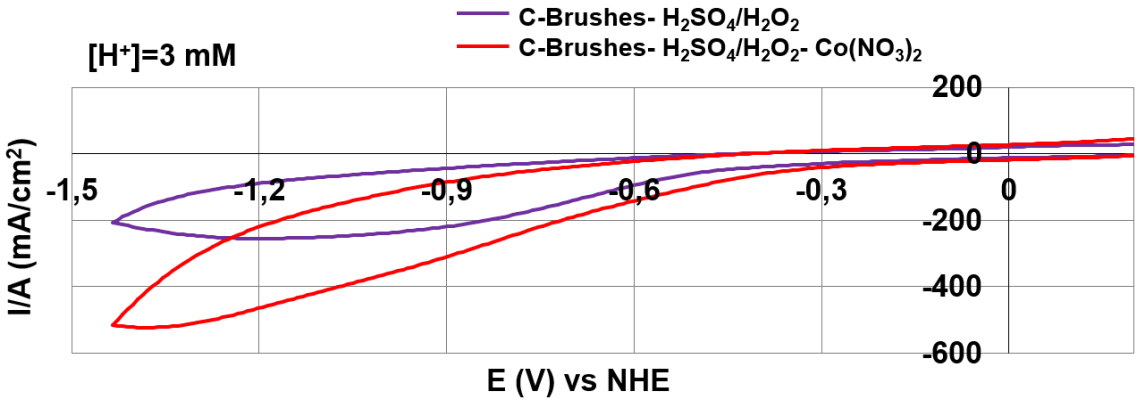
C-Brushes- H_2SO_4/H_2O_2
C-Brushes- H_2SO_4/H_2O_2- $Co(NO_3)_2$
[H+]=3 mM
I/A (mA/cm²)
-1,5
-1,2
-0,9
-0,6
-0,3
0
200
0
-200
-400
-600
E (V) vs NHE

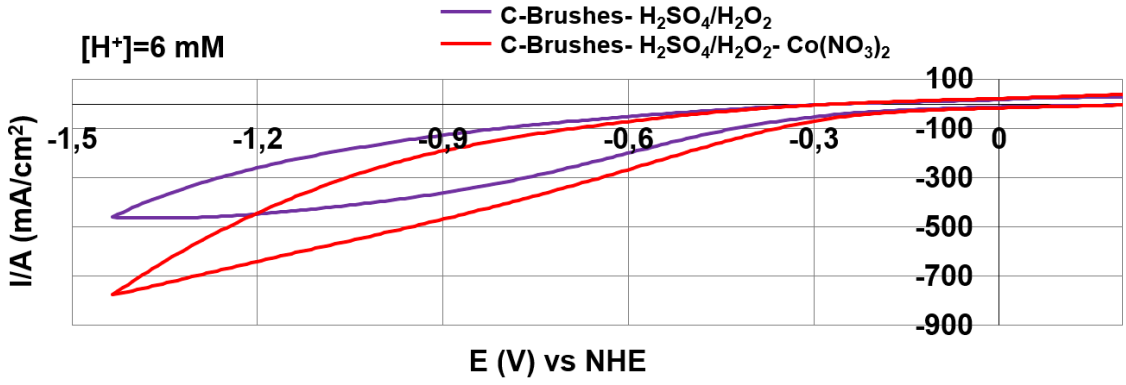
C-Brushes- H_2SO_4/H_2O_2
C-Brushes- H_2SO_4/H_2O_2- $Co(NO_3)_2$
[H+]=6 mM
I/A (mA/cm²)
-1,5
-1,2
-0,9
-0,6
-0,3
0
100
-100
-300
-500
-700
-900
E (V) vs NHE

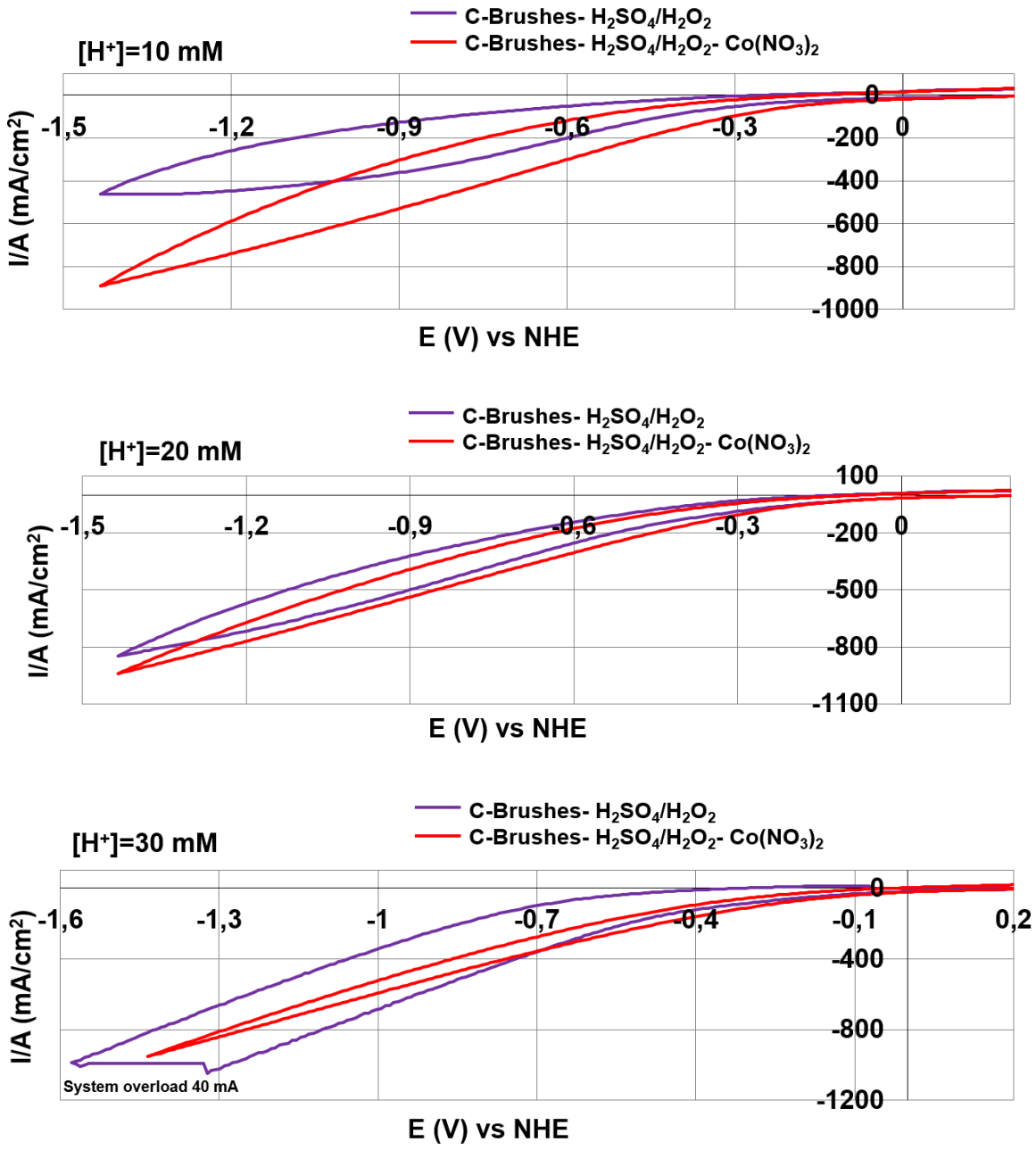

Figure 5.9: Cyclic voltammetry of C-Brushes treated with H_2SO_4/H_2O_2 with and without cobalt.

The observed catalytic effect is not present when a standard glassy carbon electrode is used. The behavior of glassy carbon was clearly different from the carbon fibers electrodes; first, the glassy carbon has a lower non-faradaic currents without H^+. On figure 5.10 it is possible to compare a glassy carbon linear sweep with several carbon fibers electrodes. The corresponding to the glassy carbon is the thinnest among them.

Bellow this lines were shown linear sweep voltammetry of several C-Brushes and a glassy carbon electrode. The HER firstly starts on the oxidized carbon electrodes, it

confirming the catalytic effect of the oxidized groups that could be generated on the carbon surface. An interesting detail is the non-dependence of the current and the $[H^+]$ further than 10 mM. It would be due to the saturation of the catalytic sites on the surface of the carbon fiber.

The last set of figures shows clearly the catalytic effect of the oxidized surface. Moreover, it is observed that cobalt ions on C-Brushes (red line) increases a little bit the cathodic current, But this effect is really small as will be confirmed by the bulk electrolysis.

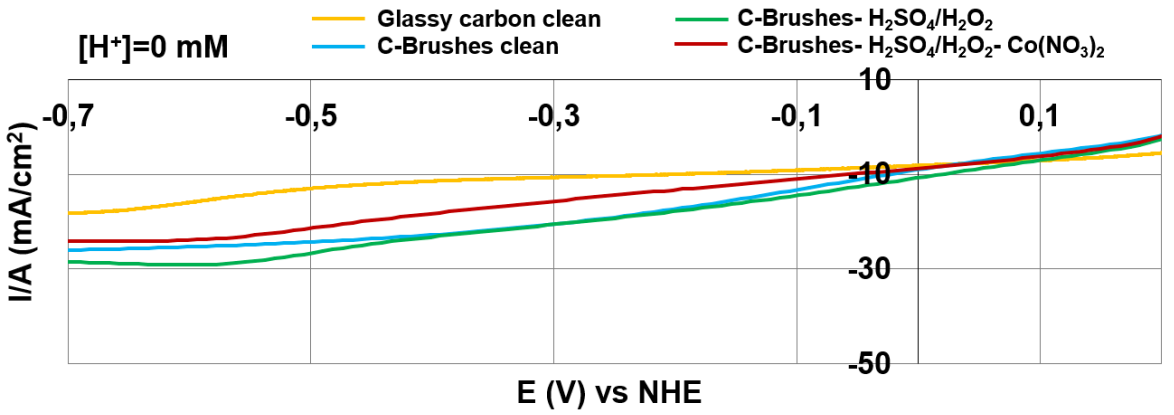

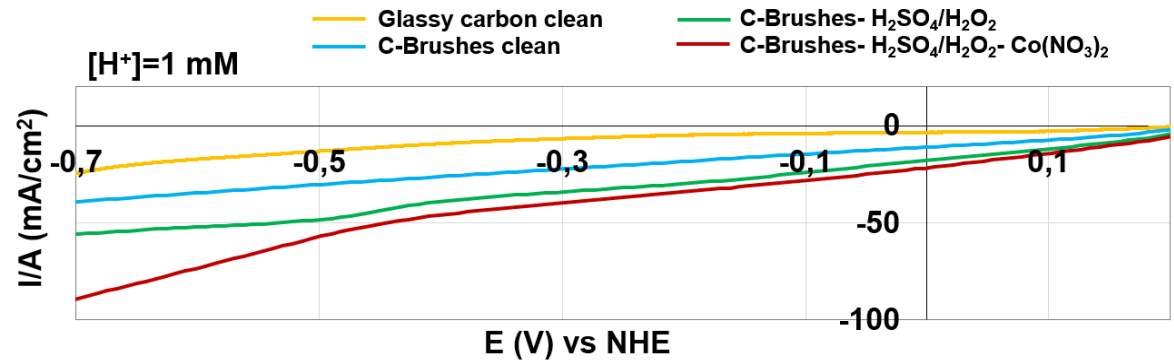

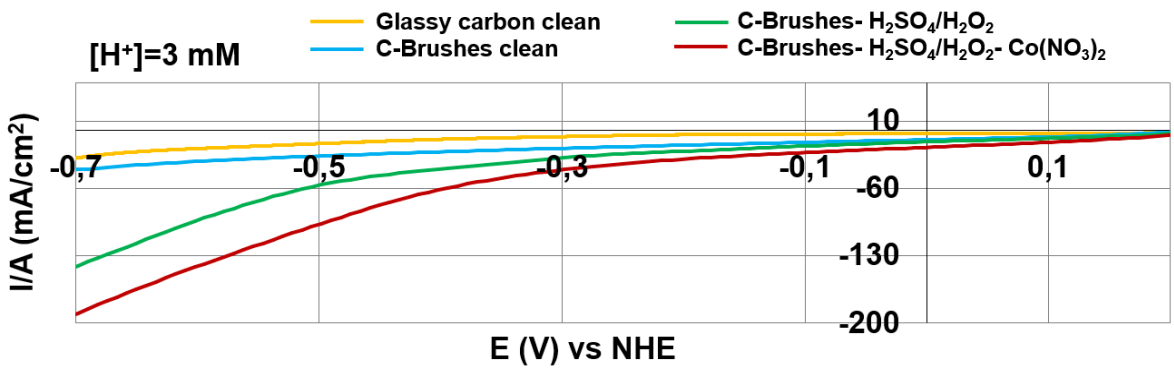

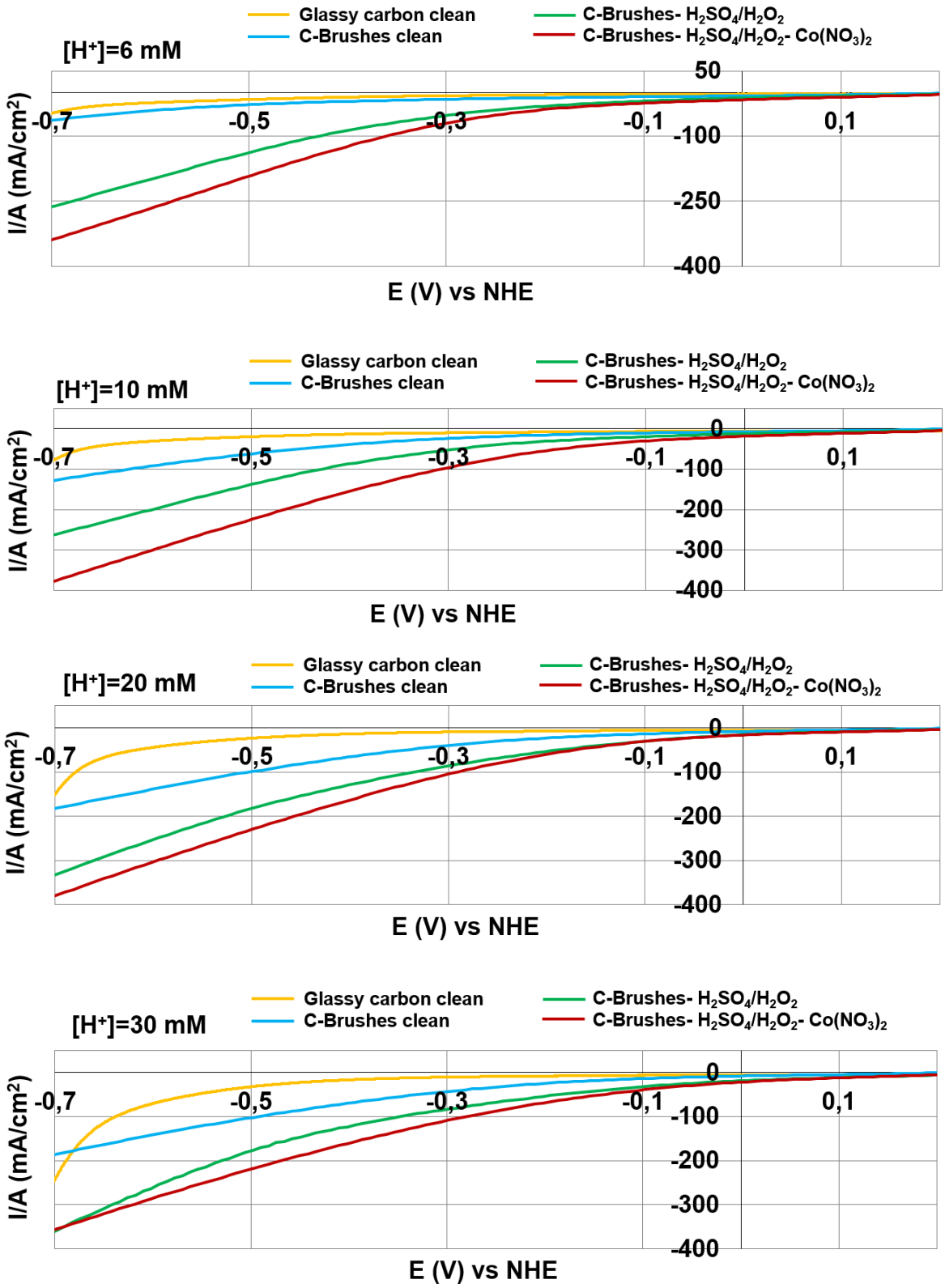

Figure 5.10: Linear sweet voltammetry of a glassy carbon and several C-Brushes with and without cobalt.

Finally, it is shown some examples of the catalytic effect at several redox potentials using another electrochemistry output. The I_{cat}/I_p (I_{cat}= Intensity in presence of catalyst and substrate and I_p= Intensity in absence of substrate) shows the current activity duo to the electrochemical process, discounting area effects. We have chosen two examples bellow -0.7 V vs NHE because at that potentials the glassy carbon electrode does not show any activity.

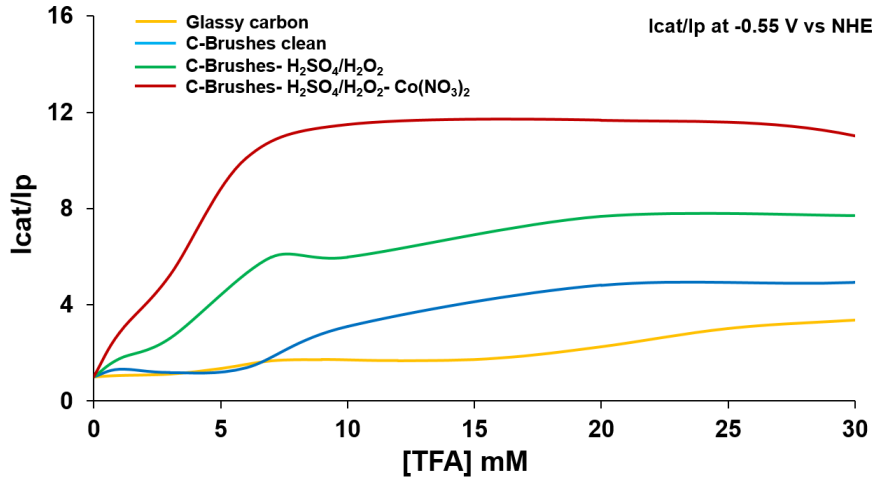

Figure 5.11: I_{cat}/I_p at -0.55 V vs NHE of a glassy carbon and several C-Brushes with and without cobalt.

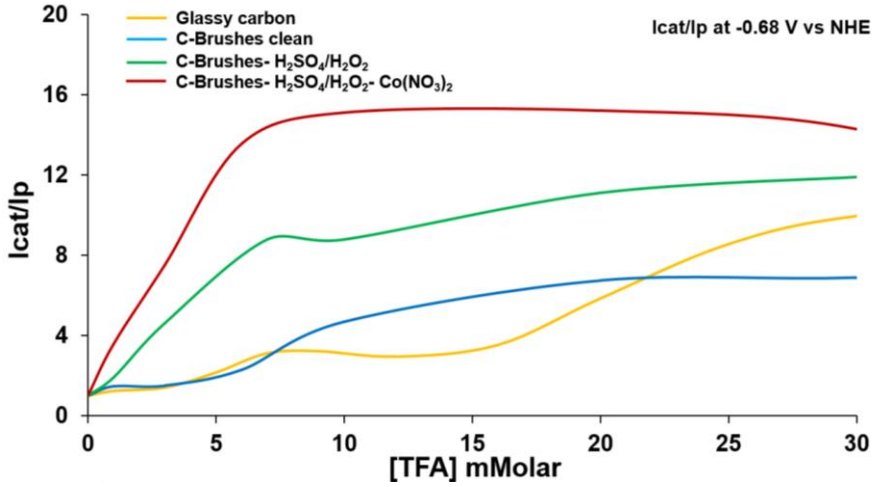

Figure 5.12: I_{cat}/I_p at -0.68 V vs NHE of a glassy carbon and several C-Brushes with and without cobalt.

From figures 5.11 and 5.12, we have observed the catalytic effect for C-Brushes. It is observed an enhancement of the activity when Cobalt is added to C-Brush oxidized electrodes. The intensity of the glassy carbon and C-Brushes clean are lower especially at

low concentration of acid. The I_{cat}/I_p shows the current activity but after around 10 mM of acid it will be constant because after this all the catalytic sites are saturated.

IV.2. Chronoamperometry with coulombmetry of C-Brushes

Several sets of experiments were done to check the actual capability of the carbon fibers electrodes to carry out a hydrogen evolution reaction. These experiments were done in dry acetonitrile, where some nitrogen were bubbled few minutes, using a Bu_4NPF_6 0.1 molar as electrolyte.

An Ag/AgCl electrode has been used as reference electrode and a Pt wire in a separated cell as counter electrode (figure 5.13). The working electrodes were three types of carbon brushes: first one C-Brushes clean without any chemical treatment, second one C-Brushes activated with a chemical treatment of 30 min. in H_2SO_4 and 30 min. in a mixture H_2O_2/H_2SO_4 (1:1) and third one C-Brushes activated with H_2SO_4/H_2O_2 like previous one but with an additional cobalt dipping of 4 hours in a $Co(NO_3)_2$ solution (1mg/mL) in acetonitrile.

Before all the experiments, the working electrode suffered a cathodic pretreatment at -1.15 V vs SCE during 1000s to remove any traces of acid or oxygen form the surface of the electrode. This pretreatment slightly increases the efficiency of the working electrode.

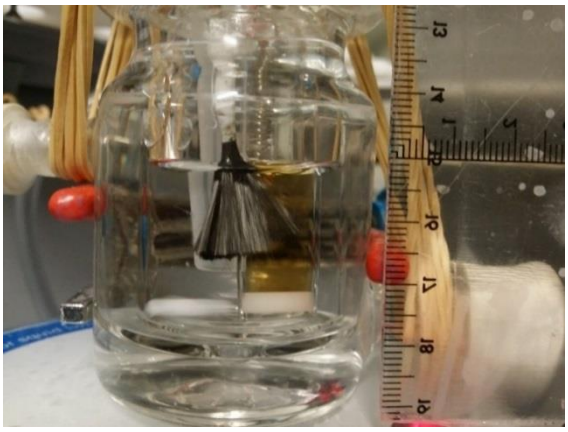

Figure 5.13: Example of a chronoamperometry and coulombmetry experiment of a carbon fiber brushes.

The bulk experiments were carried out in an especial 100 ml electrolytic vessel. That vessel allows us to monitor the pressure into the cell at the same time that we record the current during the 2000-3000 seconds of the experiment and once the experiments are done it allows us to analyze the gas atmosphere with a gas chromatographer. This systems gives

us three ways to check the hydrogen evolution: measured gas (GC) that generally underestimates the H_2 generated, the increment of pressure (Δp) in the cell, that usually overestimates the hydrogen generation and the transferred charge (C transfer) that records the amount of electrons moved into the solution, not all the electrons generate hydrogen.

Those experiments were carried out at three H^+ concentrations 5, 10 and 20 mM at a constant potential of -0.9 V vs SCE (-0.68 V vs NHE).

The current recorded on each experiment indicates a very low current on the non-oxidized carbon electrodes (C-Brushes-clean) at any proton concentration and a null H_2 evolution in any case.

Those experiments highlight the different chemical behavior of the oxidized carbon fibers. The intensity is much higher for oxidized electrodes than for the non-oxidized ones. Moreover, the presence of cobalt on the electrode increases a bit more the recorded intensity.

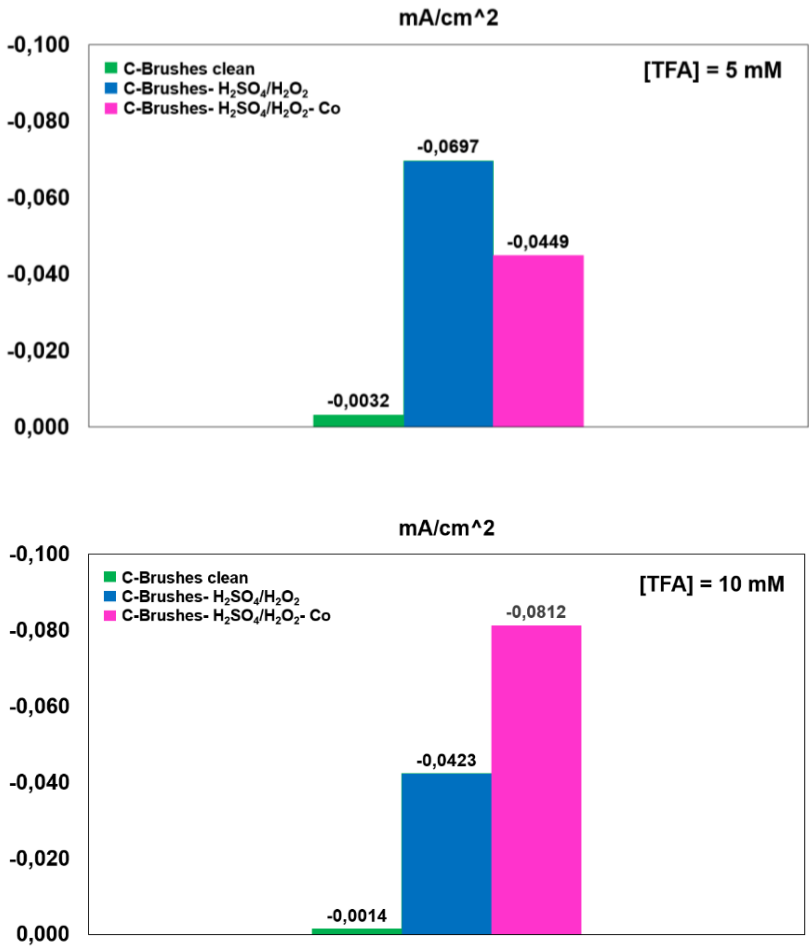

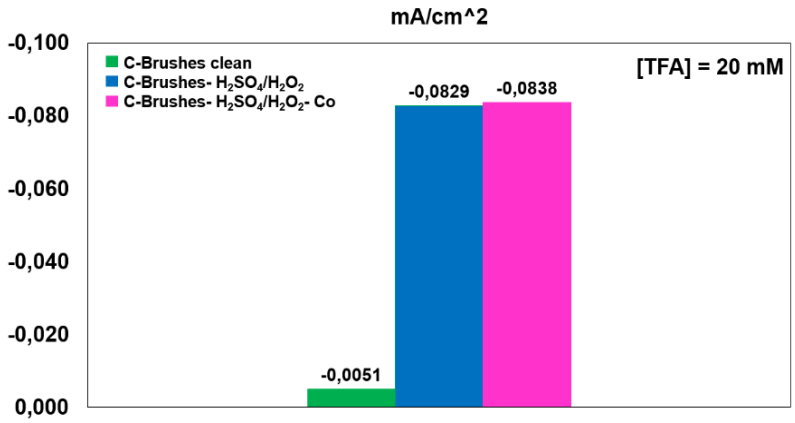

Figure 5.14: Average currents on the chronoamperometry experiments at several H^+ concentrations.

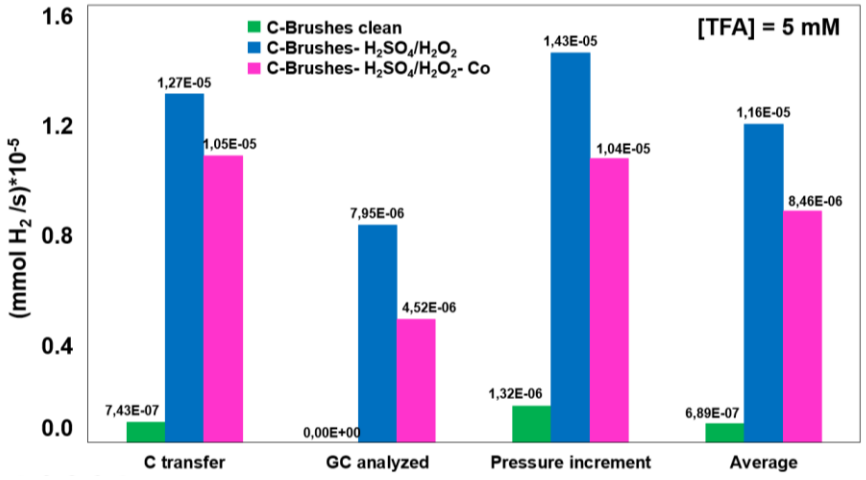

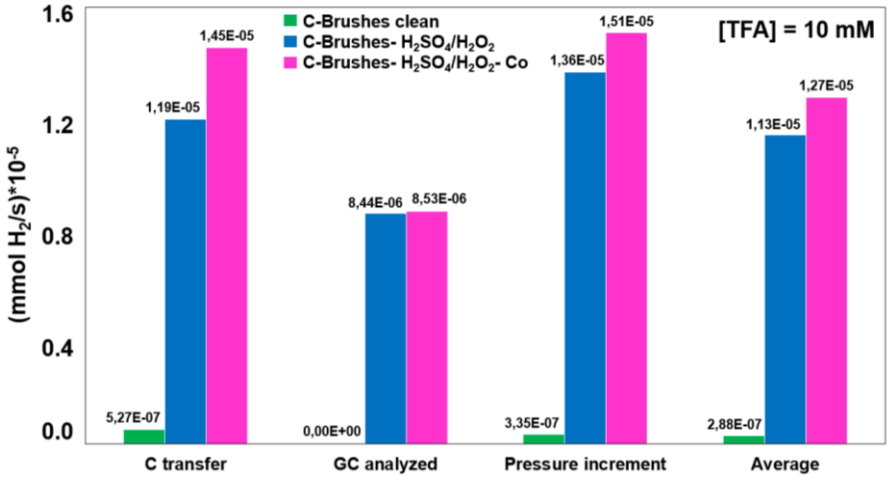

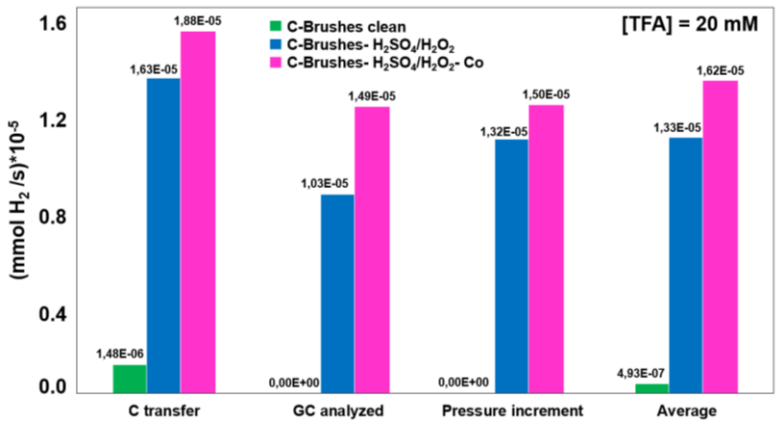

Figure 5.15: Estimated H_2 evolution on bulk experiments.

Figure 5.15 shows three different ways to check the hydrogen evolution: charge transfer (Δp), gas chromatography (GC), increment of pressure and the average of them in three different concentration of acid (5, 10, 15 mM). As it is clear, all the experiments confirm that the clean C-Brushes do not generate too much H_2, but there is H_2 evolution for oxidized C-Brushes and oxidized C-Brushes-Co, although, there are not any important different between them.

GC analysis confirms the hydrogen evolution in electrochemical cells. It is important to highlight that H_2 is generally underestimated by GC because the experimental conditions always imply H_2 leaks. So, it is possible that the yield would be even higher than indicated in figure 5.16.

Faradaic yields have been calculated by comparing the theoretical amount of the H_2 for currents measured and the amounts of H_2 determined by GC.

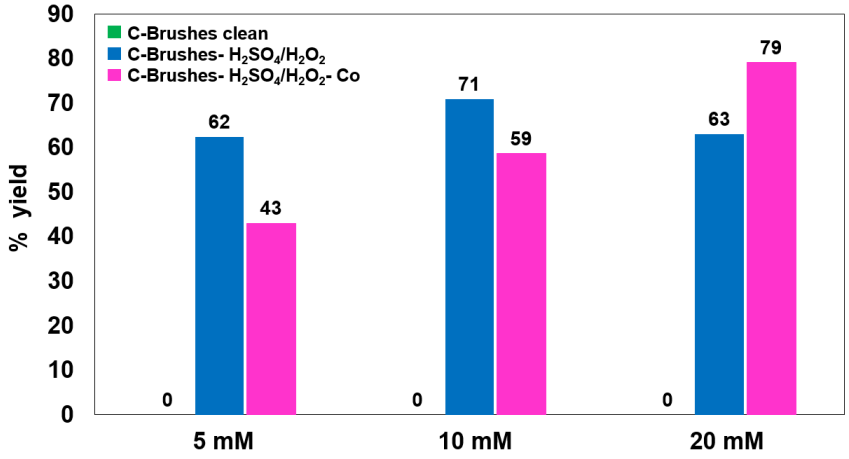

Figure 5.16: Faraday yields of several C-Brushes electrodes by GC determination.

IV. 3. C-Brushes electrochemistry in water/H_2SO_4

During work from Cui et al that suggested a chemical activated carbon nanotube as metal free catalyst for HER.[32] Almost at the same time, another paper from Das et al also reported the chemical activation of several carbon-based materials as nanotubes or graphitic materials for hydrogen evolution reaction.[18]

Both papers describe another method for the oxidation of carbon-based materials and they perform their research in water. Because of that, we carried out a small benchmark in water to see the efficiency of the oxidized carbon fibers.

To carry out an activity benchmark in acid we prepared a 0.5 M solution of H_2SO_4 as Cui et al describe on their paper. The experiments were carried under argon atmosphere, bubbling argon into the solution for 15 minutes to eliminate any oxygen trace. The counter electrode was a carbon fiber electrode without any chemical treatment (C-Brushes clean) and using an Ag/AgCl electrode as reference.

To keep a constant active area the working electrodes were dipped into the solution around 1 to 1.5 cm and a real area estimation was done by taking a picture of the electrode in the solution.

Linear sweep voltammetries were recorded between -0.8 and 0.4 V vs NHE. (V(NHE)=V(SCE)+0.22V) to study the different activity of C-Brushes clean and C-Brushes activated with H_2SO_4/H_2O_2 (figure 5.17).

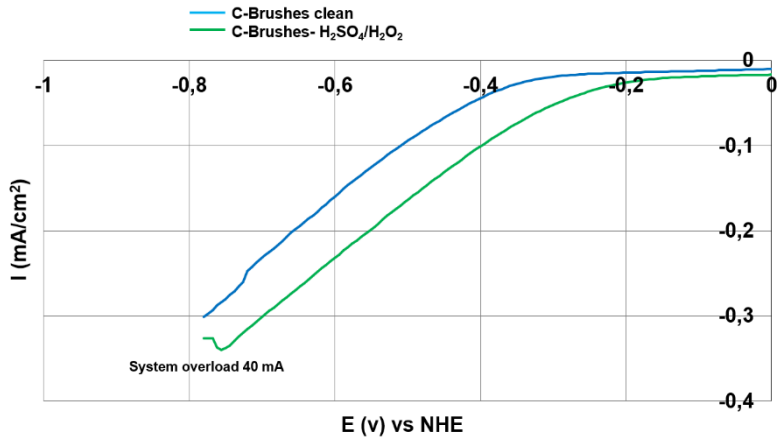

Figure 5.17: Linear sweep voltammetry of several C-Brushes in H_2SO_4 solution (0.5M).

The different activity between the non-oxidized and the oxidized carbon fiber electrode is clear. The last one starts HER around 0.1 V before the other but as shown in figure 5.18 because there is a massive bubbling in the cell and it was difficult to measure correctly.

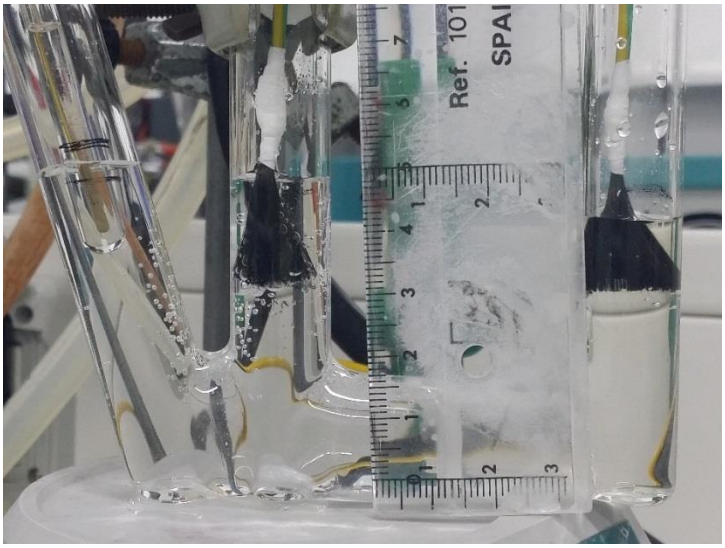

Figure 5.18: Hydrogen evolution reaction by C-Brushes oxidized in acid solution during a LSV.

V. Conclusions

In this chapter, we have prepared clean C-Brushes electrodes in Isopropanol, and H_2SO_4 then we have activated some of them with the mixture of H_2SO_4/H_2O_2 (1:1). Then the electrodes were treated with cobalt salts ($CoCl_2$ or $Co(NO_3)_2$). We have characterized these electrodes by SEM, XPS and TXRF. Also to evaluate the electrocatalytic behavior of this electrodes, we have carried out different experiments with several electrochemical techniques like linear sweep voltammetry, cyclic voltammetry or chronoamperometry.

Those experiments already highlight the different chemical behavior of the oxidized carbon fibers. In all the experiments the intensity of the oxidized C-Brushes is so much higher than the clean electrodes. Moreover, the presence of cobalt on the electrode increases a bit more the record intensity but this effect is not too much, because the amount of the Co in comparison with the oxidized group are low.

Also with three different ways, we have checked the hydrogen evolution: charge transfer (Δp), gas chromatography (GC), increment of pressure. These methods also confirmed the effect of the oxidized C-Brushes and oxidized C-Brushes- Co on the H_2 generation.

In summary, in this chapter we used the C-Brushes fiber as electrode for HER. We have succeed to increase the intensity of the cathodic currents and also generate the H_2 by oxidizing these electrodes with H_2SO_4/H_2O_2 and improved the catalytic behavior by deposition $Co(NO_3)_2$ on activated electrodes.

References:

(1) Panwar, N. L.; Kaushik, S. C.; Kothari, S. *Renewable and Sustainable Energy Reviews* **2011**, *15*, 1513.
(2) Wrana, N.; Sparling, R.; Cicek, N.; Levin, D. B. *J. Cleaner Prod.* **2010**, *18*, S105.
(3) Bullen, R. A.; Arnot, T. C.; Lakeman, J. B.; Walsh, F. C. *Biosens. Bioelectron.* **2006**, *21*, 2015.
(4) Kundu, A.; Sahu, J. N.; Redzwan, G.; Hashim, M. A. *Int. J. Hydrogen Energy* **2013**, *38*, 1745.
(5) (a) Barber, J.; Morin, S.; Conway, B. E. *J. Electroanal. Chem.* **1998**, *446*, 125(b) Barber, J. H.; Conway, B. E. *J. Electroanal. Chem.* **1999**, *461*, 80.
(6) Angelo, A. C. D. *Int. J. Hydrogen Energy* **2007**, *32*, 542.
(7) Inoue, H.; Wang, J. X.; Sasaki, K.; Adzic, R. R. *J. Electroanal. Chem.* **2003**, *554-555*, 77.
(8) Liu, C.-H.; Wu, Y.-C.; Chou, C.-C.; Chen, B.-H.; Hsueh, C.-L.; Ku, J.-R.; Tsau, F. *Int. J. Hydrogen Energy* **2012**, *37*, 2950.
(9) Huot, J. Y.; Brossard, L. *J. Appl. Electrochem.* **1988**, *18*, 815.
(10) Wu, Y. M.; Li, W. S.; Long, X. M.; Wu, F. H.; Chen, H. Y.; Yan, J. H.; Zhang, C. R. *J. Power Sources* **2005**, *144*, 338.
(11) Sheela, G.; Pushpavanam, M.; Pushpavanam, S. *Int. J. Hydrogen Energy* **2002**, *27*, 627.
(12) Burchardt, T. *Int. J. Hydrogen Energy* **2000**, *25*, 627.
(13) Krolikowski, A.; Wiecko, A. *Electrochim. Acta* **2002**, *47*, 2065.
(14) Hashimoto, K.; Sasaki, T.; Meguro, S.; Asami, K. *Materials Science and Engineering: A* **2004**, *375–377*, 942.
(15) Mitov, M.; Chorbadzhiyska, E.; Rashkov, R.; Hubenova, Y. *Int. J. Hydrogen Energy* **2012**, *37*, 16522.
(16) Dominguez-Crespo, M. A.; Ramirez-Meneses, E.; Torres-Huerta, A. M.; Garibay-Febles, V.; Philippot, K. *Int. J. Hydrogen Energy* **2012**, *37*, 4798.
(17) Cui, W.; Liu, Q.; Cheng, N.; Asiri, A. M.; Sun, X. *Chemical Communications* **2014**, *50*, 9340.
(18) Das, R. K.; Wang, Y.; Vasilyeva, S. V.; Donoghue, E.; Pucher, I.; Kamenov, G.; Cheng, H.-P.; Rinzler, A. G. *ACS Nano* **2014**, *8*, 8447.
(19) Landmarks., N. H. C. In *American Chemical Society*, 2014.
(20) Zhang, W.; Liu, J.; Wu, G. *Carbon* **2003**, *41*, 2805.
(21) Sauder, C.; Lamon, J.; Pailler, R. *Carbon* **2004**, *42*, 715.
(22) (a) Sedghi, A.; Farsani, R. E.; Shokuhfar, A. *Journal of Materials Processing Technology* **2008**, *198*, 60(b) Shokuhfar, A.; Sedghi, A.; Farsani, R. E. *Mater. Sci. Technol.* **2006**, *22*, 1235.
(23) (a) Eslami Farsani, R.; Shokuhfar, A.; Sedghi, A. *Fibre Chem.* **2006**, *38*, 383(b) Eslami Farsani, R., Shokuhfar, A., Sedghi, A. *E-Polymers.* **2006**, *6*, 1.
(24) (a) Chung, D. D. L. *J. Mater. Sci.* **2004**, *39*, 2645(b) Markham, D. *Materials & Design* **1999**, *21*, 45(c) Tzeng, S. S.; Chang, F. Y. *Mater. Sci. Eng., A* **2001**, *A302*, 258.
(25) (a) Chung, D. D. L. *Carbon* **2001**, *39*, 279(b) Fu, S. Y.; Lauke, B.; Mader, E.; Yue, C. Y.; Hu, X. *Composites, Part A* **2000**, *31A*, 1117(c) J.B. Donnet and R.C. Bansal; Marcel Dekker, Ed. New York (1990).
(26) Zhao, Z.; Gou, J. *Sci. Technol. Adv. Mater.* **2009**, *10*, No pp. given.
(27) Gamby, J.; Taberna, P. L.; Simon, P.; Fauvarque, J. F.; Chesneau, M. *Journal of Power Sources* **2001**, *101*, 109.
(28) Leitner, K.; Lerf, A.; Winter, M.; Besenhard, J. O.; Villar-Rodil, S.; Suarez-Garcia, F.; Martinez-Alonso, A.; Tascon, J. M. D. *J. Power Sources* **2006**, *153*, 419.
(29) Shiraishi, S.; Kurihara, H.; Shi, L.; Nakayama, T.; Oya, A. *J. Electrochem. Soc.* **2002**, *149*, A855.
(30) Huang, H. X.; Chen, S. X.; Yuan, C. e. *J. Power Sources* **2008**, *175*, 166.
(31) Blakemore, J. D.; Gupta, A.; Warren, J. J.; Brunschwig, B. S.; Gray, H. B. *J. Am. Chem. Soc.* **2013**, *135*, 18288.
(32) Cui, W.; Liu, Q.; Cheng, N.; Asiri, A. M.; Sun, X. *Chem. Commun. (Cambridge, U. K.)* **2014**, *50*, 934.

Chapter **6**

General conclusion

1) We analyzed the activation of H_2 promoted by the products of iron complex [Fe(BPMCN)$(OTf)_2$] (BPMCN =N,N'-bis(2-pyridylmethyl)-1,2-diaminocyclohexane) and H_2O_2. While the active species generated in the presence of acetic acid barely activate the hydrogen molecule, in the absence of such acid high oxidation state iron species activated efficiently the H-H bond by an unprecedented oxidative homolytic cleavage (see scheme).

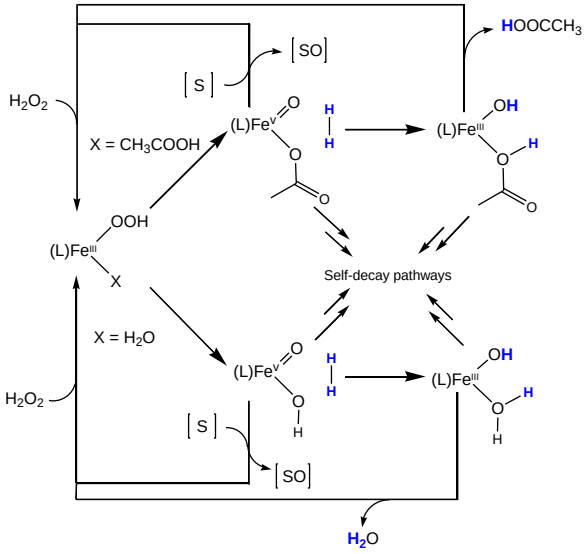

2) The incorporation of metalloporphyrins to graphene oxide through supramolecular interactions (π- π) or by covalent functionalization results in new nanostructured functional materials. These GO-porphyrin hybrids, may be present aqueous in dispersions of porphyrins that would otherwise be completely insoluble in water.

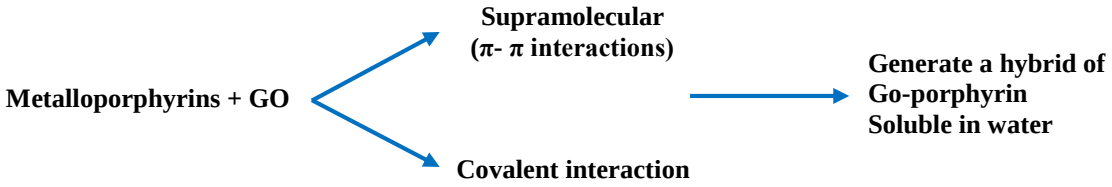

3) Few layers graphene suspensions were obtained in low boiling point solvents such as EtOH, THF and their mixtures with water. This work contributes to solving the problem of dispersibility of the suspensions of graphene in different solvents and makes more universal use of graphene in suspension. These suspensions may be used as graphene inks for homogeneously coating surfaces by spray deposition to prepare transparent conductive films.

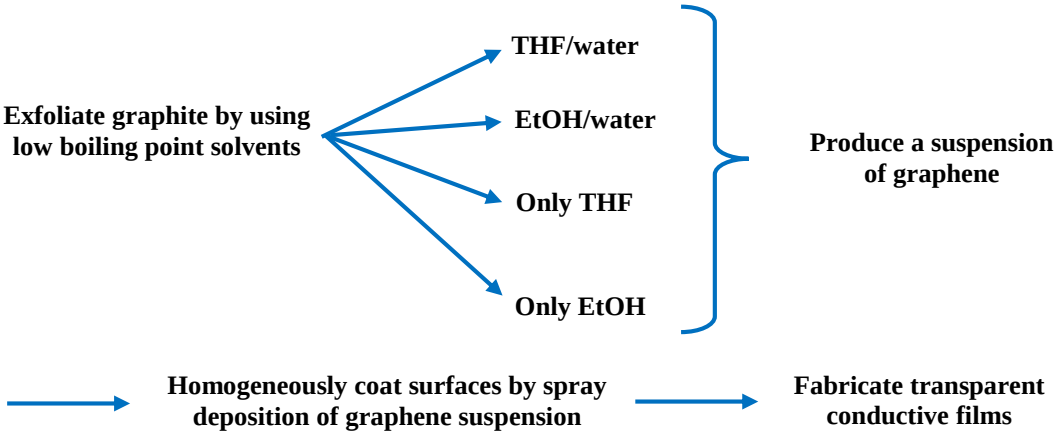

4) High superfical area carbon fibers based electrodes were prepared. While clean fresh electrodes not show electrocatalytic activity, activated electrodes with the mixture of H_2O_2 / H_2SO_4 show good activity as electrocatalysts for H_2 electrogeneration in acidic media.

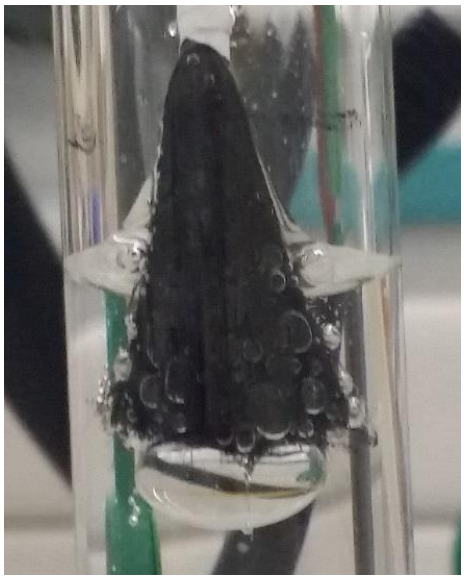

Spanish:

1) Se ha analizado el proceso de activación de H_2 promovido por los productos resultantes de la reacción del complejo de hierro [Fe(BPMCN)$(OTf)_2$] (BPMCN =N,N'-bis(2-pyridylmethyl)-1,2-diaminocyclohexane) y H_2O_2. Mientras que la especies activa generada en presencia de ácido acético apenas activa la molécula de hidrógeno, en ausencia de dicho ácido las especies de hierro en alto estado de oxidación activan de manera eficiente el enlace H-H mediante un proceso hasta ahora no descrito de ruptura homolítica oxidativa.

2) La incorporación de metaloporfirinas a óxido de grafeno, mediante interacciones supramoleculares (π- π) o mediante funcionalización covalente resulta en nuevos materiales nanoestructurados funcionales. Con estos híbridos de GO-porfirina, es posible tener dispersiones acuosas de porfirinas que de otro modo serían completamente insolubles en agua.

3) Se han obtenido suspensiones de grafeno de pocas capas en disolventes de bajo punto de ebullición tales como EtOH, THF y en la mezcla de ellos con agua. Este trabajo contribuye a resolver el problema de la dispersabilidad de las suspensiones de grafeno en diferentes disolventes y hacer más universal el uso de grafeno en suspensión. Estas suspensiones pueden ser utilizadas como tintas de grafeno para recubrir homogéneamente superficies mediante deposición por pulverización con el fin de preparar películas conductoras transparentes.

4) Se han preparado electrodos con elevada area superfical basados en fibras de carbono. Mientras los electrodos limpios no muestran actividad electrocatalítica, los electrodos activados con la mezcla de H_2O_2/H_2SO_4 muestran una buena actividad como electrocatalizadores para la electrogeneración de H_2 en medios ácidos.

Appendix

Technical details

Dichloromethane and tetrahydrofuran were purchased from SDS. CH_3CN, thionyl chloride, EtOH, Sulforic acid, H_2O_2, N,N-Dimethylformamide, trimethylamine, 4-(dimethylamino) pyridine, 4-hydroxypyridine were purchased from Sigma-Aldrich. All solvents were used as received unless noted otherwise.

CH_3CN solvent was distilled over CaH_2 before use. Dichloromethane was distilled over calcium hydride under argon atmosphere. Tetrahydrofuran was distilled over sodium and benzophenone under argon atmosphere. Water for preparation of solutions was purified with a Milli-Q Milli-RO water system (Millipore).

Meso-tetraphenyl porphyrin (TPP) and meso-tetra(pentafluorophenyl)porphyrin (F20TPP) were purchased from Frontier Scientific. 5,10,15,20-Tetraphenyl-21*H*,23*H*-porphyrin cobalt(II) (CoTPP) and 5,10,15,20 Tetraphenyl- 21*H*,23*H*-porphyrin nickel(II) (NiTPP) were purchased from Sigma-Aldrich. 5,10,15,20-Tetrakis- (2,3,4,5,6-pentafluoro-phenyl)- porphyrin-Co(II) (CoF20TPP) and 5,10,15,20-tetrakis-(2,3,4,5,6- pentafluoro-phenyl)- porphyrin-Ni(II) (NiF20TPP) were purchased from Tripor Tech GmbH. High quality graphene oxide (GO) large flakes was provided by Nanoinnova Technologies S.L. (www.nanoinnova.com). The starting commercial graphite source (NGS Naturgraphit) is based on natural graphite with particles sizes < 150 µm (100 mesh) up to < 45 µm (325 mesh). The carbon fibers were purchased from clipcarbono.com.

Fourier transformer infrared (FTIR):

Fourier transformer infrared spectras were recorded on a Perkin-Elmer 1650 spectrophotometer in KBr pellets.

UV-Vis spectroscopy:

Electronic absorption spectra were recorded on an Agilent 8452 diode array spectrophotometer over a 190–1100 nm range in 1 cm quartz cuvettes at room temperature.

X-ray Photoelectron spectra (XPS):

XPS spectra were obtained in collaboration with prof. José Luis García Fierro in the Institute of Catalysis and Petrochemical (CSIC) with a VG Escalab 200R spectrometer equipped with a hemispherical electron analyzer (pass energy of 50 eV) and a MgKα ($h\nu$ = 1254.6 eV, 1 eV = 1.6302×10^{-19} J) X-ray source, powered at 120 W. The kinetic energies

of photoelectrons were measured using a hemispherical electron analyzer working in the constant pass energy mode. The background pressure in the analysis chamber was kept below 6 x 10^{-9} mbar during data acquisition.

Raman-luminescence spectroscopy:

A CRM200 confocal Raman microscope (Witec GmbH, Ulm, Germany) was used to obtain the Raman-luminescence spectra of films of GO and derivatives on glass slides. This experiment were done in collaboration with Dr. Benjamin R. Horrocks, chemical nanoscience laboratory, Newcastle University, UK.

Atomic force microscopy (AFM):

Atomic force microscopy images were acquired in dynamic mode by using a Nanotec Electronica system. Olympus cantilevers were used with a nominal force constant of 0.75 N/m and 70 KHz resonance frequency. The images were processed using WSxM (freely downloadable SPM software from www.nanotec.es) operating at room temperature in ambient air conditions.

Transmission electron microscopy (TEM):

TEM images were obtained in a JEOL model Transmission Electron Microscope JEM 3000 F (field emission) with an accelerating voltage of 300 KV in the Microscopy centre of Luis Brú in Complutense university of Madrid. The microscope has a multi scan CCD camera, XDS microanalysis, TEM and STEM operation modes, annular detector (HAADF). EELS analyses were carried out on a ENFINA electron energy loss spectroscopy (EELS), 1.7 Å point resolution and 25° tilt goniometer.

Scanning electron microscopy (SEM):

Scanning Electron Microscopy (JEOL JM6400) equipped with a 40 kV microprobe in the microscopy centre of Luis Brú in Complutense university of Madrid. The substrates used for SEM were copper discs. The microscope has a multiscan charge-coupled device (CCD) camera and Energy-dispersive X-ray spectroscopy (EDXS) microanalysis system.

X-ray powder diffraction (XRD):

Powder X-ray diffraction has been done using a diffractometer PANalyticalX'Pert PRO theta/2theta primary monochromator and detector with fast X'Celerator. The samples have been analyzed with scanning theta/2theta in the Interdepartmental Research Service (SIDI) of the Autónoma University of Madrid.

Raman spectroscopy:

Raman measurements were recorded on a WITec/Alpha 300AR Raman confocal microscope at ambient conditions. The laser wavelength and power were 532 nm and 0.7 mW, respectively. The experiments were obtained in the Institute of Ceramics and Glass (ICV), (CSIC) in the Autónoma University of Madrid, in collaboration with Dr. Angel Adolfo de Campo García.

Thermal gravimetric analysis (TGA):

The thermogravimetric analyses were performed in a TGA TA INSTRUMENTS Q-500 analyzer in the Interdepartmental Research Service (SIDI) of the Autónoma University of Madrid. The temperature program was from 25 to 1000 ºC, with a temperature rate of $5^{o}C.min^{-1}$ under a nitrogen flow.

Spray coating:

The substrates were sprayed using a Meinhard TR-30-K1 nebulizer with a flow of argon. The number of spray cycles and the ink concentration can control the film thickness.

Optical transmission:

Optical transmission spectra of the films deposited on glass slides were recorded on a UV–vis spectrometer (Agilent 8452) with a glass slide as reference. Transparency was measured at a wavelength of $\lambda = 550$ nm after annealing the conductive films in 350 ºC for 15 min.

Conductivity measurement:

Sheet resistance, Rs, was measured by a KDY-1 four-probe resistivity test system (GuangZhou KunDe).

Gas Chromatography:

GC product analyses were performed on a CP-3800 Varial gas chromatograph (Factor IV-5MS column, 30 m) with a flame ionization detector in the Interdepartmental Research Service (SIDI) of the Autónoma University of Madrid.

Reactions under control pressure:

A magnetically stirred thermostated, Teflon-lined steel, Berghof reactor model BR 100, the Teflon insert have been modified to reduce the internal to a maximum volume of 15 ml, the liquid was added using a 307 Gilson HPLC pump. These experiments were done in collaboration with Dr. Jose Miguel Campos Martín and prof. José Luis García Fierro in the Institute of Catalysis and Petrochemical (CSIC).

Total Reflection X-ray Fluorescence (TXRF):

TXRF analysis of the samples was performed in collaboration with Dr. Ramón Fernández Ruiz in the Interdepartmental Research Service (SIDI), with a benchtop S2 PicoFox TXRF spectrometer from Bruker Nano GmbH (Germany), equipped with a molybdenum X-ray source working at 50 kV and 600 μA, a multilayer monochromator with 80% reflectivity at 17.5 keV (Mo Kα), an XFlash SDD detector with an effective area of 30 mm^2, and an energy resolution better than 150 eV for Mn Kα.

Electrochemical measurements:

Electrochemical measurements are performed in collaboration with Dr. Octavio González del Moral with using a one-compartment cell, all voltammetric scans were recorded using C-Brushes fiber as working electrode. An Ag/AgCl and Pt wire were used as reference and counter electrodes, respectively. All materials for electrochemical experiments were dried at room temperature before use. All experimental procedureswere conducted at ambient temperature under nitrogen atmosphere and using degassed acetonitrile.We carried out several cyclic voltammetries at increasing H^+ concentrations (trifluoroacetic acid as H^+

source). The working solution was made with fresh dry acetonitrile (10 ml) and Bu_4NPF_6 as electrolyte (100 mM). All the experiments were done under argon atmosphere, bubbling argon into it few minutes and dipping 1 cm of the C-brushes into the working solution.

Titration of produced H_2O_2 with $KMnO_4$:

To know amount of the H_2O_2 produced in the reactor, after filtration the solution of the reactor, 3 ml of the solution was added to 47 ml distilled water and 10 ml H_2SO_4 (4M) and was titrated by $KMnO_4$ (0.0025 M).

Then by considering the equation we have calculated the amounts of H_2O_2 produced:

$$2\ MnO_4^- + 5\ H_2O_2 + 6\ H^+ \longrightarrow 2\ Mn^{2+} + 5\ O_2 + 8\ H_2O$$

Moles of H_2O_2 = 5/2 (Moles of $KMnO_4$)

Determination calibration factor for GC analysis of oxidized olefins substrates:

To obtain the calibration factor three different concentration of each sample were prepared and then 1mM Naphthalene as an internal standard was added and the sample was injected to gas chromatography. Then the K was calculated for each one by using the integration and concentration and then was averaged between three different K.

$$\text{Concentration} = \frac{I_{\text{oxide}}}{I_{\text{naphtalene}}} * K$$

Table 2. Determination calibration factor for all the substrates that we have used.

	K
Cyclooctene oxide	$\mathbf{1.21*10^{-6}}$
phenyl propylene oxide	$\mathbf{1.4*10^{-6}}$
sulfoxide	$\mathbf{1.62*10^{-6}}$
sulfone	$\mathbf{1.72*10^{-6}}$
Cyclohexanole	$\mathbf{2.77*10^{-6}}$
Cyclohexanone	$\mathbf{1.67*10^{-6}}$
cyclohexane- OAC	$\mathbf{1.16*10^{-6}}$